Development of a Novel Porogen Insertion System Used in Solid Freeform Fabrication of Porous Biodegradable Scaffolds with Heterogeneous Internal Architectures

by

Hajar Sharif

A thesis
presented to the University of Waterloo
in fulfillment of the
thesis requirement for the degree of
Master of Applied Science
in
Mechanical Engineering

Waterloo, Ontario, Canada, 2009

AUTHOR'S DECLARATION

I hereby declare that I am the sole author of this thesis. This is a true copy of the thesis, including any required final revisions, as accepted by my examiners.

I understand that my thesis may be made electronically available to the public.

Hajar Sharif

Abstract

This thesis is concerned with the design of a novel system for inserting porogen particles within internal structure of the bone scaffold. The proposed system would be integrated with a 3D printing machine to create macro-pores based on the conventional porogen leaching method. The system is capable of inserting porogens on pre-designed locations within the scaffold structure to realize the generation of macro-porosity within scaffolds. Several alternatives for such a porogen insertion mechanism are proposed based on employing a mechanical actuator for opening and closing the path of porogen particles from a porogen reservoir to the build chamber. Another possible design that offers significant advantages over its actuator-based alternatives is a pneumatic-based mechanism that picks up porogens from a porogen reservoir and places them at pre-designed locations. Among all the presented alternatives, the pneumatic-based system is selected by utilizing the value matrix method, and detail design of the different parts of this system is presented. The required pilot test setups for performing the feasibility study of the proposed method have been designed and successfully developed, and the practicality of the designed porogen insertion mechanism is proven through experiment.

Acknowledgements

I would like to take this opportunity to acknowledge the support of a number of individuals without whom this thesis would not have been possible. I would like to thank my supervisor, Dr. Ehsan Toyserkani who provided me an opportunity to explore more in my academic life. His dedication and support was a source of invaluable influence in my academic achievements and career. As well, I wish to express my appreciation to the readers of my thesis, Dr. Behrad Khamesee and Dr. John Wen, for their helpful comments and suggestions.

I would like to thank Dr. Armaghan Salehian for the helpful information she provided me on selecting the actuators. In addition, I would like to thank Dr. Jock Mackay and Dr. Stefan Steiner for their useful advice on the experimental design. I hope that I may have the opportunity to repay them in-kind in the future.

My fellow students and friends helped to create a tremendously rewarding experience here at the University of Waterloo. I would especially like to thank Habib Abou Saleh, Hamidreza Alemohammad, Kobra Gharali, Tahereh Garshasb, Amin Eshraghi, Michele Heng, Alireza Kasaiezadeh, Saman Mohammadi, Rafat Parsaei, Nasim Paryab, Homeyra pourmohammadali, Negar Rasti, Nima Rezaei, Ahmad Salam, Yaser Shanjani, Sherry Towfighian, and Mihaela Vlasea for their help, friendship, and encouragement.

I cannot find a suitable word, but I would like to express my special thanks to my husband, Hossein Bagheri, for all the moments he spent with me. Without him, I could not have come as far.

In closing, I would like to dedicate this thesis to my family and friends, all those individuals whose love, prayer, and persistent support have always accompanied me, no matter how far away I may be, thank you!

Table of Contents

List of Figures

List of Tables

Chapter 1
Introduction

1.1 Biodegradable Scaffolds with Heterogeneous Internal Architecture

Traumatic bone fractures, congenital disorders, and bone defects caused by bone cancer decrease the quality of life significantly. Different methods such as bone grafting and using orthopaedic implants have been applied to repair such defects, since in these cases bone cannot cure itself without any external assistance [1, 2, 3]. Tissue engineering that is an interdisciplinary field and relates to biology, as well as, material, chemical, and mechanical engineering, emerged in the early 1990s, in order to address the limitations of the traditional clinical treatments. Tissue engineering proposed utilizing of biodegradable porous structures, known as scaffold, for transplanting a biofactor such as cell, gen, and protein into the host body. Scaffold is built similar to the damaged tissue and supports the new tissue growing in vitro and/or in vivo. Since every tissue has specific mechanical and structural properties, different criteria must be satisfied by their appropriate scaffolds [4, 5].

Both mechanical and biological properties of bone scaffolds should be considered for assessments. In other words, a scaffold should be strong enough to withstand the applied stresses, capable of revascularizing, and able to incorporate into the host body and survive under the host biological responses [6]. To this end, several criteria such as posing specific surface chemistry and internal architecture, being fabricated from biodegradable and biocompatible materials, etc. have been recognized as crucial for the tissue engineered scaffolds [7].

High porosity and large size interconnected pores are among the most important requirements for the bone scaffolds because large pore size and pore continuity improve permeability for nutrition and oxygen delivery and waste diffusion [7, 8, 9, 10, 11, 12]. In addition, a larger pore volume provides more room for revascularization and accommodates sufficient cell mass for tissue repair. Moreover, larger surface area in pores facilitates cell attachment and growth [11, 12, 13, 14]. However, higher porosity leads to a weaker structure and accelerates the degradation rate. As a result, proposing an optimal design for pores distribution within a biodegradable structure to balance the required characteristics for mechanical support versus the target properties for tissue regeneration is crucial in production of tissue engineered

bone scaffolds [10, 15, 16, 17]. This goal can be facilitated through heterogeneous design of the scaffold. In other words, at each region of the scaffold some specific mechanical and biological properties are required; therefore, the porosity level must be optimized in a way that the local mechanical and biological requirements are satisfied. For instance, those regions aim for load bearing need stronger mechanical properties, and lower porosities should be only assigned to such regions [16].

Several conventional techniques have been recognized as successful methods for manufacturing porous 3D biodegradable Scaffolds. The most common methods are fiber bonding, particulate leaching, gas foaming, freeze drying/emulsification, and phase separation [13, 17, 18, 19, 20]. However, as will be explained in section 2.3, none of these techniques can fabricate scaffolds with complex morphology and controlled internal architecture directly from a CAD (computer aided design) model. In contrast, Solid Freeform Fabrication (SFF) has exceptional properties that make this method an excellent alternative for production of tissue engineered scaffolds. SFF is a computer-aided manufacturing technique that is compatible with a wide range of biomaterials, and manufactures parts layer by layer. The layer-wise nature of SFF enables this technique to extensively control the size and shape of the scaffold, as well as, the material distribution and pore morphology within the scaffold structure [5, 7,18,21,22].

3D printing is a powder-based SFF technique that has been applied extensively for manufacturing bone scaffolds [23,24,25,26]. A combination of SFF technique and particulate leaching has been used for generating macro-pores in the scaffold structure [18, 27,28,29,30,31]. All of these proposed SFF techniques facilitate a homogenous pore distribution in the scaffold structure; however, posing a heterogeneous design is vital for the tissue engineered scaffolds. As a consequence, proposing a new technique that is capable to control the macro pore distribution within the scaffold structure is still a crucial requirement in the field of tissue engineering.

1.2 Objectives of the thesis

This work is concerned with design of a novel system for manufacturing bone scaffolds with controlled macro-porosity and distribution. This novel device works synchronized with a SFF machine and applies the concept that has been proposed for the traditional particulate leaching method. This mechanism is capable of insertion of the porogen particles in pre-designed

locations within the scaffold structure. As a result, when the scaffold is completely fabricated by the 3D printing method and the porogens are washed out through the porogen leaching technique, a scaffold with a pre-designed internal architecture is achieved. In the current project, the overall design of the whole mechanism, as well as, the detail design of the important parts of the system is presented. The feasibility of the proposed design is proved through experimental results.

1.3 Outline

the present thesis is organized in the following order. Chapter 1 contains the introduction, problem definition, and objectives. Background information on tissue engineered bone scaffolds, effect of porosity distribution and size on bone scaffold properties, and the methods that have been used for manufacturing porous scaffolds is stated in Chapter 2. A finite element model of a dual-porous scaffold that is composed of a cartilage substrate and a bone scaffold is presented in Chapter 3. Such a scaffold can be widely used in repairing the ostecondral defects. In order to judge the effect of two distinct porous architectures on strength and capability of cell ingrowth stimulation of the presented structure, stiffness and principal strain histogram of the single and the dual-porous scaffolds are compared. The presented modeling and finite element analysis methods can be applied to optimize the porosity distribution and pore size of the bone scaffolds that can be fabricated by the proposed porogen insertion mechanism. In Chapter 4, the proposed alternatives for the porogen insertion mechanism have been presented. Afterwards, the well-known value matrix method has been applied for selecting the best design among the presented solutions. Subsequently, the selected design has been described in more details. The feasibility study methods and results on the practicality of the selected design have been demonstrated in Chapter 5. Lastly, Chapter 6 addresses the conclusion and recommendations for future work.

Chapter 2
Literature Review and Background

2.1 Tissue Engineered Bone Scaffold as a Promising Bone Substitute

Around 6.3 million fractures occur in the United States yearly [32]. At the first glance, this does not seem to be a considerable issue because bone can heal itself [33]; however, in traumatic cases such as large crushes or extremely complex fractures the consequence is different. Usually in those conditions, there is an extensive amount of damage and they pose a significant risk to the patient or fail to heal properly. In such situations, as well as congenital disorders or defects in bone caused by bone cancer, bone cannot cure itself without any external assistance [2, 3].

the extent of the problem is evident from the fact that the bone cancer (osteosarcoma) has been reported as the fourth most common type of cancer among children. Moreover, about half a million bone graft operations are done yearly in the United States, and bone grafts are the second most transplanted materials after blood transfusions [34, 35].

Depending on the site and type of the bone problem, different methods have been applied to facilitate and speed up the bone healing. One of the techniques commonly applied to complex fractures is bone grafting. In bone grafting, the defected area is determined by applying diagnostic tests such as x-rays, magnetic resonance imaging (MRI), and computed tomography (CT) scan. Then new bone or material is replaced into the fracture (space between or around broken bone) or defect (hole in bone) via surgery. Since immobilization at the graft-host interface is necessary for a successful bone grafting, rigid internal fixations such as pins, plates, or screws are used to hold the graft immovable after replacement. Therefore, employing standard osteosynthesis techniques are highly recommended. Additionally, a splint or cast is often applied to prevent movement of the bones during recovery. When the bone graft is accepted by the body, the transplanted bone converts into the new living bone and integrates into the body as a functional unit [3, 36].

In general, the bone grafts are classified on the basis of donor and structure types. Donor types include autograft (from the same person, usually from hip bones or ribs), allograft (from the same species, usually from a cadaver), isograft (from an identical twin), xenograft (from a

different species), and synthetic. Also, structure type, which is associated with the application of the graft, is used for categorization. These categories include cortical, cancellous, and corticocancellous [3, 6].

Job van Meekeren, a Dutch surgeon, documented the first bone graft procedure in 1668. A traumatic defect in a soldier's cranium was repaired by a graft taken from a dog's skull. For the first time in 1674, another Dutch scientist, Anton van Leeuwenhoek, described bone structure which was followed by an explanation of the phenomenon of callous formation around bone ten years later [6].

the first allograft was taken from the tibia of a child and implanted in the humerus of a 4-year-old boy, by Macewen in Scotland. Von Walter performed the first autograft implant which replaced parts of a surgically removed skull after trephining the bone. During and after World War II, bone banking gained popularity; however, development of reliable bone banks started in the 1960s. In that decade, the histologic and immunologic natural history of allografts became well established by Burwell [6].

A bone graft can facilitate defect healing in three ways. The first one is osteogenesis in which the new bone can form from the cells contained within the graft. In osteoinduction, the second way, molecules within the graft (a variety of growth factors including bone morphogenetic proteins abbreviated as BMP) convert the host body cells into cells with the ability to differentiate into the bone-forming cells through a chemical process. Migration, proliferation, and differentiation of host’s cells are mandatory for osteoinduction. Thirdly, the graft can act as a scaffold to enhance the ingrowth of the new capillaries and the bone tissue. This gradual process is referred as osteoconduction [3, 6].

Using autograft has a lower risk of graft rejection and disease transfer to the patient. In addition, compared to allograft, isograft, and xenograft, a shorter time may be required for autograft to incorporate with the host tissues. Using autograft has some drawbacks too. For example, less bone is available for grafting and it requires a second operation, which results in more pain, longer operation and anesthesia time (usually around 30 minutes per surgery), additional cost and higher risk of infection. Allograft, isograft, and xenograft provide variability of bones from different donors and one surgery per person is required. However, their

osteoinductive ability may be destroyed during the preparation processes such as sterilizing [3, 6, 37].

Synthetic bone grafts offer remarkable advantages over both allograft and autograft. When applying a synthetic graft, the patient undergoes only one surgery and, since there is no donor, there is no possibility of disease transfer. Moreover, it can be manufactured in the variety of structures to mimic the replaced bone geometrical features. In other words, synthetic grafts eliminate most of the cost and pain associated with using other types of grafts. However, their integration with the host tissue and their failure due to wear and fatigue over the time are considerable issues in employing them [5].

Tissue engineering is an interdisciplinary field and emerged in the early 1990s. Tissue engineering, which relates to biology on one hand, and material, chemical and mechanical engineering on the other hand, addresses the limitations of the traditional grafting methods. The proposed concept by tissue engineering is to transplant a biofactor such as cell, gen, and protein within a porous structure called scaffold. In this way, scaffold functions in the role performed by conventional grafts in osteogenesis, osteoinduction, and osteoconduction. By using MRI, X-Ray and other imaging methods, along with image processing, the scaffold is built similarly to the damaged tissue and supports the new tissue growing in vitro and/or in vivo. As every tissue has specific mechanical and structural properties, their appropriate scaffolds must satisfy different criteria [4, 5].

the success of a bone scaffold is determined by both its mechanical and biological properties. In other words, its strength to withstand the applied stresses, its capability of revascularization, and its ability to incorporate into the host body and survive under the host biological responses should be taken into account [6]. To facilitate this aim, several criteria have been recognized as crucial in producing the tissue engineering scaffolds [7]. First of all, scaffolds need to be made of biocompatible materials, so no adverse response will be induced by it after implantation [8, 9]. Secondly, the scaffold materials should degrade into non-toxic components with controlled biodegradability or bioresorbability, because eventually tissue will replace the scaffold and the scaffold materials should be excreted from body over the time [7, 8, 9, 10]. In addition, high porosity along with a large surface to volume ratio is required to provide sufficient room for cell

seeding. Such pores should be interconnected with the channels of appropriate scale to facilitate cell/oxygen/nutrition/waste products diffusion, tissue integration, and vascularisation [7, 8, 9, 10, 11, 12]. Furthermore, to favour cellular attachment, differentiation and proliferation, specific surface properties are essential [7]. Moreover, to match the intended site of implantation, the scaffold should possess appropriate mechanical properties. For instance, it requires being strong enough for load bearing during in vitro or in vivo growth and remodeling process [7, 8, 10]. Additionally, the structure should have similar apparent stiffness to the apparent stiffness of the surrounding bone [11]. At last, the material should be easily manufacturable to fabricate scaffolds with any desired shape and size to fit complex anatomical defects. Because scaffold guides tissue regeneration in three dimensions and dictates the final shape of the grown tissue [7, 10].

2.2 Effect of Porosity Distribution and Size on Bone Scaffold Properties

Porosity, which is a morphological property, is defined as the percentage of void fraction in a solid [13]. Porosity of the bone scaffold is usually characterized by micro and macro-porosity that is usually assigned to the porosity caused by the pores of the sizes larger than 50 μm [18]. Regardless of the scaffold material or the applied manufacturing technique, high porosity and large size interconnected pores are desired for the bone scaffolds due to several reasons. First of all, large pore size and pore continuity improve permeability for nutrition and oxygen delivery and waste diffusion. It should be emphasized that, one of the most significant challenges in tissue engineering is mass transportation [8, 10]. Secondly, a larger pore volume provides more room for revascularization and accommodates sufficient cell mass for tissue repair [8, 10]. In addition, larger surface area in pores facilitates cell attachment and growth [8]. It has been claimed that micro-pores and submicron porosity (associated with the pore size less than 1 μm) affect surface topography and accordingly cell-surface interaction. As a result, cell attachment, proliferation, spreading, differentiation, and function depend on micro and submicron porosities, as well. Furthermore, micro-pores and submicron pores may serve as reservoirs for growth factors or other drugs for local release and induce bone ingrowth and vascularization [14]. In turn, more tissue ingrowth in pores enhances stronger interlocking between implant biomaterial and the natural bone which results to more mechanical stability at their interface [8, 13].

the minimum recommended pore size for successful bone regeneration was 100 μm based on the work of Hulbert et.al. [38]; however, subsequent works have been claimed that the optimal pore size is between five to ten times the cell's diameter i.e., 100-300 μm for bone cells [17]. Also, the optimum pore size for different tissues has been identified through experiments. The experimentally recommended values are 5 μm for neovascularization, 5–15 μm for the ingrowth of fiberblast, close to 20 μm for hepatocytes ingrowth, 20–125 μm for regeneration of adult mammalian skin, 40–100 μm for osteoid ingrowth and 100–350 μm for regeneration of bone. In fibrovascular tissues, pores' size greater than 500 μm is required for the survival of transplanted cells [8].

For designing scaffolds, in addition to optimum pore size and porosity, the possible changes in internal structure over time should be taken into consideration. After implantation, the biodegradable scaffolds, such as scaffolds from polylactic acid (PLA), polyglycolic acid (PGA), and calcium polyphosphate (CPP), degrade, and, consequently, the average pore size increases, and the interconnecting channels open. In the case of non-degradable scaffolds, pore volume will be occupied by new grown tissues and the void fraction decreases. In addition to mentioned parameters, the morphology of the pores influences tissue ingrowth. Reproducibility of pores is also a vital parameter in designing the bone scaffolds and selecting the appropriate technique for producing them [8, 18].

theoretically, the scaffold is a temporary mechanical support for tissue ingrowth and it has to present mechanical properties similar to the mechanical properties of the host site. To accomplish this goal, bone scaffold needs to offer adequate stiffness and strength to bear the loads applied to the implantation site during the new bone ingrowth [10, 13, 15].

Typically, required characteristics for mechanical support conflict with target properties for tissue regeneration, i.e., high porosity with large size interconnected pores [10, 15]. In other words, by increasing the volume fraction, which results to obtaining a stiffer and stronger scaffold, permeability decreases [10, 15]. In contrast, higher porosity leads to a weaker structure and accelerates the degradation rate [16, 17]. As a result, attaining an optimal design for material distribution within a porous structure to balance load bearing versus permeability/porosity is a necessity for manufacturing tissue engineered bone scaffolds [10, 15, 16, 17].

Furthermore, manufacturing bone scaffolds with desired mechanical properties as well as internal and external architecture is essential in application of bone scaffolds in tissue reconstruction studies. For instance, scaffolds with well controlled mechanical properties enhance investigation of the effect of external loads and mechanical properties of scaffold on tissue regeneration. Furthermore, the influence of cell migration, nutrition delivery and wastes removal from the cells on tissue reconstruction can be studied by using scaffolds with well controlled pore structure [5, 10].

2.3 Porous Scaffold Manufacturing Methods

Traditionally, because of the manufacturing and design limitations, the scaffolds were designed with homogeneous porosity. A single level porosity limits the scaffold design and cell growth. In fact, since different mechanical and biological properties are required at different regions of the scaffold, porosity must be optimized in different areas to satisfy local mechanical and biological requirements [16]. For instance, lower porosity should be only assigned to those parts aim for load bearing and need stronger mechanical properties. Homogenous design, based on worst case scenario, offers the higher mechanical properties and in turn lower porosity for the entire scaffold. As a result, the cells that require high level of porosity may not grow efficiently [16]. Conversely, if a higher porosity is assigned for the whole scaffold to facilitate efficient cell growth in all regions, the scaffold may fail to bear applied loads on the implantation site. Moreover, the degradation rate would increase undesirably due to the higher degradation surface area and lower volume of material especially in the areas that are more exposed to the biological fluids [13, 16, 17]. As a result, posing a heterogeneous internal architecture is of interest in manufacturing of bone scaffolds. In addition, bone scaffold dictates the overall shape of the regenerated bone and it should fit the complex anatomical defects for every individual patients [10, 18]. To facilitate these requirements, the material used for producing bone scaffold should be easily processable to a solid structure with complex geometrical features [17, 20]. In the same way, an efficient low-cost automated manufacturing process is essential [18]. As another considerable issue, it should be taken into account that properties of manufactured scaffold primarily depend on both the characteristics of the applied biomaterial and the fabrication process [13]. In turn, the appropriate method is selected depending on the biomaterial being used.

Several successful techniques have been reported for manufacturing of porous 3D biodegradable scaffolds. The most common methods are fiber bonding, particulate leaching, gas foaming, freeze drying/emulsification, phase separation and solid freeform fabrication [18, 19, 20].

Scaffolds made by fiber bonding method, were some of the earliest tissue engineered structures proposed in 1993. This method is usually used for PGA fibers, which are attached to each other through two different ways. The first method was proposed by Mikos et al. at 1993. They immersed PGA fibers in a poly-L-lactide acid (PLLA) solution, so solvent's evaporation left a composite of PGA fibers embedded in PLLA. The composite then was heated up to the melting point of the both materials. PLLA melted first and filled all the gaps between PGA fibers, therefore when PGA melted fibers did not collapse. In this way, PGA fibers welded in their cross-points and PLLA was washed out by methylene chloride left a porous structure of PGA fibers with the porosities of up to 81% and pore sizes as large as 500 μm. These foamy scaffolds showed promising results for Hepatocytes culturing in vitro. In the second method of PGA fibers attaching, a solution of PLLA or polylactic-co-glycolic acid (PLGA) in chloroform is sprayed onto the PGA fibers. When the solvent evaporates, leaves PGA fibers glued with PLLA or PLGA. In vivo test of this kind of scaffold confirmed its ability to stimulate neotissue formation. This method was used by Mooney et al. at 1996 [39].

Fiber bonding techniques provide high porous scaffolds with interconnected pores; however, both methods use solvents which should be removed completely to avoid toxic residuals in the scaffold structure. To facilitate this aim, the scaffolds are vacuum dried for several hours, so they cannot be used in a clinical setting immediately. Additionally, in the first method there is a combination of high temperature and toxic materials which can be a concern if cells or bioactive molecules need to be included in the scaffold [39, 40].

the particulate leaching technique, also known as solvent casting, is based on using a particulate material as the pore maker or porogen. Particles or fibers with pre-determined sizes are included in the scaffold structure during the manufacturing process. When the parts are completed, porogen particles are leached out with an appropriate solvent. In a primary alternate form of this method [41], a polymer such as PLLA is dissolved in a solvent like chloroform and

mixed with a particulate material (e.g., salt) that is stable in the polymer solvent. When the solvent is removed through 48 hours evaporation and complimentary vacuum drying, a composite of polymer with porogen particles is left. Next, the porogens are washed out in another solvent such as distilled water or one which does not affect the polymer. This process produces a porous polymeric structure. The porosity of the resultant scaffold depends on the amount of porogens, and its pore sizes are controlled by the porogen sizes. By using 70-90 weight percent of salt, homogenous interconnected pores are achievable in 93% porous PLLA scaffold [41]. However, the side exposed to air is rougher than the other side which is not exposed. To provide a more homogenous surface morphology, pieces of the polymer/porogen composite are molded into a cylindrical form under pressure and at a temperature just above the melting/glass transition temperature of the polymer. Discs with desired thickness can be cut out of the resulted cylinder. This method provides scaffolds with more uniform surface properties, but thermal degredation of the polymer during the process is an issue [41]. Furthermore, the porogen leaching step makes the scaffold preparation process longer. In addition, specifically in the case of scaffold with poorly interconnected pores, there is a possibility of undesirable residuals in the scaffold structure. However, scaffolds manufactured through the porogen leaching method have been used extensively for culturing different types of cells without posing any adverse effect on new tissue regeneration. Different minerals such as tartrate, salt, citrate, etc. and organic materials like sugar, saccharose, naphtalene, polymer, etc. have been used as porogen [18, 27, 39, 40, 42].

To avoid usage of organic solvents in the pore-making process, gas foaming technique was proposed by Mooney et al. at 1996 [43]. In this method polymeric disks are kept in high pressure CO2 for 72 hours at room temperature. When the “gas-containing” disks suddenly go back to atmospheric conditions, gas forms bubbles. By applying this method, porosities of up to 93% with the pore sizes of up to 100 μm are achievable. In a variation of gas foaming method, a foaming agent is added to the scaffold structure and the pores are created by the agents in the exposure of heat. Usually the pores generated by gas foaming are not interconnected and therefore cell migration is hard in the scaffold structure [40].

Other common methods for manufacturing porous structures, which were proposed at 1995, are emulsification/freeze-drying and liquid-liquid phase separation. With the first method a

polymer such as PLGA is dissolved in a solvent (for example methylene chloride) and mixed with an immiscible liquid like distilled water to leave an emulsion. The resulted liquid mixture is cast into a mold and then frozen quickly. By freeze-drying the resulted solid structure at -55°C, immiscible liquid (i.e., water) evaporates and leaves pores behind. Although manufacturing of porous structures with up to 95% porosity is possible by applying this method, the small size of pores (13-35 μm) is a significant issue. In addition, in this method organic solvents are required and removing the residuals is a concern. In liquid-liquid phase separation, a polymer is dissolved in a low melt-point solvent such as naphthalene or phenol. Then, a bioactive molecule is dissolved or dispersed and the resulted homogenous solution is quenched down to the melting point of the solvent in a controlled fashion to a liquid-liquid phase separation and then a solid-solid phase separation induced. The solvent phase is removed by sublimation and leaves 90% porous scaffolds with interconnected pores of approximately 100 μm, which includes bioactive molecule as well [20, 39, 40].

Although all of the mentioned conventional methods are promising for manufacturing of porous structures, none of them can precisely control the architecture within the scaffold [5, 18, 21]. Moreover, they are not capable to fabricate scaffolds with complex morphology directly from a CAD model [18]. In contrast, the specific properties of Solid Freeform Fabrication (SFF) make it an excellent candidate for tissue engineered scaffold production. SFF is a computer-aided manufacturing technique, which is compatible with a wide range of biomaterials. SFF can extensively control the size and shape of the scaffold and the material distribution and pore morphology within the scaffold structure. Scaffolds made by SFF pose significantly better mechanical properties [5, 7, 21, 22].

In next section SFF methods will be discussed in more details.

2.3.1 Solid Freeform Fabrication (SFF)

SFF, also known as Rapid Prototyping (RP), layered manufacturing, and automated fabrication; is the name of a group of manufacturing technologies that fabricate parts directly from CAD data source. All of these methods use the same approach for fabrication, i.e., they add and bond materials in a layer wise fashion to form the part, contrast to conventional methods in which parts are manufactured by mechanically removing material. SFF technologies have lots of

applications these days. Different parts with a wide range size, from microscopic to entire buildings can be produced by them. Also variety of materials, from plastics, to metals and ceramics, and different combination of them can be processed by these techniques [22, 44].

In all of the SFF methods, first a 3D model is prepared by using CAD. Then, it is exported to "STL" or "SLC" file formats to be readable by an SFF machine. The SFF machine divides the part to thin horizontal cross sections and then builds these layers from the bottom to the top one after other until the part is completed. Since the layers are manufactured independently and can have totally different shapes, solid parts with very complex geometries can be fabricated. In fact, SFF methods are known as a solution for manufacturing parts with complex geometrical features. The layers are joined together by use of a laser beam or a binder injection system. Although, the resulted "Green Part" may still need some finishing processes, but these processes are usually less than what are needed in most of the conventional manufacturing methods. In addition, since there is not much human intervention during the operation, precise parts can be fabricated [45, 46].

SFF techniques are classified according to the primary material they use. Hence, there are three main SFF systems including liquid based, solid based and powder based systems [45].

Most systems of the liquid-based class build parts in a vat of an organic liquid resin, which is cured or solidified by laser light especially in the UV range. When the first layer of resin solidified, an elevation control system lowers it and next layer of resin will fabricated similarly on top of the first layer. This process will continue to complete the whole part. Then the resin exhausted and the part removed for post processing if needed. It should be noted that, different vendors use different kind of liquid resins, method of scanning or exposure, elevation mechanism and optical system. Therefore some variations to this technique exist. Stereolithography (SLA), Solid Ground Curing (SGC), Solid Creation System (SCS), and Solid Object Ultraviolet Laser Printer (SOUP) are some of these varioations [45].

Solid-based group of SFF systems are not so similar to each other; however, all of them use solids as the primary material to build parts. Laminated Object Manufacturing (LOM) processes paper sheets with laser beam, Fused Deposition Modeling (FDM) builds the part from polymer filament, and Multi-Jet Modeling System (MJM) works on thermoplastics [18, 45, 47, 48].

Powder-based group can be considered as a branch of solid-based SFF systems, because they use solid powder as the raw material to create parts. Three Dimensional Printing (3DP), Selective Laser Sintering (SLS) and Laser Engineered Net Shaping (LENS) are categorized in this group. Powder layers are bonded to each other by fusion caused by a laser beam or a binder injected from a print head [45, 49].

2.3.1.1 Application of 3D Printing in Manufacturing Bone Scaffolds

3D printing system was developed at Massachusetts Institute of Technology (MIT) in 1989. A schematic figure and the flow chart of the 3D printing process are demonstrated in Figure 2-1 and Figure 2-2, respectively. As presented in these figures, powder delivery piston comes up to a pre-set height. Then counter-rotating roller spreads and compacts powder on the build bed. Consequently, the adhesive binder is injected by the inkjet (print) head on the appropriate sectors of the layer to glue the powders together and make the desired shape for each cross section of the part. After completion of one layer, the fabrication piston goes down to the zero level, and roller returns to its initial place. The process continues and the part is manufactured layer by layer. When the part is completed, it is left in the machine at a pre-set temperature for drying. When the binder evaporates completely, the part is ready for post-processing stage [18, 50, 51].

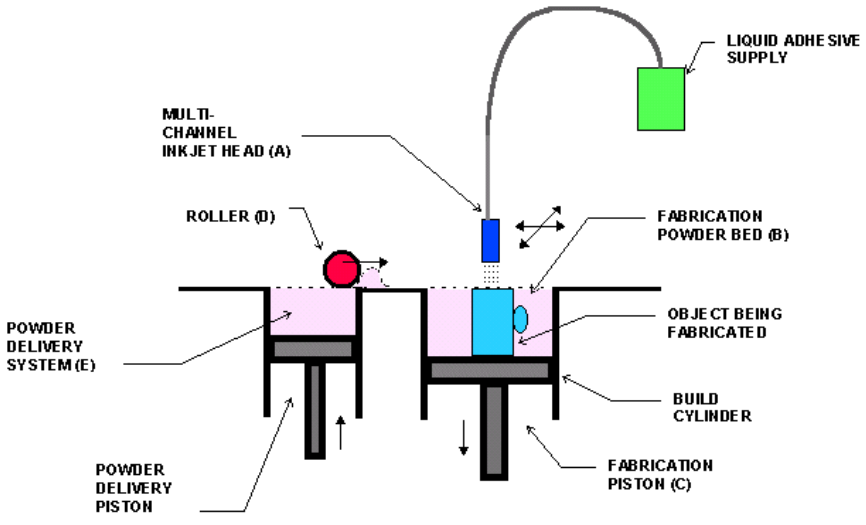

Figure 2-1- Schematic of the 3D Printing Mechanism [50]

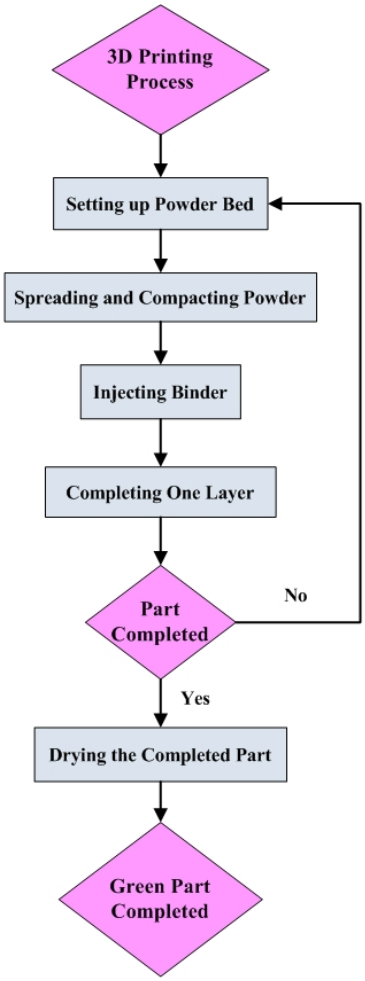

Figure 2-2- Flowchart of the 3D Printing Mechanism

3D printing method has been applied extensively for manufacturing bone implants and tissue engineering applications [23, 24, 25, 26]. Lam et al. [30] claimed that the fusion of powder particles during sintering does not fill all the voids between the particles. As a result, the scaffolds fabricated by 3D printing technique pose micro-pores. A combination of SFF technique and particulate leaching has been used for generating macro-pores in the scaffold structure [18].

Sherwood et al. [31], employed 3D printing technique for fabricating osteochondral scaffolds from Calcium phosphate tribasic (TCP) in the range of 38–106 μm. The upper part of the fabricated scaffolds that composed of D,L-PLGA and L-PLA, was aimed to support cartilage ingrowth, and it was 90% porous. The lower part had a cloverleaf shape, and it was designed to

simultaneously improve bone ingrowth and maintain the required mechanical properties. This bone portion was 55% porous and consisted of a L-PLGA/TCP composite. A transition region that had a gradient of materials and porosity was considered between these two regions to prevent delamination. NaCl particles in the range of 106–150 μm were used as porogen [31].

Tay et al. [29], utilized a blend of polycaprolactone (PCL) and polyvinyl alcohol (PVA) in fabricating biodegradable scaffolds with 3D printing method. They designed and fabricated Rectangular bars with the dimensions of 15×9×3.5 by Zcorp 3D printer. They used a water-based ink to bind different proportions of the PCL powders, in the range of 150-212 μm, and the PVA particles, in the range of 106–150 μm. The resulted scaffolds were air-dried at room temperature and, subsequently, heated at 65 ˚C. Next, the PVA particles were removed at the particulate leaching step to leave a porous scaffold [29].

Taboas et al. [27], used an indirect SFF manufacturing technique to control the internal architecture of the scaffold. By utilizing 3D printing method, as well as some other SFF techniques, they fabricated molds with desired structures that were determined through computer aided design techniques and/or image based design methods. Afterwards, the scaffolds were casted in the molds. Porogen leaching was applied to produce pores in the range of 50-100 μm. The presented technique was compatible with a number of polymers or combinations of polymers and ceramics and/or cements [27].

Lee et al. [28], employed an indirect 3D printing method as well. A polymer solution composed of dissolved PLGA in a mixture of chloroform and methanol was mixed with sucrose. Then, the mixture was cast into the 3D printed molds. The resulted scaffolds were dried, and the solvents were evaporated by freeze-drying. After that, Molds and sucrose were removed simultaneously by immersing the scaffolds in deionized water overnight [28].

2.4 Summary

Several methods have been applied for manufacturing bone scaffold. SFF fills the gap of conventional methods by manufacturing complex structures and among all the SFF techniques, 3D printing has shown promising results for bone scaffold manufacturing. The combination of porogen leaching technique and 3D printing has been applied to generate macro-pores in the

bone scaffold; however, the proposed techniques facilitate a homogenous pore distribution in the scaffold structure. Because of the different mechanical and biological conditions in the different areas of the scaffold, a heterogeneous design is vital for the tissue engineered scaffolds. As a consequence, proposing a new technique which is capable to control the macro pore distribution of the scaffold is still a requirement in the tissue engineering field.

To facilitate this goal, the current work presents a porogen insertion mechanism which is capable to insert the porogen particles in pre-determined positions in a controllable fashion. This mechanism works with a 3D printing machine and inserts porogens in pre-set locations between the layers. In this way, the distribution of macro-pores in three dimensions can be designed and generated selectively.

Chapter 3
Numerical Analysis[1]

3.1 Motivation

Osteochondral defects, resulted from accident, disease or cancer, decrease the quality of life significantly. Nowadays, different methods are used for repairing such defects. One fairly new technique is generating biphasic structures composed of a grown cartilage tissue on a substrate, which serves as the bone interfacing component. On the one hand, the substrate should be porous for supporting cartilage formation and its fixation to bone after implanting by bone ingrowth inside the pores. On the other hand, the size and organization of the pores should allow fluid flow without cell infiltration into the full thickness of the substrate [1].

A dual-porous scaffold can be used for repairing osteochondral defects. The top portion of this kind of scaffold, which has smaller pore size, is used as the substrate for cartilage ingrowth. The resulted biphasic scaffold can be seeded with bone stem cells and placed inside the defected site of the body, causing the second portion of the structure to act as a bone scaffold. Figure 3-1 demonstrates a schematic of the dual-porous biphasic scaffold.

Such a scaffold structure makes it possible to implant both the *in vitro*-formed cartilage and the bone scaffold at the damaged site with a one-time surgery. Additionally, applying one structure for both bone scaffold and cartilage substrate may provide a better fixation between the grown cartilage and the bone tissues. Subsequently, the scaffold and the substrate can be manufactured simultaneously that reduces the production cost and time.

1 This chapter is also published in the proceeding of IMECE2008 by ASME.
Sharif, H., Shanjani, Y., Vlasea, M., Toyserkani, E., "On the Bio-Mechanical Properties of a Dual-Porous Osteochondral Scaffold"

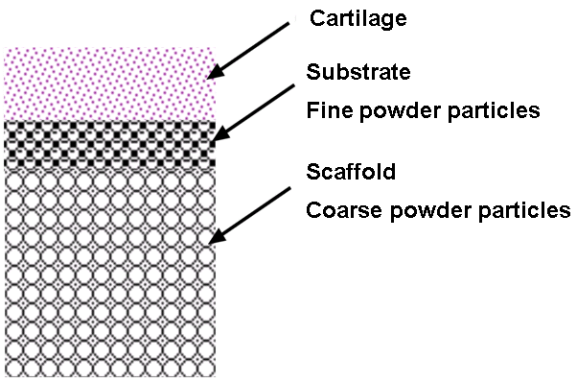

Figure 3-1: Schematic of a Dual-Porous Biphasic Scaffold

Calcium phosphates are widely used as a structural backbone in both cartilage substrates and bone scaffolds. Among all calcium phosphates, the specific properties of calcium polyphosphate (CPP) are superior for such applications, because CPP is a biocompatible and biodegradable ceramic and can form porous structures that approximate cancellous bone properties. Porous CPP cylinders with approximately 35 vol% porosity and interconnected pores in the 25–75 micron size range are used as cartilage substrate [1, 52, 53].

the potential of CPP as a material for biodegradable synthetic bone substitutes is confirmed through a number of investigations [54, 55, 56, 57, 58, 59]. Studies have been performed on the biocompatibility, rate of degradation, and the bone ingrowth *in vitro* [60] and *in vivo* [61]. Pilliar and his group demonstrated that CPP promotes rapid bone ingrowth and can be tailored in terms of *in vivo* degradation rate if the properly selected starting particle size would be.

CPP substrates have also been shown to provide a suitable support for chondrocytes to form cartilage tissue *in vitro* with mechanical stimulation [62, 63, 64]. The mechanical properties of the cartilage improved after implantation of *in vitro*-cultured biphasic CPP construct [56].

Since the biphasic scaffold will function as an implant at the damaged site, it calls for having specific mechanical properties. First of all, it should be strong enough for load bearing during the *in vitro* and *in vivo* growth and remodeling process. Also the structure should have similar apparent stiffness to the apparent stiffness of the surrounding bone [7].

the second portion of the dual-porous scaffold is used as a bone scaffold. Research has shown that the growth of bone cells is stimulated by existing mechanical strains in the scaffold. As a result, the dual-porous scaffold should have a special principal strain range for bone cells growth stimulation [65].

Finite element methods have been widely used for assessing these parameters in the scaffolds. Cleynenbreugel et al. [66] have worked on Micro-CT-based screening of bio-mechanical and structural properties of scaffolds using finite element analysis. They also investigated bio-mechanical design of porous structures for bone growth stimulation [67]. Telen et al. [68] produced a study on mechanical considerations for micro-porous titanium as an orthopedic implant material and compared the experimental, analytical and FEM results. Shanjani et al. [10] investigated the effect of porosity on the apparent stiffness and principal strain histogram, for seven biocompatible materials.

In the previous studies, single–porous scaffolds were taken into account, while in this work, a finite element model of a dual-porous scaffold is presented. Stiffness of the dual-porous scaffold is compared to that of a single-porous scaffold. To assess the scaffold capability of cell ingrowth, principal strain histograms are obtained as well.

3.2 Analysis Method Description

CPP is considered as the third generation of biodegradable materials that is used for producing bone scaffolds and cartilage substrate. CPP powder particles of 75 to 150μm in diameter are used for building bone scaffold samples by gravity sintering methods [60]. CPP samples are sintered at 965 or 970˚C for 2 h in an air muffle furnace (heat-up rate of 10˚C/min). Such process yields samples of approximately 30-40 vol% porosity and with interconnected pores in the 100 micron range. The macroscopic pore size range is selected according to [60] to make scaffold appropriate for bone ingrowth. To facilitate cartilage substrate production, finer particles in the range of 45-75μm are used which make smaller pore size and interconnectivity channels of about 20μm.

This chapter provides insight into the mechanical behaviour of the dual-porous scaffold by constructing an appropriate geometrical model and applying finite element techniques to this

approximation. For this purpose, CPP particles are geometrically simplified and modeled as spheres with the average diameter of powder particles. The distance between the spheres is designed to provide the desired porosity and neck size between the particles, which makes a good estimation of the real sintered part. For the sake of simplification, the finer particles part of the scaffold is named substrate and the coarser particles part is called scaffold in the rest of the current chapter.

Generally, bone scaffolds within a range of millimetres are used in clinical treatments and *in vivo* testing. For example, cylinders with the diameter and height of 4mm are used by Kandel and her workers [69]. The actual size of the dual-porous scaffold parts contains an extensive number of facets that would force the finite element analysis to be very memory-consuming and cumbersome. Limited computational capacity imposes dimensional constraints on the specific size of the dual-porous scaffold that can be modeled. As a result, a smaller geometrical model containing both layers is developed and analyzed.

It is significant to correlate the dependency of the results on the sample size analyzed in order to improve the numerical results and reduce the discrepancies between the modeling and experimental observations. For this purpose, the apparent stiffness and histograms of micro-strain for two single-porous scaffolds, with different pore shapes, were investigated. The same material and boundary conditions as the principal model and similar porosity to it were applied to these two structures. Figure 3-2 shows the generated geometries.

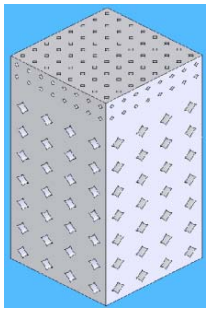

(a)

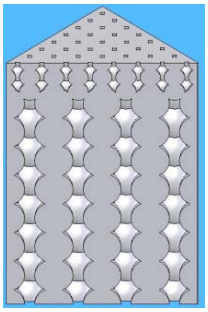

(b)

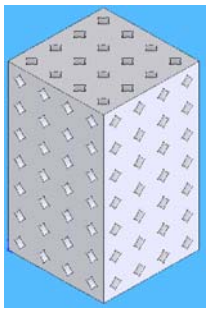

(c)

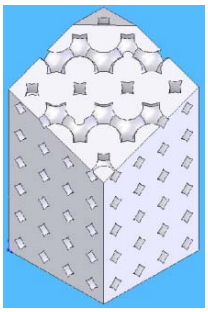

(d)

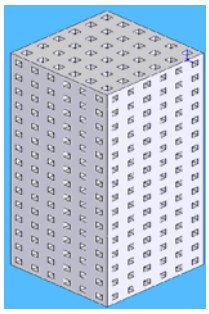

(e)

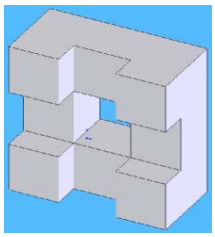

(f)

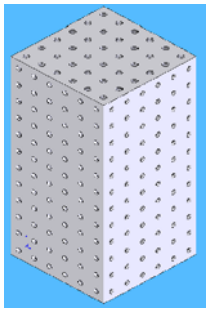

(g)

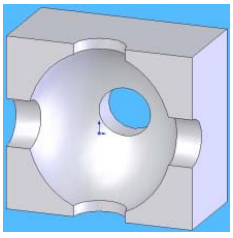

(h)

Figure 3-2: Generated Models a) Dual-Porous Scaffold Model, b) Dual-Porous Scaffold Model Section View, c) Single-Porous Scaffold Model, d) Single-Porous Scaffold Model Section View, e) Cubic-Pore Model, f) Unit-Cell Section View of the Cubic-Pore Model, g) Elliptical-Pore Model And h) Unit-Cell Section View of the Elliptical-Pore Model

Each scaffold is subject to the same boundary conditions to study the biomechanical properties. The bottom surface has a zero-displacement boundary, while the top surface must

meet a certain vertical displacement. The boundary conditions are shown in Figure 3-3 and described mathematically as Equation (3-1), respectively.

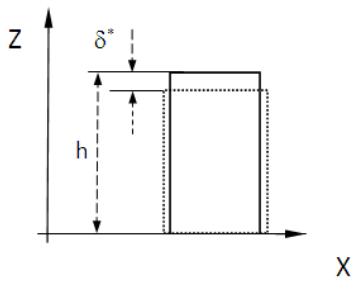

Figure 3-3: Proposed Boundary Conditions

$$\delta=\delta^{*} \ @\ z=h$$
$$\delta=0 \ @\ z=0 \qquad (3\text{-}1)$$

where h is the height of the scaffold, δ is vertical displacement, and δ^{*} is a certain vertical displacement.

3.3 Results

For modeling the dual-porous scaffold, spheres with the diameter of 110 μm and 60 μm are assumed for bone scaffold and cartilage substrate, respectively. The distances between the spheres are selected as 0.1 mm for bone scaffold and 0.05 mm for cartilage substrate, which make a realistic approximation of the actual sintered scaffold. These values provide 26% porosity for both portions of the dual-porous scaffold, and a neck size of 50 μm for the scaffold and 30 μm for the substrate. CPP's mechanical properties, as listed in Table 3-1, were assigned to the model.

Table 3-1: Mechanical Properties of CPP

Material	Stiffness (GPa)	Poison's Ratio
CPP	48	0.3

A compression with a typical apparent strain of 1% in the vertical direction [70] was imposed on the model to assess the apparent stiffness. For evaluating the probability of bone formation stimulation, according to [71], a compressive "apparent" strain of -4000 micro-strains in the vertical direction is imposed on the structure. This analysis is performed on the bone scaffold model as a single-porous scaffold, as well.

In order to examine the independency of results from the size of geometrical model, two extra models were used. For each of these two models five single-porous scaffolds with the 100, 80, 60, 40, and 20% size ratio of the actual part were taken into account. Table 3-2 shows the properties of models used. Material properties and boundary conditions were kept unchanged for this study.

Table 3-2: Properties of Proposed Models

	Unit Cell Shape	Pore Shape	Pore Size (mm^3)	Height (mm)	Cross Section (mm)	Porosity (%)
Dual-Porous Scaffold Model[1]	sphere	Formed by merged spheres	N/A^2	0.84	0.4×0.4	26
Single-Porous Scaffold Model[1]	sphere	Formed by merged spheres	N/A^2	0.7	0.4×0.4	30
Model1[3]	cube	cube	$\{6.54\times10^{-5}\}$[4]	4	2×2	30
Model2[3]	cube	ellipse	$\{6.54\times10^{-5}\}$[4]	4	2×2	33

Two bio-mechanical properties of the proposed scaffolds including apparent stiffness and stimulation of the bone formation are evaluated. The results are presented in the next tow sections.

3.3.1 Apparent Stiffness

the proposed scaffold architecture and material properties must promote cell growth but at the same time it has to provide the structural support necessary for initial load bearing. An analysis of apparent stiffness is necessary to characterize the performance of this bone replacement. Homogenization theory [72] has been applied to obtain the apparent stiffness of the scaffold implant. The Equation (3-2) defines the apparent modulus.

1 20% size ratio of the real sample
2 So big to provide 26% porosity for the structure
3 100% size ratio of the real sample
4 Equal to the volume of a 300-µm sphere

$$E_{app} = \frac{\sum R_f}{A\varepsilon} \qquad (3\text{-}2)$$

where E_{app} is the apparent modulus, $\sum R_f$ is the total reaction force, A is the area of the face upon which the displacement boundary conditions are applied, and ε is the applied strain. The apparent Stiffness for all the proposed models is presented in Table 3-3. Figure 3-4 shows how the apparent stiffness changes versus size in cubic-pore and elliptical-pore models.

Table 3-3: Apparent Stiffness of Models

Model	Dual-Porous Scaffold[1]	Single-Porous Scaffold[1]	Cubic-Pore Model[2]	Elliptical-Pore Model[2]
Apparent Stiffness (Gpa)	21	19.9	25.6	25.3

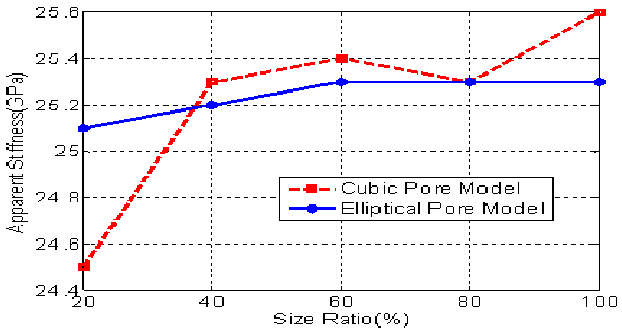

Figure 3-4: Apparent Stiffness versus Size

3.3.2 Stimulation of the Bone Formation

Strain in the underlying substrate has been shown to promote bone cell proliferation and differentiation [65]. This finding illustrates the importance of designing a scaffold that would

1 20% size ratio of the real sample
2 100% size ratio of the real sample

enforce the appropriate mechanical strains on the cells under *in vivo* loading. This feature is evaluated by calculating the histogram of the major principal strains over all the elements in the model under the applied loading. The histogram is compared to the strain regions defined in the Mechanostat theory formulated by Frost [73]. According to this theory, the optimal strain region to stimulate new bone formation is situated between 1500 and 4000 micro-strain. The histograms of the major principal strains in the dual-porous scaffold and other models are presented in Figure 3-5 and Figure 3-6, respectively.

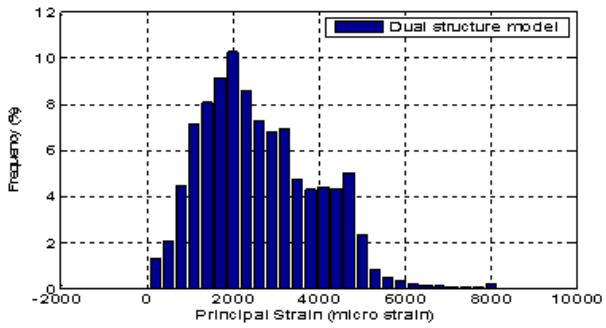

Figure 3-5: Histogram of Principle Strain in Dual-Porous Scaffold at 20% Size Ratio

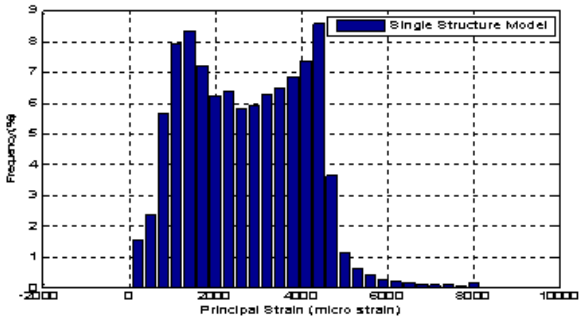

(a)

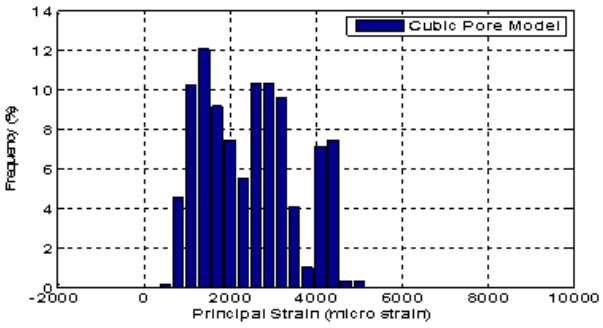

(b)

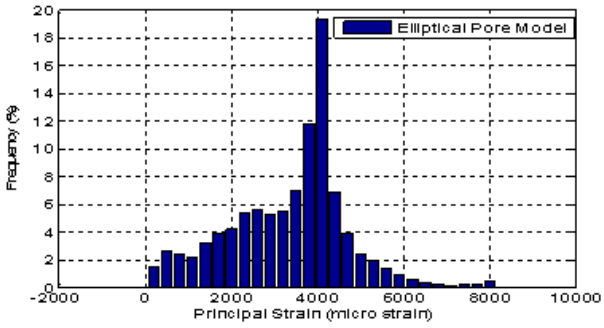

(c)

Figure 3-6: Histogram of Principle Strain a) Single-Porous Scaffold at 20% Size Ratio, b) Cubic-Pore Model at 100% Size Ratio c) Elliptical-Pore Model at 100% Size Ratio

Figure 7 shows the corresponding principal strain histograms of different size ratios for the elliptical model.

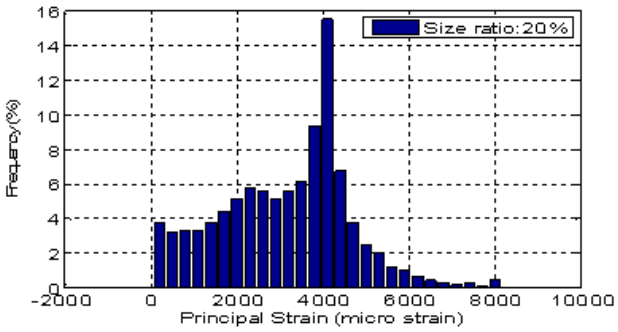

(a)

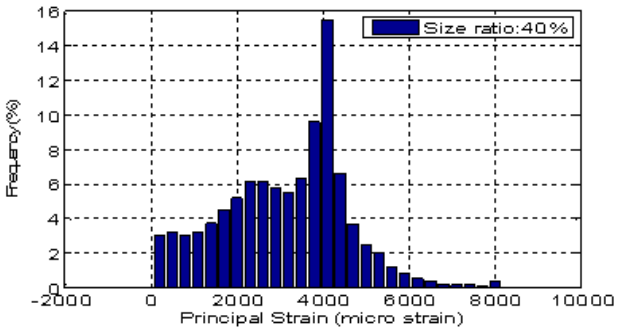

(b)

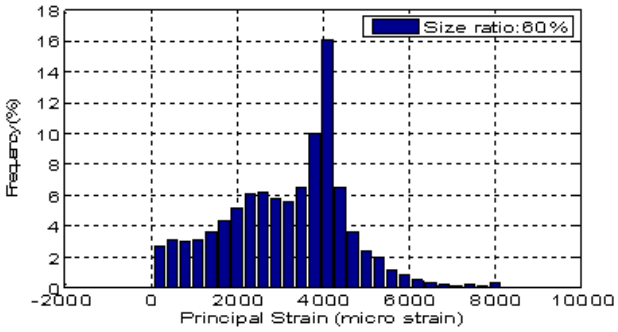

(c)

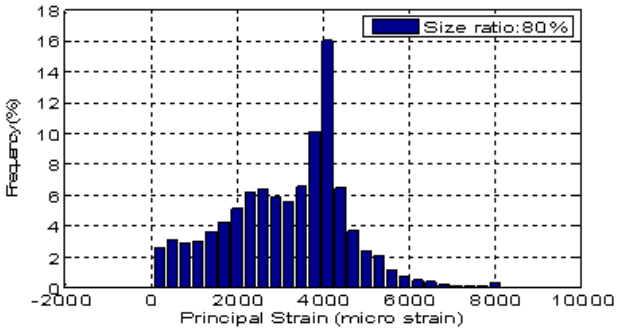

(d)

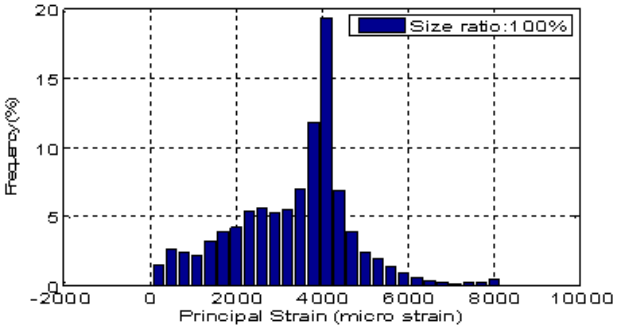

(e)

Figure 3-7: Histogram of Principle Strain for the Elliptical-Pore Model a) 20% Size Ratio, b) 40% Size Ratio, c) 60% Size Ratio, d) 80% Size Ratio e) 100% Size Ratio

3.4 Model Validation – Analytical Method

When *n* springs with different stiffness are connected in series, the stiffness of the equivalent system is calculated as Equation (3-3).

$$\frac{1}{K_{eq}} = \sum_{i=1}^{n} \frac{1}{K_i} \qquad (3\text{-}3)$$

where K_i is the stiffness of the spring i. As a result, the equivalent stiffness of the system is lower than all K_i values.

This concept can be applied for bulk materials as well. Stiffness of a bulk of a solid material under compression or tension loading is defined as Equation (3-4) [74].

$$K = \frac{AE}{L} \tag{3-4}$$

where A is the cross-sectional area, E is the Young's modulus and L is the length of the element.

When *n* layers of material with different stiffness are stacked in a series fashion, under axial loading they can be modeled by a system composed of n series springs. Equivalent stiffness of the system is smaller than all assigned stiffness to parts, as well.

Consequently, the dual-porous scaffold, which consists of substrate and scaffold with different stiffness due to their different structures, should have a lower stiffness than both substrate and scaffold. In other words, adding substrate to the scaffold for making a dual-porous scaffold, results in a lower stiffness for the whole structure. This fact is investigated in section 3.5.

3.5 Discussion

To assess how the designed structures mechanically support the *in vivo* loading, their apparent stiffness is calculated.

According to Table 3-3, the apparent stiffness of the cubic and the elliptical models (at 100% size ratio) are approximately equal. The small discrepancy between the two values is due to the fact that the analyzed samples had different pore shapes.

According to Figure 3-4 the apparent stiffness of the elliptical-pore model remains constant for all size ratios with an acceptable estimation. The apparent stiffness of the cubic-pore model

has about 1 GPa variation between 20% and 40% size ratios; however, it doesn't have a significant change for models bigger than 40% size ratio. In addition, such variations can be assigned to sharp edges and corners in cubic-pore model. These results lead to the conclusion that the apparent stiffness for each model is roughly independent of the size ratio. This finding is important when considering the dual-porous scaffold. Although the modeled dual-porous scaffold in this investigation is about 20% of the actual part size, according to Figure 3-4, it can be concluded that the actual part has an apparent stiffness of about 21 GPa similar to the value listed in Table 3-3.

Based on Table 3-3 and Equation (3-4) stiffness of the single-porous scaffold and the dual-porous scaffold can be found $4.5\times10^{6}\frac{N}{m}$ and $4\times10^{6}\frac{N}{m}$, respectively. As a result, although the apparent stiffness of the single-porous scaffold is smaller than the corresponding value of the dual-porous scaffold, its equivalent stiffness is greater. It means that, adding the substrate to scaffold reduces the stiffness of the composed structure, which verifies the correctness of the modeling.

Figure 3-6 shows the principal stain histogram for all three single-porous scaffold models. All three of these histograms have the desired range of principal strain, since in all of them the majority of elements have principal micro-strain in the range of 1500-4000. However they have different trends, which can be attributed to the fact that the actual sample has been modeled in three different ways.

the principal strain histogram for the dual-porous scaffold at 20% size ratio is presented in Figure 3-5. This figure shows that the principal strain is within the desired range and it follows a Gaussian-like distribution.

To assess the effect of the added substrate on the principal strain histogram, the histograms for the dual-porous scaffold (Figure 3-5) and the single-porous scaffold (Figure 3-6) were compared. Both graphs have a similar distribution in the desired principal strain range; however the corresponding histogram for the single-porous scaffold has a top-hat distribution, while the dual-porous scaffold has a Gaussian-like distribution. In the dual-porous scaffold case, the concentration of micro-strain distribution is pushed to the left side of the desired range that may

cause different activation of cell ingrowth. As well, the out-of-range peak present in the single-porous scaffold case has been significantly reduced in the dual case.

Figure 3-7 shows the histogram of principal strains in the elliptical-pore model for various size ratios. The principal strain histogram distribution is approximately constant regardless of the size ratio. As well, all histograms demonstrated in Figure 3-7 have the bulk of the data between 1500-4000 micro-strains, which is the appropriate range for cell ingrowth stimulation. The peak in all these histograms is at 4000 micro-strain. These results show that the principal strain histogram distribution is highly independent of the size ratio of the model considered.

This finding can be applied to the dual-porous scaffold as well, by inferring that the results from the principal strain histogram at 20% size ratio is applicable to the actual size of the part.

3.6 Conclusion

A prediction of bio-mechanical properties of a dual-porous scaffold composed of a cartilage substrate and a bone scaffold was conducted using the finite element technique. To judge the effect of two distinct porous architectures on strength and capability of cell ingrowth stimulation of the resultant structure, stiffness and principal strain histogram of the single and the dual-porous scaffolds were compared. Subsequently, to conquer the software limitations in modeling the actual size of the dual-porous scaffold, the results' (apparent stiffness and principal strain histogram) independency of size of the model was investigated as well. It can be concluded that the investigated mechanical properties of the dual-porous scaffold at 20% size ratio can be used to infer the mechanical properties of the actual size of the part.

Chapter 4
Development of Porogen Insertion Mechanism

4.1 Motivation

A combination of 3D printing and particulate leaching has been used extensively for generating macro-pores in bone scaffolds [28, 29, 31]; however, the manufacturing processes have resulted in homogenous pore distribution for the fabricated scaffolds. As discussed in Chapter 2, heterogeneous pore distribution is a crucial requirement for the bone scaffold. In this work, a novel method has been presented that facilitates the manufacturing of bone scaffold with the desired macro-porosity. the idea is based on the layer-wise nature of the 3D printing technique. Manufacturing of the scaffold layer by layer provides the opportunity to place the porogen particles on the desired layers to provide pre-designed pore distribution for each layer and, consequently, for the whole scaffold. In other words, instead of mixing the porogen particles with the scaffold material randomly (the method which is usually used and, in the best case scenario, provides a homogenous porosity), in the new proposed system, the particles are inserted at desired locations with pre-designed (X,Y,Z) coordinates throughout the fabrication process. A schematic of the powder layers and porogen particles, before and after pushing the porogens into the powder layers by applying a pushing mechanism, is demonstrated in Figure 4-1.

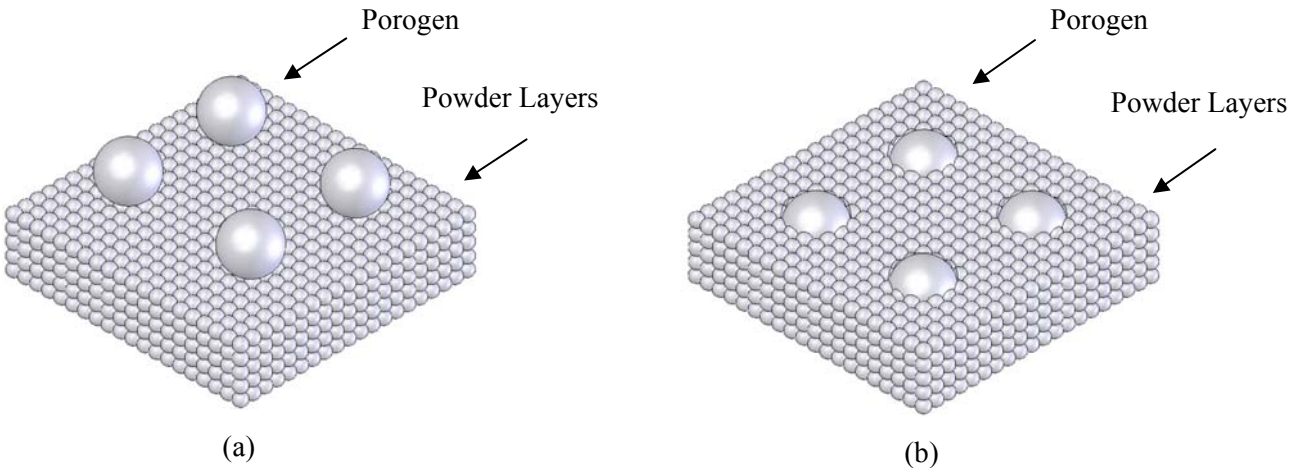

Figure 4-1: Schematic of the Porogens and the Compacted Powder Layers a) Before the Pushing Mechanism Acts b) After the Pushing Mechanism Acts

the updated flowchart of the manufacturing process has been presented in Figure 4-2. The proposed Porogen Insertion Mechanism consists of five main parts: a positioning system, which provides movement for the whole mechanism in X, Y, and Z directions; porogen reservoir; feeding mechanism; insertion head; and pushing mechanism. First, the positioning device brings the insertion head to the desired location. The feeding mechanism carries porogens from the porogen reservoir to the insertion head. The insertion head places the porogens at pre-designed (X-Y) locations on the compacted powder layers. The positioning device brings the pushing head to the desired location, and the pushing head pushes the porogens into the powder layer to provide a flat surface.

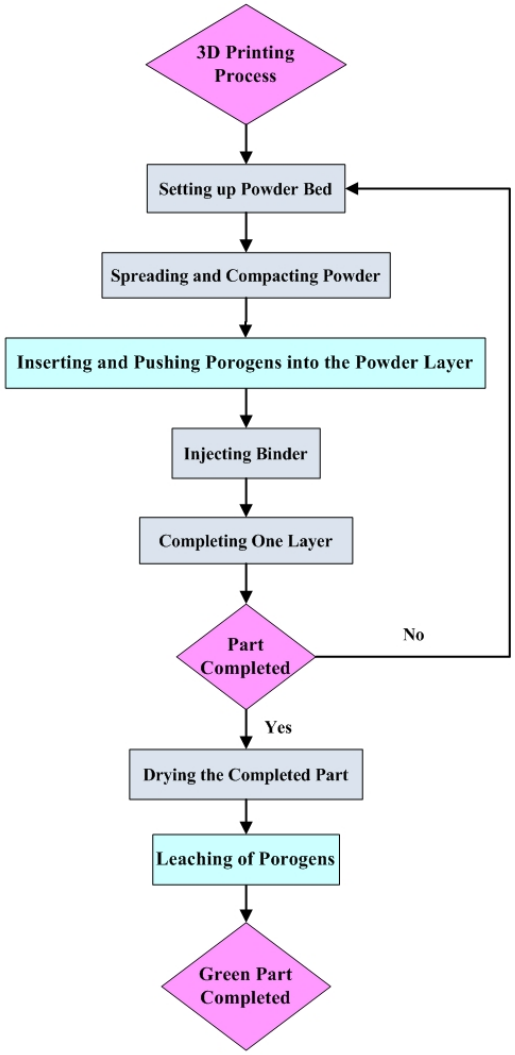

Figure 4-2: Flowchart of 3D Printing Process with Porogen Insertion Mechanism

This work is mainly concerned with the design of the insertion head; however, for each proposal, the general design of the required feeding mechanism and porogen reservoir are also taken into account.

the porogen insertion mechanism is joined to a 3D printing machine that is currently being designed and manufactured by the Rapid Prototyping Laboratory at the University of Waterloo. This 3D printing machine has been equipped with an X-Y positioning stage to carry different parts of the system to the workspace. The whole porogen insertion mechanism is installed on the

X-Y positioning system. Figure 4-3 demonstrates a schematic of the porogen insertion mechanism position in the 3D-printing system.

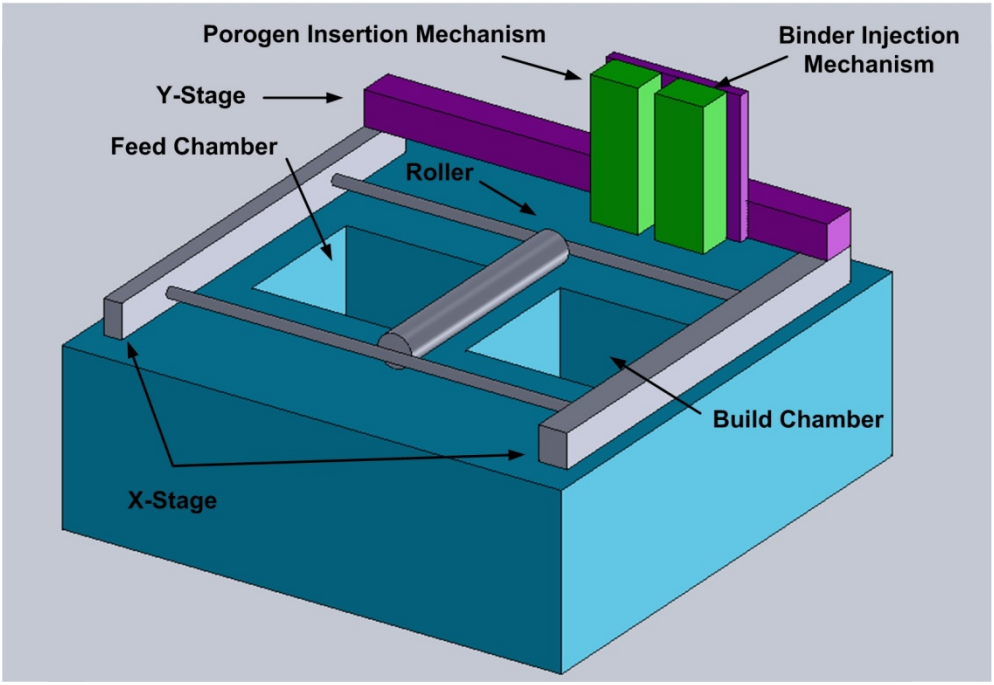

Figure 4-3: Schematic of Porogen Insertion Mechanism Position in 3D-Printing System

4.2 Proposed Solutions: Actuator-Based Mechanisms

Several designs have been presented for the insertion head, and for each option some common steps are followed. First, the micro-positioning stage should bring the insertion head to the desired location. Then, an actuator, which is located at the lowest level of the insertion head, acts and places porogens at the appropriate positions. This work continues until the porogens are placed on the entire workspace.

4.2.1 Single Insertion Head

In the first group of designs, the system is composed of a single insertion head.

4.2.1.1 Syringe -Type Reservoir

Porogens can be fed to the head directly from the reservoir by using a syringe type mechanism that applies pressure on top of the porogens. The schematic of the system is presented in Figure 4-4. In the syringe-type design, many porogens are brought to the head, as a result, more than one particle is inserted. To limit the number of inserted particles to one each time the actuator acts, a smaller nozzle should be fabricated at the end of the insertion head. Figure 4-5 shows a schematic of the system with an integrated nozzle. The drawback of this improved system is that the extra porogen particles that cannot travel through the integrated nozzle are stuck on the bottom of the insertion head. The second way to control the number of inserted porogens is to manufacture the head with a diameter slightly bigger than the porogen size, i.e., around 250 μm. To examine the feasibility of the presented syringe-type system, a test was conducted with 98% hydrolyzed PVA particles, which were sieved with the number 60 sieve (250 μm). The particles were poured into a syringe and pressure was applied by the syringe piston to push the porogens out. The test was repeated using different amounts of powder, and one consistent result was obtained. In all of the experiments, the particles stuck in the syringe and did not come out when pressure was applied.

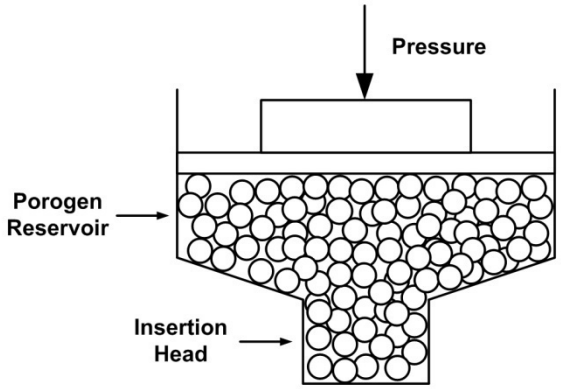

Figure 4-4: Schematic of the Syringe -Type Reservoir for the Single Insertion Head

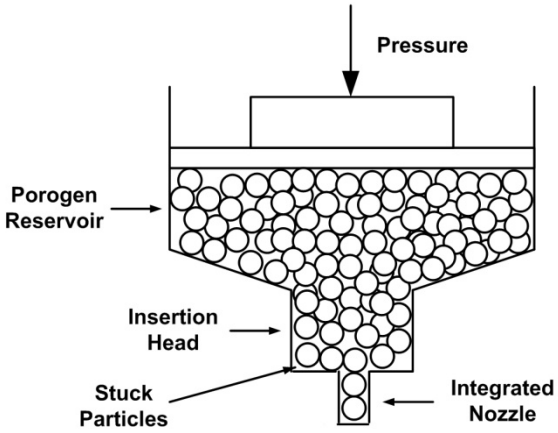

Figure 4-5: Schematic of the Syringe -Type Reservoir with an Integrated Nozzle

4.2.1.2 Funnel-Type Reservoir

Since using the syringe-type system is not practical based on the mentioned experiment, a funnel-type design is presented. This modified version of the reservoir for the single head design group is shown in Figure 4-6. To investigate the feasibility of funnel-type reservoir, 98% hydrolyzed PVA powders were sieved with the number 60 sieve (250 μm) and fed into a paper funnel. The narrow opening of the funnel measured 2 mm in diameter. The experiment revealed that the powder particles come out of the funnel easily without applying any pushing force. Therefore, the funnel-type reservoir was selected for the next steps of design.

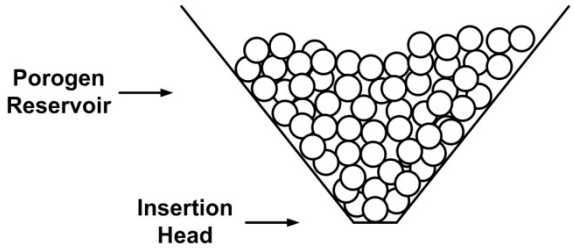

Figure 4-6: Schematic of the Funnel-Type Reservoir for the Single Insertion Head

4.2.1.3 Single-Hole Disk Insertion Head

the insertion head should be able to place a specific number of porogens on the desired locations of the workspace in a controlled fashion. A way that this goal can be facilitated is to design the insertion head so that the porogens' flow path is kept closed except at the moment of insertion. A possible design to achieve this aim is a single-hole disk as presented in Figure 4-7. The diameter of the hole is equal to the diameter of the narrow mouth of the funnel, i.e., slightly larger than the diameter of a porogen. The disk is mounted below the funnel and off center with respect to the funnel. The distance between the funnel center and the disk center is designed in a way that the hole is located just under the funnel mouth, so, when the disk rotates, the funnel is closed except when the distance between the centers of the funnel and the hole is equal to zero. Therefore, by controlling the rotational speed of the disk, the system can insert the porogens at pre-determined locations.

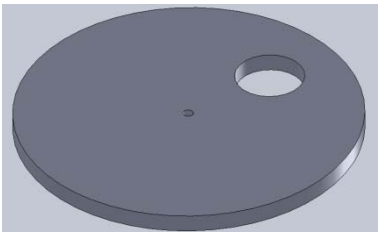

Figure 4-7: Insertion Head - Single-Hole Disk

4.2.1.4 Multiple-Hole Disk Insertion Head

the single-hole disk design, which has only one hole, limits the system to only one porogen size. To make system capable to insert more than one size of porogen, a multiple-hole disk design is presented in Figure 4-8. The funnel diameter is equal to the biggest hole's diameter. The disk is set for the desired porogen size by placing the desired hole under the funnel. In this case, instead of a complete rotational movement, the disk passes an arc by clockwise-counter clockwise rotations and in this manner opens and closes the funnel mouth to insert porogens. The significant point is when the holes with smaller diameters than the funnel diameter are used, the

opening motion should continue to open the porogen path for inserting the first particle and then the closing motion should start. In other words, it is not needed to continue the opening motion to make the distance between the funnel center and the hole center equal to zero.

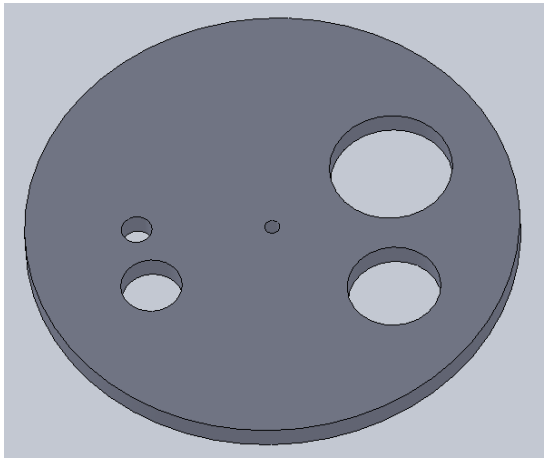

Figure 4-8: Insertion Head - Multiple-Hole Disk

4.2.1.5 Four-Plate Design Insertion Head

Although the multiple-hole disk design is compatible with more than one porogen's size, it is still limited to the pre-designed porogen sizes. To facilitate insertion of porogens with any required size, a new design is demonstrated in Figure 4-9. In the presented system, the proposed plates have linear movement along X and Y axes. The radius of the funnel is selected equal to the maximum possible radius of the required porogens. By using the proposed four-plate design, a semi-circular hole is obtained for porogen seeding. The radius of the hole is controlled by the distance between the plates. For any desired porogen size, three plates can be set and fixed in the required distances and the hole is opened and closed by the linear movement of the fourth plate. By designing the feeding mechanism in a way that makes it capable of bringing porogens from different reservoirs, which carry porogens with different sizes, the presented insertion head system provides the possibility of inserting more than one size of porogen on a single workspace.

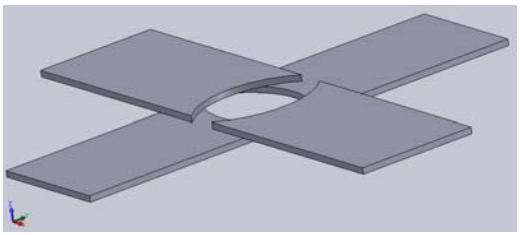

Figure 4-9: Insertion Head - Four-Plate Design

4.2.2 Matrix of Insertion Heads

Although the porogen particles move to the head easily in the funnel-type reservoir design and the proposed insertion systems are capable of inserting porogens of different sizes, a single head needs more time to cover the entire workspace. In fact, if the single insertion head be replaced by a matrix of heads the required time for inserting the porogens on the desired layers and consequently the manufacturing process time would decrease significantly. Figure 4-10 shows a possible design of an insertion system that consists of a matrix of insertion nozzles. The proposed system includes two plates that are mounted on the top of each other with no distance between them. The lower plate is fixed and the upper plate moves linearly to open and close the insertion head. A matrix of holes is made in each plate, so when the holes meet each other the porogen flow path opens. The holes of the upper plate have a conical shape with a smaller diameter than the lower plate's holes diameter to reduce the possibility of trapping the porogens between two plates.

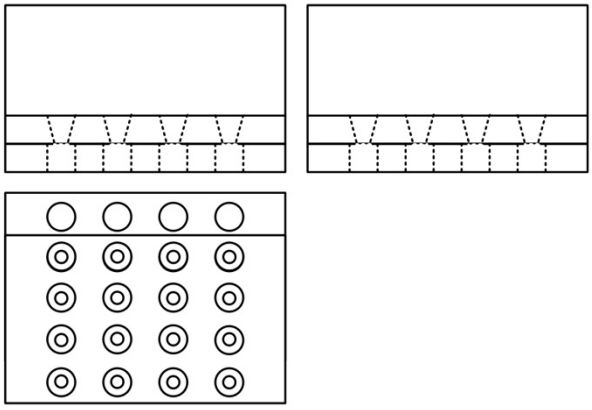

Figure 4-10: Insertion Head - Matrix of Insertion Nozzles

4.2.3 Optimizing Stage Velocity, Actuator Frequency and the Number of Insertion Nozzles

Porosity is defined as the ratio of the pores' volume to the whole structure's volume, and is usually presented in percentage. In this work, a simplified model consists of several cubic unit cells with a spherical pore at the center of each unit cell is assumed for calculation of the porosity. This model is presented in Figure 4-11. According to the proposed simplified model, porosity of one unit cell, which is equal to the porosity of the whole structure, is defined according to Equation (4-1).

$$\alpha = \frac{V_s}{V_c} = \frac{4\pi d^3 / 3 \times 8}{D^3} \qquad (4\text{-}1)$$

where α is porosity, V_s is the pores' volume, V_c is the whole structure's volume, d is pore diameter, and D is the unit cell's length.

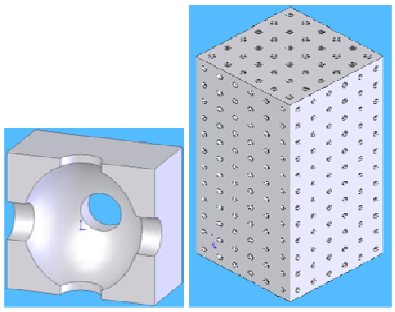

Figure 4-11: Simplified Model of the Porous Scaffold (Whole Scaffold and a Section View of the Unit Cell)

the involved parameters in the porogen insertion process, as well as their ranges, are listed in Table 4-1.

Since the bone scaffold should mimic the geometrical features of the real bone, the porosity in human bones is considered for calculating the desired range of porosity for the bone scaffold. Human body consists of two different types of bone including cortical bone, with the porosity of 5% to 30%, and cancellous bone, with the porosity of 50% to 95% [33]. As discussed in Chapter 2, the scaffolds that are fabricated from the powder form of the material may have micro-porosity, because voids between the powder particles are not filled completely during the sintering process. The resulted porosity depends on the powder size, the material characteristics, and the sintering conditions. For instance, Calcium Polyphosphate powder particles of 75 to 150μm in diameter that are sintered at 965 or 970˚C for 2 h in an air muffle furnace with the heat-up rate of 10˚C/min yields samples of approximately 30-40% porosity [60]. As a result, the main goal of the porogen insertion mechanism is to control macro-pores distribution within the bone scaffold structure. Specially, manufacturing bone scaffolds with the range of pore sizes between 100-300 μm that is the best pore sizes range for successful bone regeneration is a significant target. Recall from Chapter 2, pores larger than 50μm are referred as macro-pores. The pore sizes in cortical bone are smaller than 50μm [75], therefore, Porogens are mainly used for creating scaffolds similar to cancellous bone. Although a few portion of porosity in cancellous bone is due to porosity in individual trabeculae, the most portion of porosity is because of the voids in intertrabecular spaces [33]. As a result, the porosity in trabeculae is

ignored, and the target porosity of the porogen insertion mechanism is selected between 50%-95%.

Table 4-1: Involved Parameters in Porogen Insertion Process

Nomenclature	Description	Range of Changes
d	Porogen Diameter	50-600 micron [76] [77]
α	Porosity	50%-95%
L	Length of Workspace	Depends on the Application
V	Linear Velocity of the Micro-Positioning Stage	1-50 mm/s [78]
f	Frequency of the Porogen Insertion Actuator	1-125 Hz[77]

4.2.3.1 Optimizing V and f

For a unit workspace with the length of $L = 1cm$, the total required time versus the porogen diameter at different porosities and the total required time versus the porosity at different porogen diameters for the fastest and the slowest conditions are demonstrated in Figure 4-12 and Figure 4-13, respectively. The fastest condition is associated with $V = 50\,\frac{mm}{s}$ and $f = 125Hz$ and the slowest condition is associated with $V = 1\frac{mm}{s}$ and $f = 1Hz$. These figures provide an accurate estimation of the total required time in each condition.

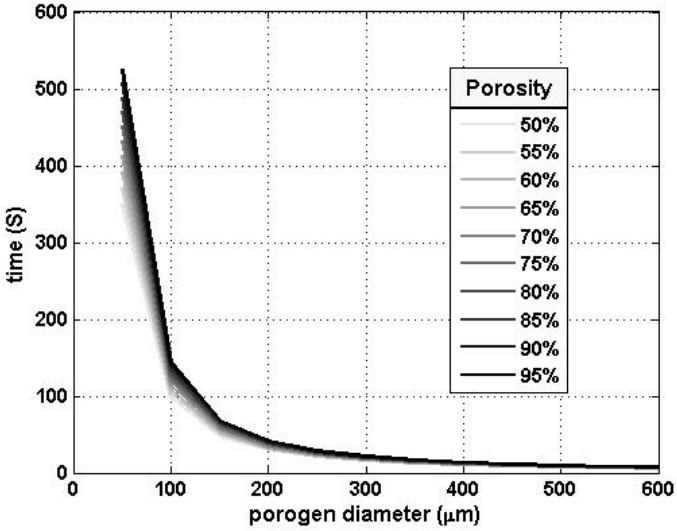

(a)

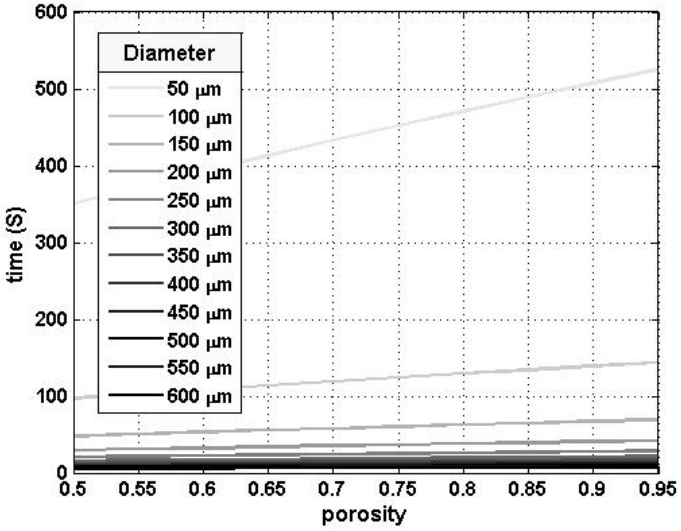

(b)

Figure 4-12: Total Time for the Fastest Condition a) Versus Porogen Diameter b) Versus Porosity

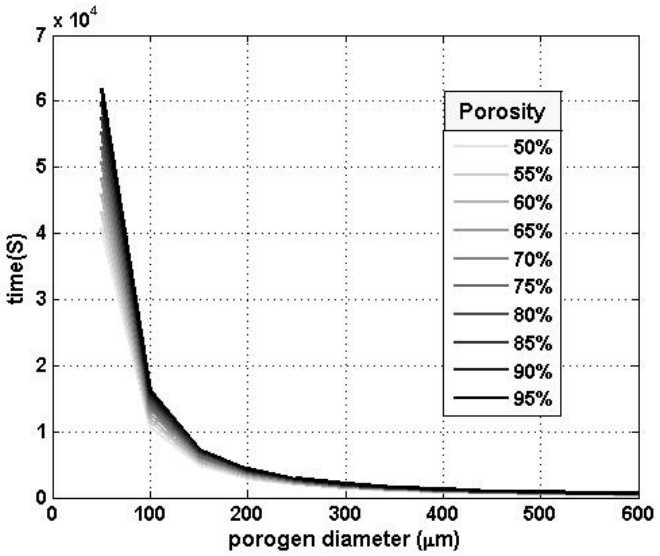

(a)

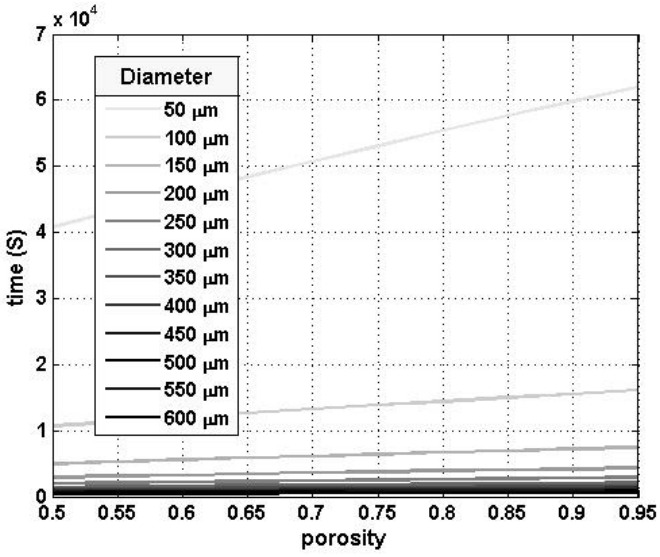

(b)

Figure 4-13: Total Time for the Slowest Condition a) Versus Porogen Diameter b) Versus Porosity

the total number of porogens at each row of cells is calculated by (4-2)

$$n = \frac{L}{D} \tag{4-2}$$

where n is the total number of porogens at each row with the length of L, and D is the unit cell's length. By applying Equation (4-1) and the presented values for the range of d and α in Table 4-1, minimum and maximum values of D are determined as $41\,\mu m$ and $609\,\mu m$, respectively. For the assumed value of $L = 1cm$, which is the unit length of the workspace, the range of n can be calculated according to Equation (4-2). Therefore, the minimum value of n is 16 and its maximum value is 243. the total required time for inserting porogens on the entire workspace at different velocities of the stage is presented in Figure 4-14. According to this figure, in all frequencies of the inserter actuator, there is no significant change in the required time for the velocities equal or greater than $15\frac{mm}{s}$. As a result, $V = 15\frac{mm}{s}$ would be an appropriate velocity for the stage.

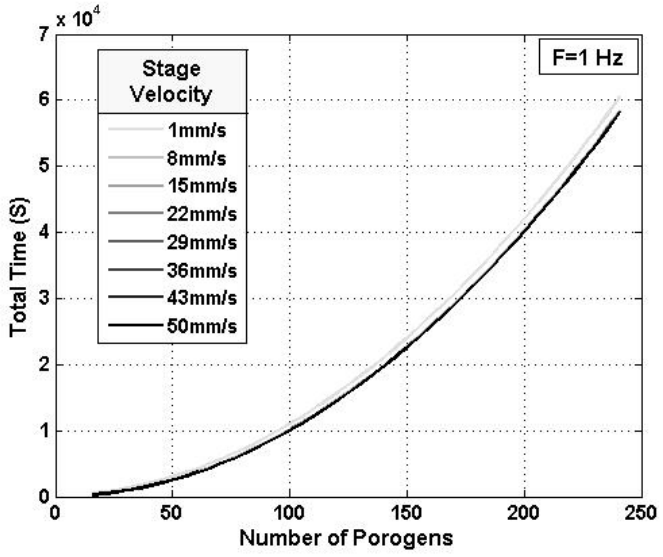

(a)

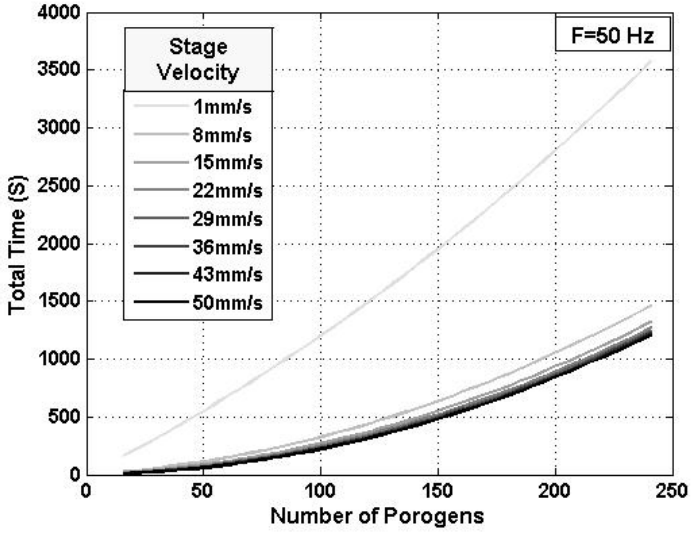
F=50 Hz
Stage Velocity
1mm/s
8mm/s
15mm/s
22mm/s
29mm/s
36mm/s
43mm/s
50mm/s
Total Time (S)
Number of Porogens
0
500
1000
1500
2000
2500
3000
3500
4000
0
50
100
150
200
250

(b)

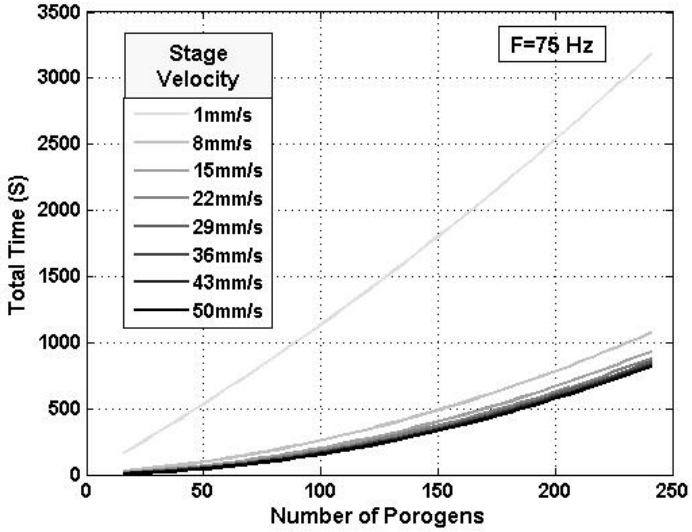
F=75 Hz
Stage Velocity
1mm/s
8mm/s
15mm/s
22mm/s
29mm/s
36mm/s
43mm/s
50mm/s
Total Time (S)
Number of Porogens
0
500
1000
1500
2000
2500
3000
3500
0
50
100
150
200
250

(c)

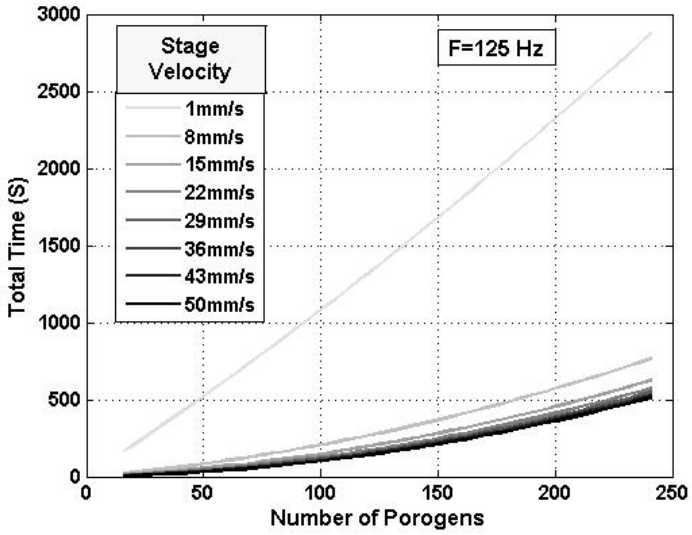

(d)

Figure 4-14: Time Versus Number of Porogens at Different Stage's Velocities a) $f = 1Hz$ b) $f = 50Hz$ c) $f = 75Hz$ d) $f = 125Hz$

the total required time for inserting porogen on the entire workspace at different frequencies of the inserter actuator is shown in Figure 4-15. $V = 15\frac{mm}{s}$ has been selected for the stage velocity. According to this figure, for different amount of porogens time does not have any considerable changes at the frequencies equal or greater than $71Hz$. Therefore, $f = 71Hz$ can be used for the rest of the analysis. Figure 4-16 demonstrates the total required time versus the porogen diameter at different porosities and the total required time versus the porosity at different porogen diameters for the optimized, i.e., $V = 15\frac{mm}{s}$ and $f = 71Hz$, condition in a workspace with the length of $1cm$. Comparing Figure 4-16 with Figure 4-12 confirms that, except for the porogens in the lower part of the size range, the optimized condition is not significantly slower than the fastest condition and the optimized values for the stage velocity and the actuator frequency are acceptable with a good estimation.

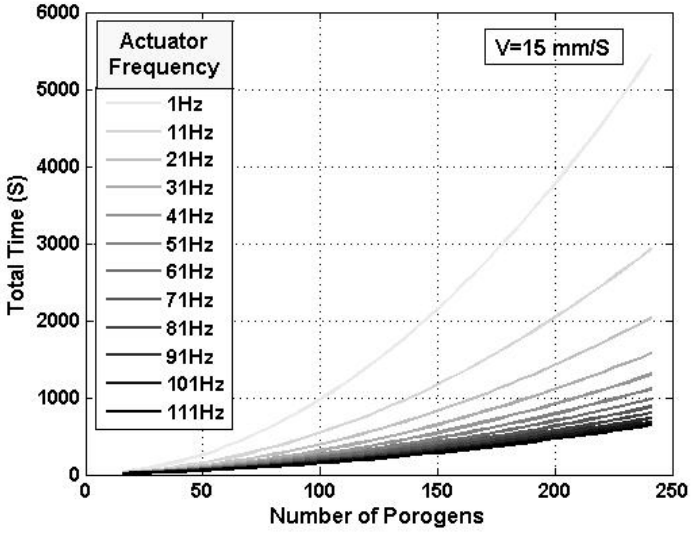

Figure 4-15: Time versus Number of Porogens at Different Actuator's Frequencies

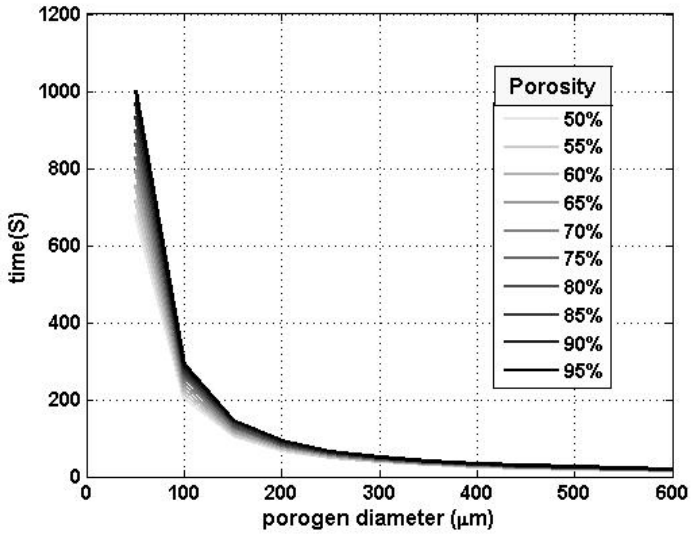

(a)

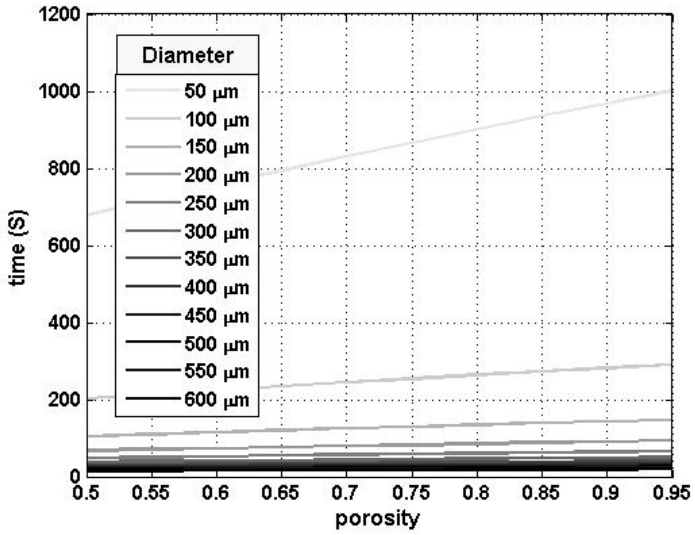

(b)

Figure 4-16: Total Time for the Optimized Condition a) Versus Porogen Diameter b) Versus Porosity

4.2.3.2 Optimizing the Number of Integrated Insertion Heads

To decrease the total process time, a matrix of the insertion heads can be used. Obviously, increasing the number of the insertion heads decreases the total required time; however, the distance between the insertion heads also is a significant parameter in designing the system. The distance between each pair of the insertion heads is determined based on some parameters. First of all, the fabrication process may impose some limitations. In addition, the porogen insertion mechanism should be capable of manufacturing bone scaffolds with any desired porosity in the range of the bone porosities that is presented in Table 4-1. Furthermore, this mechanism should be able to insert the porogen particles with every required size to fabricate scaffolds with any porosity needed. Therefore, the distance between the insertion heads should be set such that the system provides the possibility of manufacturing a bone scaffold with the minimum possible porosity by using the largest diametarl size for available porogen.

the center-to-center distance between each pair of neighbour porogens (λ) is equal to the distance between the two heads they insert the porogens. It has been assumed that each porogen

is exactly located at the center of the cubic unit cell; therefore, as demonstrated in Figure 4-17, $\lambda = D$. The optimum value of λ is calculated by replacing $\alpha = 50\%$, the lowest porosity, and $d = 600\mu m$, the largest porogen diameter, in Equation (4-1). As a result, $\lambda_{optimum} = 609.29\mu m$ and the number of insertion heads for covering a complete row with the length of $L = 1cm$ is equal to 16.

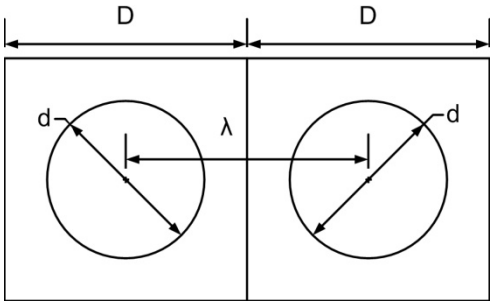

Figure 4-17: Distance between Porogens and the Length of the Unit Cell

To confirm the obtained value for λ, the size of the matrix (the number of the insertion heads in X and Y directions) is considered as $\xi \times \eta$. Therefore, the required time for inserting the porogens on one row along x-axis is calculated through the following steps:

the distance that the micro-positioning device should pass in the horizontal direction is $L'' = L - L'$, where L' is the length of the array in X direction and is equal to $\xi \times D$

then the required time for micro-stage to pass one side of the workspace is calculated as $t_s = L''/V$.

the required time for insertion heads' actuators to insert porogen on one row is equal to $t_i = (\frac{1}{f})n/\xi$.

the total time for inserting porogens on one row is calculated as $t_x = t_i + t_s$.

t_x versus the unit cell's length for the different values for ξ is demonstrated in Figure 4-18. In this figure, $t_x < 0$ represents the conditions in which the porogens have overlap. Overlap of the porogens is not an acceptable condition because it means that the porogens are not used perfectly. So, the ξ at which t_x remains positive for all the unit cell's lengths can be considered as an optimum ξ. therefore, $\xi = 16$ can be chosen as an optimum value. Similarly, $\eta = 16$ can be selected as the optimized number of the insertion heads along the Y-axis.

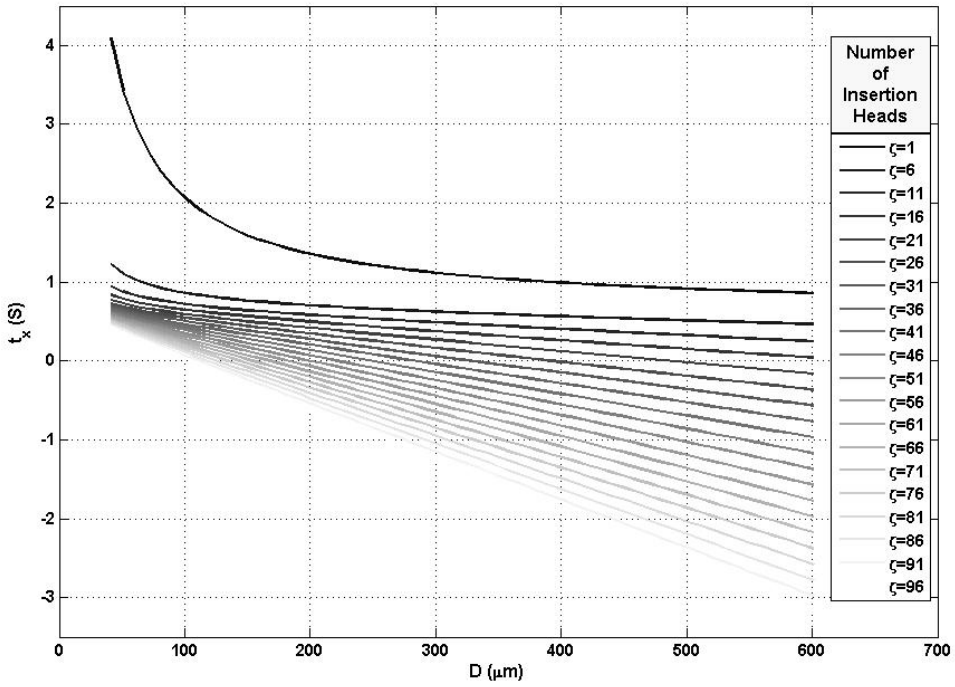

(a)

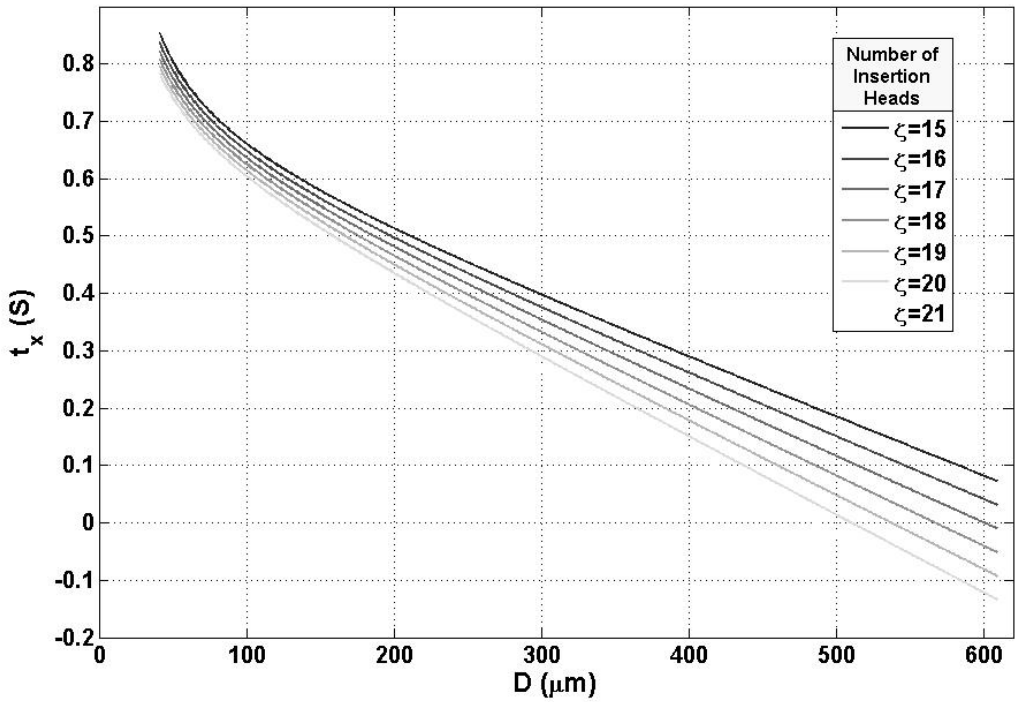

(b)

Figure 4-18: t_x versus unit cell's length for different ξ a) $1<\xi<96$ b) $6<\xi<11$

4.3 Proposed Solutions: Vacuum-Based Mechanisms

In the vacuum-based system, the porogens are picked up and placed by the vacuum force. The schematic of the process is demonstrated in Figure 4-19. In this type of system, the porogen reservoir is separated from the insertion head. The insertion head is connected to a vacuum-producer system that turns on when the insertion head comes to the porogen reservoir and generates a negative pressure to suck the porogen particles in the insertion head's holes. Then the insertion head is moved by the X-Y positioning stage to the workspace at the desired location. For inserting the porogens, the insertion head is moved down close to the compacted powders surface by the Z-stage. Then, the vacuum-producer system turns off so the negative pressure is eliminated, and the porogen particles drop on the compacted powder layer due to their weights.

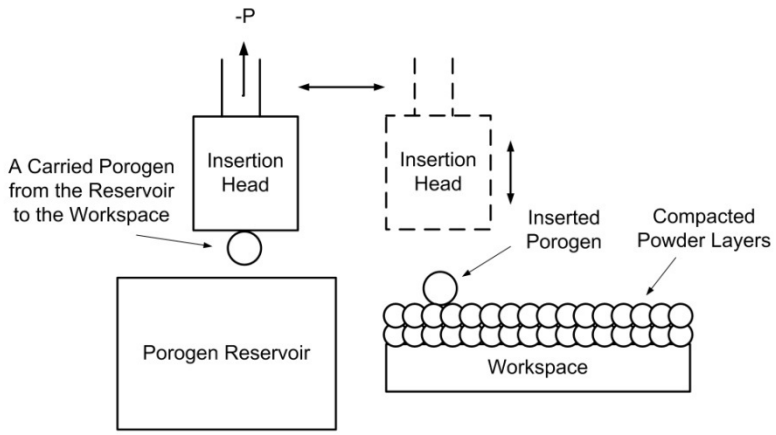

Figure 4-19: Insertion Process in the Vacuum-Based Design

4.3.1 Setup for Feasibility Study

To investigate the feasibility of the presented system, a test set-up including a pipette, a pipette bulb, and a piece of aluminum foil has been used. A schematic of the system is presented in Figure 4-20. As depicted in this Figure 4-20, a sub-millimeter hole is made in the aluminum foil by a needle. The 98% hydrolyzed PVA particles of 250 μm size were picked up at the sub-millimeter hole by the suction made by the pipette bulb. The result of this experiment emphasizes that the presented system has the capability of picking up and placing the porogens.

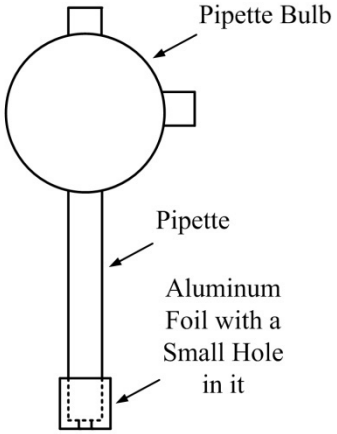

Figure 4-20: Schematic of the Feasibility Test Set-Up – Vacuum-Based Design

4.3.2 Calculation of the Hole Diameter

Figure 4-21 demonstrates a free body diagram of a grabbed particle at a hole. The vacuum force is proportional to the hole area and the vacuum pressure, i.e., $F_{vacuum} = P_{vacuum} \times A_{hole}$ when $A_{hole} = \pi D^2/4$ and D is the hole diameter. g is gravity acceleration and m is the mass of the picked up porogen. m can be rewritten as $\rho_{porogen} V_{porogen}$, so Equation (4-3) is driven. The volume of porogen can be calculated based on the porogen diameter (d). As a result, depending on the porogen's density and size, the diameter of the head's hole and the applied vacuum pressure in the system can be determined. The presented model is a simplified model in which the electrostatic force has been neglected. The rational is, based on the conducted experiments presented in Chapter 5, the electrostatic force is negligible compare to other presented forces in the system. Moreover, by connecting the insertion head and the powder reservoir to the ground it can be ensured that there are not any induced charges in the particles and the insertion head to cause electrostatic force.

$$P_{vacuum} \frac{\pi D^2}{4} = \rho_{porogen} \frac{4\pi d^3}{3 \times 8} g \qquad (4\text{-}3)$$

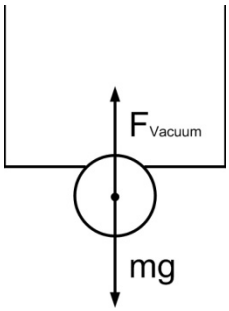

Figure 4-21: Free Body Diagram of the Picked up Porogen

4.4 Selection of the Best Design

To select the most appropriate system among the presented designs, the well-known value matrix method has been applied. According to this method, first the important factors in selecting the best method should be determined. Then, a value should be assigned to each parameter according to its importance in and effect on the system's function and performance. For evaluation, a matrix of insertion heads that works based on the vacuum-based design is compared to both the single head and the array of nozzles that are made according to the actuator-based design. The resulted value matrix is presented in Table 4-2.

the most important parameter in designing a porogen insertion mechanism is the capability of the system for inserting porogens with the different sizes within a single part. In the array of nozzles in the actuator-based systems, the reservoir is filled with the porogens of a certain size and it is not practical to remove the porogens from the reservoir and refill it with the porogens of a different size during the fabrication process. None of the presented single head designs, except the four-plate design, is able to insert porogen with a variety sizes. The four-plate design head is capable of inserting the porogens of any required sizes; however, a feeding mechanism should be designed to bring porogens of the appropriate sizes to the head. In contrast, as shown in Figure 4-19a, in the vacuum-based system the porogens are picked up from the reservoir and consequently different reservoirs with a variety of porogen sizes can be used. During the

manufacturing process, the vacuum-based insertion head can pick up porogen from any desired reservoir that may vary from the last or the next used reservoirs.

All the three competitive systems are adoptable with a variety of porogen sizes. In the vacuum-based head, for any hole's diameter the vacuum pressure can be changed according to the porogen size to satisfy the equality presented in (4-3). In the actuator-based systems, the holes can be opened in a controllable fashion to be adopted with any required porogen size.

Although inserting a controlled number of porogens on the workspace is a crucial requirement for the porogen insertion system, evaluating this parameter requires preliminary test that is impossible without using a pilot test setup. However, it can be predicted that in the actuator-based design there is a possibility for the porogens to be trapped between the moving plates and inserted accidently on the workspace. In addition, since in this type of design the reservoir is connected to the insertion head directly and carried on top of the workspace, a continuous flow of particles can be inserted in the case of malfunctioning.

Figure 4-22 demonstrates some sample graphs of the evacuation time versus the generated vacuum pressure for a couple of typical vacuum generators, which evacuate 1 litre volume of air at 6 bar pressure. VADM and VADMI, which are presented in Figure 4-22, are two models of vacuum generator that are manufactured by the Festo Company. The numbers after the name of these models demonstrate the nominal laval nozzle size in each vacuum generator. For picking a small porogen up, a lower amount of air need to be evacuated, and perhaps the evacuation process will take shorter time than what has been presented in Figure 4-22. Since the evacuation process should be done for each set of porogens, depending on the number of the insertion heads in the array, the required time for inserting all the required porogens on the entire workspace may increase significantly. Moreover, releasing the porogens from the insertion head may have delay in a pneumatic system. Figure 4-16 shows the required time for the optimized single-head design of the actuator-based system to insert the porogens on the entire workspace. The required time decreases m^2 times by using a matrix of $m \times m$ heads.

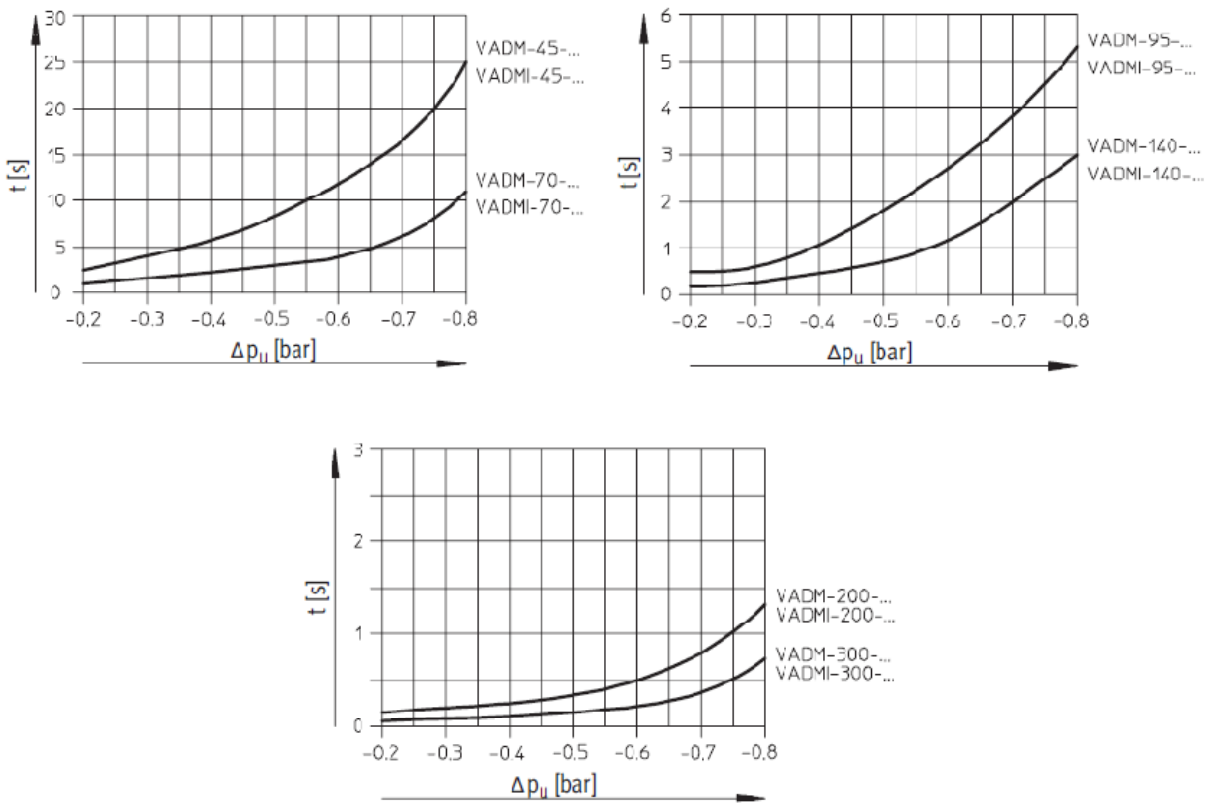

Figure 4-22: Evacuation Time versus Generated Vacuum Pressure [79]

the vacuum-based system composed of a head that has a simple structure as presented in Figure 4-19b, and a vacuum producer system that can be found off the shelf. In contrast, the actuator-based systems need the custom-designed insertion heads and the linear actuator with the accuracy in the range of micron to make the system capable of inserting the porogens with the different sizes. The custom-designed insertion heads, such as the heads presented in Figure 4-9 and Figure 4-10, with very precise and geometrically small features may increase the cost and complexity of installing a pilot test set up or manufacturing the final functional system.

Since the porogens are in the range of 50 µm to 600 µm, the physical behaviours of the materials in micro-domain, which are different from these behaviours in macro-scale, should be taken into account. For instance, in macro-scale problems the electrostatic force is usually negligible compared to the other effective forces in the system such as gravity. However, in micro-scale systems the electrostatic force has a significant effect. In the vacuum-based system,

since the powder reservoir is separated from the insertion head, different methods such as shaking, heating, etc. can be applied to reduce the effect of attractive forces between the porogen particles and avoid them to stick together or to the reservoir's walls. In contrast, in the actuator-based systems, the insertion head is directly mounted under the reservoir and vibration or heat cannot simply be applied to the reservoir without affecting the insertion head and the connected actuators to it.

According to the results of the value matrix, which is presented in Table 4-2, the vacuum-based design has a significantly greater score comparing to both actuator-based designs. Therefore, this type of system is selected in this work.

Table 4-2: Value Matrix for Selecting the Most Appropriate Design

		Proposed Systems		
		Pneumatic-Based	Actuator-Based	
Parameters	Rank	Matrix of Nozzles	Matrix of Nozzles	Single Head
Capable of Inserting the Porogens with Different Sizes in a Single Part	7	10	0	9
Adoptable with Different Porogen Sizes	6	10	10	10
Controlled Number of Inserted Porogens	5	-	-	-
Work Faster	4	3	10	6
Pilot Test Setup	3	10	7	6
Manufacturability	2	10	7	6
Less Affected by the Forces Between Particles	1	10	7	7
Total Score		202	142	184

4.5 Pneumatic-Based Porogen Insertion Mechanism

Remarkable advantages of the pneumatic systems make them excellent choices for many industrial applications such as assembly machines, packing devices, paper industry, printing and

labeling machinery, pick and place applications. The pneumatic systems usually have low cost and their implementation is easy. In addition, these systems usually interface with the electrical and the mechanical components without any difficulties [80].

there are two basic methods for vacuum production. The first way is to use a pump that is driven by an electro-motor. The second way is to applying a venturi, which has no moving part and is known as vacuum generator. Figure 4-23 shows a schematic of a vacuum generator. A flow of compressed air enters the vacuum generator and exits from the exhaust port, causes a lower pressure than the atmospheric pressure in the vacuum port through venturi action. Therefore, the surrounding air is sucked into the vacuum port and leaves the vacuum generator with the supply air (compressed air) from the exhaust port [80].

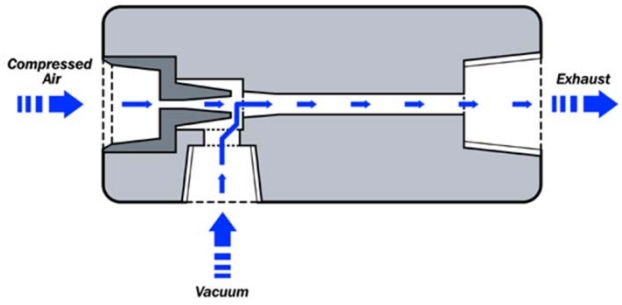

Figure 4-23: Schematic of Vacuum Generator [81]

Absence of moving part in the vacuum generator is advantageous over the vacuum pump alternative. First of all, the required time for producing vacuum is lower hence the vacuum generator is ideally suited for the fast cyclic applications such as pick and place, labeling, etc. Secondly, the only generated noise is due to the air flow that can be minimized by applying the noise reducers in the system. In addition, the vacuum generators are less sensitive to contamination, high temperatures, and corrosive environments. Moreover, the vacuum generators practically do not require maintenance and because of their simplicity they are low cost components. At last, they are fairly compact, so they can easily be mounted near the work station. As a result, the vacuum line's length is minimized that in turn reduces the size of the

vacuum generator and increases the efficiency of the system. However, the vacuum generators need compressed air for function and their efficiency in production of constant vacuum flow or large vacuum flow at high vacuum pressure is lower than the vacuum pumps [80].

In the current work, vacuum is required for picking and placing the porogens and is calculated by Equation (4-3). Since the exponent of d is three in this equation, P_{vacuum} would have relatively a small value. For example, if PVA with the bulk density of $0.4 - 0.7 \frac{g}{cm^3}$ [82] is used as the porogen material, the required P_{vacuum} for picking up one porogen versus the porogen size is demonstrated in Figure 4-24. The value of P_{vacuum} is calculated for various hole sizes between 30 to 90 µm in the insertion head. $\rho = 0.7 \frac{g}{cm^3}$ is selected for PVA in this graph. As presented in Figure 4-24, the maximum required P_{vacuum} is 137 Pa that corresponds to the porogen size of 300 µm and the hole size of 30 µm.

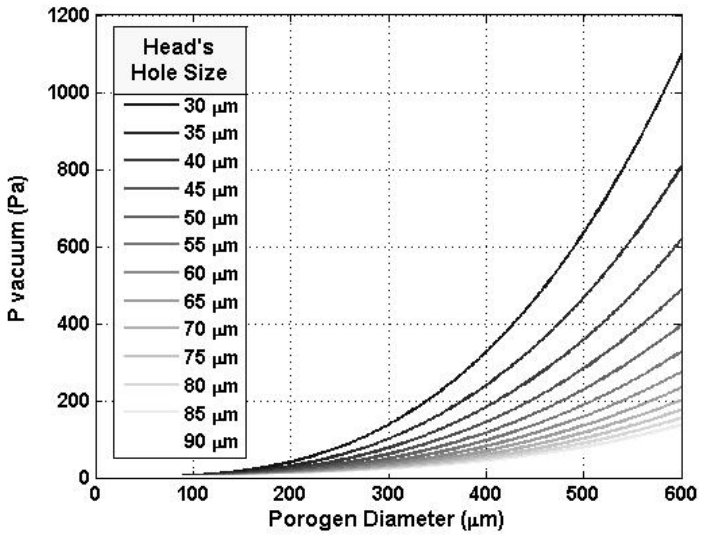

Figure 4-24: Vacuum Pressure versus Porogen Size at Different Hole Sizes

As a result, there is no need for production of a large vacuum flow or a high vacuum pressure. In addition, picking up and placing the porogens is a discontinuous process. Therefore,

the remarkable advantages of the vacuum generator make it an excellent choice for providing vacuum in the pneumatic-based porogen insertion mechanism.

4.5.1 Pneumatic circuit

Figure 4-25 demonstrates the pneumatic circuit for producing vacuum to pick up and place the porogens. Port 1 of the filter-regulator is connected to the compressed air reservoir. The filtered compressed gas leaves the filter regulator at a desired pressure that is set by the regulator, and enters port 1 of the distributer [83]. In picking up step, the flow path from port 1 to port 2 of the distributer is open. As a result, the compressed air passes the distributer and enters port 1 of the vacuum generator. In the vacuum generator, as depicted in Figure 4-23, the compressed air exits from port 2, causes a vacuum pressure in port 3 that is connected to port 1 of the 2-inlet selector [83]. Since port 1 is opened to port 3 in the 2-inlet selector, suction is transmitted to the porogen insertion head and the porogens are grabbed at the holes of the porogen insertion head. For placing the porogens on the workspace, the compressed air is guided from port 1 to port 3 in the distributer. Then in the 2-inlet selector, the path between port 2 and port 3 will be open, therefore, instead of the vacuum, a back pressure is transmitted to the porogen insertion head and push the porogens from the head to the workspace.

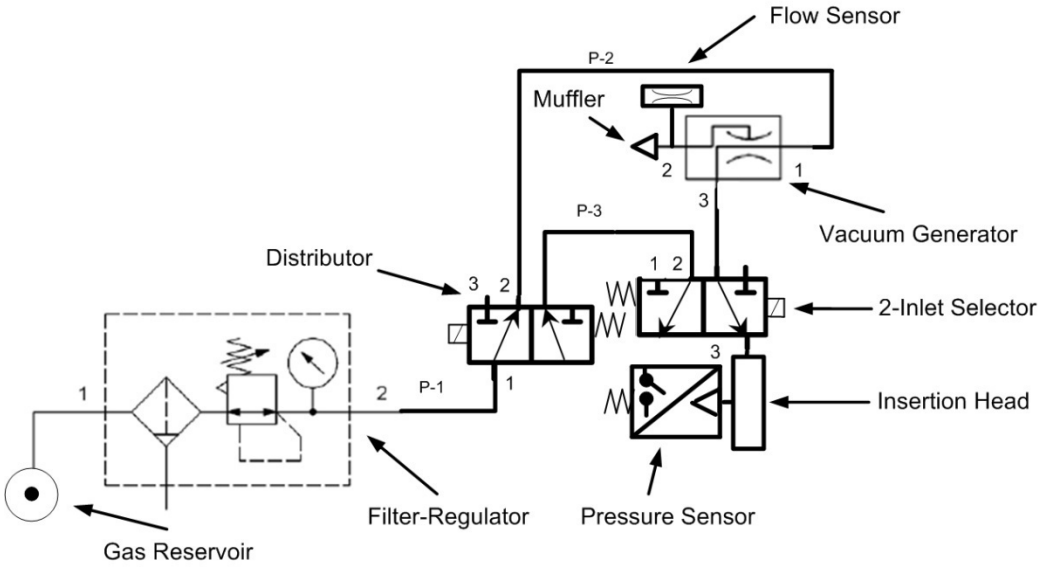

Figure 4-25: Pneumatic Circuit to Pick Up and Place Porogens

As discussed earlier in section 4.5, in the current project the absolute value of the required vacuum pressure is fairly low. As a result, the different parts of the pneumatic circuit should be selected in a way that they work properly in low pressures. This may provide the opportunity to minimize size and weight of the pneumatic circuit's parts such that they will be mounted in the whole 3D printing machine easily and be carried by the positioning devices if it will be necessary. Lower cost; higher accuracy; easier installation; better efficiency; and faster operation, specifically faster evacuation time for the vacuum generator, are the important parameters that are considered in the selection of the pneumatic circuit's components.

therefore, the vacuum generator VN_05_M_I2_PQ1_VQ1 and the filter-regulator LFR-1/8-D-5M-MINI-RR-SA were selected from the Festo Company. The information about these parts is presented in Appendix C.

A sensor is required in the system to detect the pressure or flow changes at some appropriate points of the pneumatic circuit. In this way, when the system picks up the porogens it can be ensured that, all of the holes in the insertion cap are blocked with the porogens, and, there is no air leakage at the holes. Usually two types of sensor are used in pneumatic systems including flow sensor and pressure sensor. To select the most appropriate sensor for employing in the current circuit, the law of conservation of mass is applied for the schematic system that is presented in Figure 4-26. In Equation (4-4), output and input of the venturi, and the suction point in the insertion head are presented by indices "O", "I", and "S", respectively.

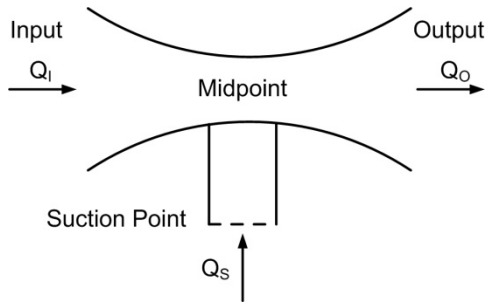

Figure 4-26: Schematic System Including Venturi and Insertion Head

$$Q_I + Q_S = Q_O \qquad (4\text{-}4)$$

the equation is assumed for two conditions of the system, including before picking up any porogen (condition 1) and after picking up the porogens when the holes are completely blocked with the particles (condition 2). When the holes are blocked with the porogens, no air is sucked into the insertion head and $Q_S = 0$, therefore, the output flow rate decreases, i.e., $Q_{O1} > Q_{O2}$. As a result, employing only one flow sensor at the output of the venturi, i.e., at port 2 of the vacuum generator in Figure 4-25, is enough to detect if all the holes are blocked with the porogens. In fact, since the input port of the venturi is connected to a compressed air reservoir, Q_I is constant for the entire process, and, according to Equation (4-4), all of the holes are blocked when $Q_O = Q_I$.

Since flow sensors are usually more expensive than pressure sensors, it is more cost effective to use a pressure sensor instead of the flow sensor. The pressure sensor can be connected to the insertion head as presented in Figure 4-25. Such a sensor can detect the air pressure changes in the insertion head (insertion rod which will be presented in section 4.5.2) before and after picking up the porogens. The system can be calibrated by measuring the pressure when the holes are completely blocked, for example, when the head is put on a clean, flat surface such as a microscope slide. The pressure that is measured in this condition is selected as the reference point of the pressure sensor at every line pressure, which is set by the filter-regulator. As a result, for any applied line pressure the corresponding reference pressure for the pressure sensor should be determined in advance.

4.5.2 Porogen Insertion Head

Figure 4-27 presents a schematic of the porogen insertion head. Porogen insertion head consists of two main parts including an insertion rod and an insertion cap that interfaces with the porogen particles. By considering Figure 4-25 and Figure 4-27 it can be understood that, the insertion rod is connected to the outlet port of 2-inlet selector. Therefore, the upper part of the insertion rod should be designed to provide flexibility for connecting to the pneumatic components. For instance, threading the upper part of the insertion rod makes it possible to

mount a push-in-fitting with a desired size to the thread and connect the 2-inlet selector's outlet port to the insertion rod with a tube. Additionally, the insertion rod can be fixed on the Z-positioning device to facilitate precise displacement along the Z axis. The Z-positioning device is in turn mounted and fixed on the X-Y positioning stage; therefore, the accurate displacements along X and Y axes can be provided as well. Conclusively, the insertion rod has to be fixed on the Z-stage by the screws. The size of the screws should be determined according to the size of the threaded holes in the Z-stage plate, which will be selected in section 4.7. At last, the flexibility for connecting to a pressure sensor, if required, is an asset.

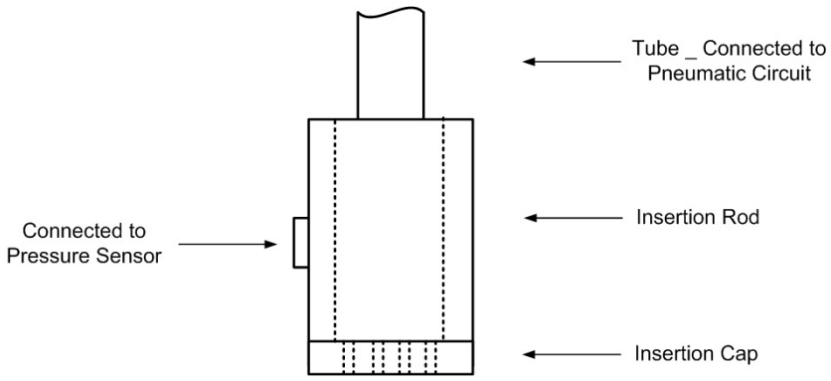

Figure 4-27: Schematic of the Porogen Insertion Head

For fabrication of the insertion cap, some parameters should be taken into account. First of all, the insertion rod and the insertion cap should be connected together in a way that their interface be sealed perfectly to avoid any leakage. In addition, the distance between the lower face of the insertion cap and the porogen powder surface in the porogen reservoir should be minimized to increase the efficiency of the system. In other words, in the closer distances between the insertion cap and the powder surface a lower vacuum level would be enough, so the line pressure can be reduced as well. Lastly, the insertion cap should be easily processable for generating the desired hole pattern in it.

the first proposed design for the insertion cap is to use a thin sheet of metal and make tiny holes in it by using the laser micro-drilling method. For example, the desired pattern of the holes can be made in a small piece of clean flat aluminum foil, which was used for feasibility test in section 4.3. Then the metallic sheet can be fixed at the end of the insertion rod by using a pair of magnets. For this purpose, a ring of magnet with the perfectly flat surface should be permanently connected to the end of the insertion rod and the sheet of metal will be trapped between this fixed magnet and a similar moveable magnetic ring. A schematic of the system has been presented in Figure 4-28. Such a system provides a perfect sealing between the insertion cap and the insertion rod and it is mounted easily, neatly, and fast. However, a distance equal to the thickness of the moveable magnet is added to the distance between the porogen powder surface in the reservoir and the holes in the metallic plane. In addition, finding perfectly flat magnetic rings with the small dimensions off the shelf is an issue.

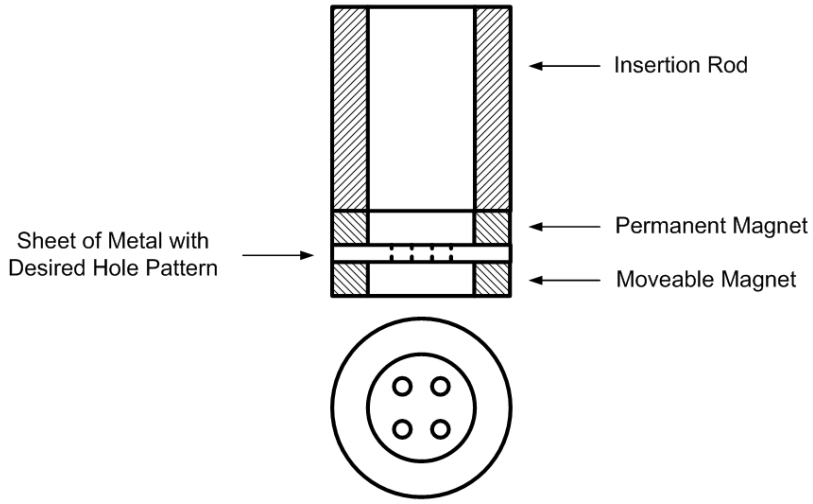

Figure 4-28: Insertion Cap - Magnetic Design

the second idea involves using glue, instead of magnetic rings, for connecting the insertion cap to the insertion rod. In this case, the sheet of metal can be simply glued to the lower face of the insertion rod, as demonstrated in Figure 4-29. Furthermore, for installing pilot test setup to run feasibility tests, using the aluminum foil may be more cost efficient and faster. However, if

the aluminum foil be glued to the insertion rod directly, it would be difficult to replace an old aluminum foil with a new one, because the insertion rod is fixed to the stage and its lower face is not easily in hand to clean it from the dried glue. In addition, rubbing glue on the insertion rod surface and washing it out frequently may damage the insertion rod that in turn reduces the accuracy of the system and increases the experiment's cost significantly.

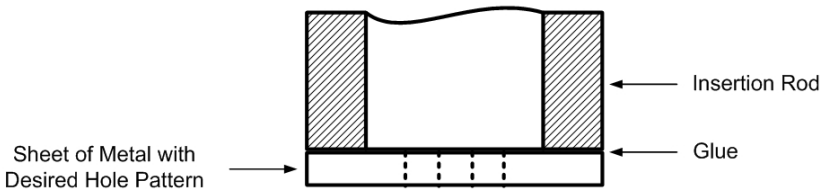

Figure 4-29: Insertion Cap - Directly Glued Design

To overcome the problems caused by using directly glued design of the insertion cap, a nut-screw design of the insertion cap can be used. In this method, the insertion cap is built as an empty cylinder with a fairly thick wall that is threaded from the inside. The aluminum foil is glued on the lower face of the cylindrical cap. The lower part of the insertion rod should be fabricated like a screw, i.e., it should be cylindrical with threads on its outer face. After connecting the aluminum foil to the insertion cap with glue, the completed insertion cap is fastened on the insertion rod as demonstrated in Figure 4-30.

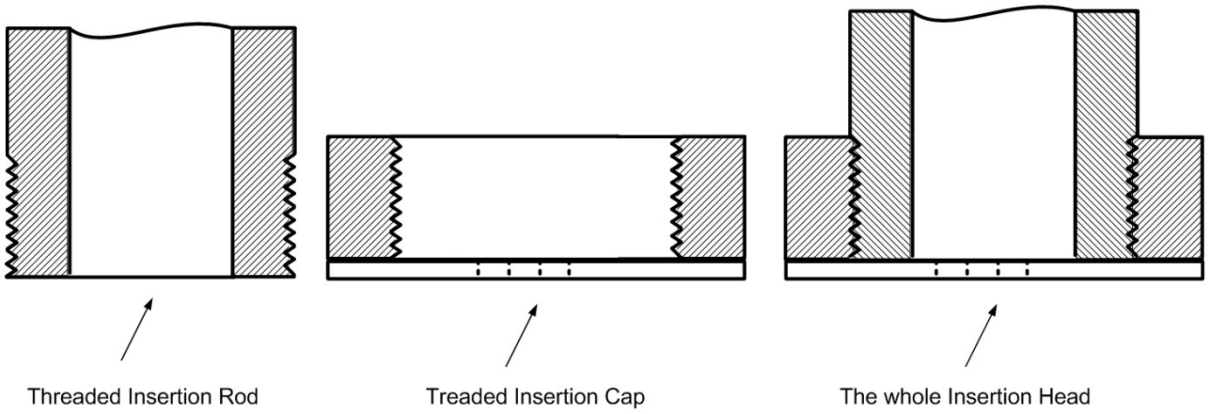

Figure 4-30: Insertion Cap - Nut-screw Design

Using glue for connecting the metal sheet with the desired holes pattern to the insertion cap may be workable for the pilot test setup and for connecting very thin sheets of metal such as aluminum foil. However, for connecting the thicker planes of metal, especially in the final machine, a more precise and consistent design is required. In fact, due to temperature, humidity, and vibrations in the system, the glued-connection between the metal plate and the insertion cap may loosen, and, to avoid accuracy's scarification, applying a more robust connection is mandatory. As a result, a unified design as presented in Figure 4-31 can be used for the insertion cap.

Figure 4-31: Insertion Cap - Unified Design

4.5.2.1 Laser Micro-Drilling for Manufacturing Insertion Cap

At the insertion step, before turning the vacuum producer system off, it would be better that if the insertion head comes down and be very close to the compacted powder layers. In this way, the porogens are placed slowly at the pre-determined locations and are not dropped from a far height, so they do not change the compacted powders' distribution. Any leakage at the holes may move the compacted powders and suck them toward the insertion head. As a result, for manufacturing the insertion cap, holes with small sizes are required to ensure that there is no leakage at the holes after grabbing the porogens.

Distinguished features of laser drilling have nominated it as an excellent technology in fabrication of the small components that have been used extensively in electronics, aerospace, biomedical, and MEMS industries. Laser drilling is a high speed process with an excellent reproducibility that has high flexibility and is capable of working with many different materials. This technique provides good quality for the fabricated parts, excellent resolution, high precision, and it is economically attractive [84, 85].

In laser drilling, a series of laser pulses, at a certain laser parameters, hit one specific spot of the workpiece. In this way, the resulted temperature gradient is large that in turn causes a smaller heat affected zone and lower heat distortion. Several parameters influence the results of the laser drilling including peak power, pulse length and repetition rate, number of pulses, focal condition, physical and material properties of the workpiece, etc. Although Nd:YAG laser is the most common laser for drilling, different kinds of pulsed lasers; in a range of wavelength from the infra-red to the UV, a variety of pulse durations from milliseconds to femtoseconds, and different repetition rates from single pulses to many tens of kilohertz; have been used world-wide [84, 85, 86].

the majority of studies and applications of the laser drilling comprise materials with less than 1 mm thickness [86]. Han et. al [84] used a pulsed Nd:YAG laser for drilling 30mils stainless steel 304 sheet and they achieved holes as small as 150 micron in their experiment. Zhu et. al [87] investigated the effect of laser parameters and workpiece material properties on the drilling of sub-10-micron holes. They compared 60-fs, 50-ps, and 10-ns pulses for drilling the foils of Al, Mo, Ti, Cu, Ag, Au, and brass. The used foils had thicknesses between 1.5 and 50 micron. They

reported a 10 by 10 array of sub-10-micron holes with fairly good quality in the 18 μm thick aluminum foil. The whole array could be fitted in a circle with the diameter of a typical human hair.

Employing laser with shorter pulse duration, higher peak power, and shorter wavelength provides the capability of drilling micro holes in the plates thicker than 1mm, as well [86]. Chichkov et. al [88] used femtosecond-pulse laser for drilling 100 and 500 micron steel sheet, 300 μm silicon wafer, 800 micron AIN sheet, and copper sheet with the thickness of 1mm. The holes they drilled in the workpieces were larger than 100 micron. Karnakis et. al [89] used Nd:YAG laser with the high intensity (15 GW/cm^2) and the wavelengths of 375nm and 532nm for drilling micro holes (around 100 micron) in stainless steel and silicon wafer with the thicknesses between 0.275-1.5mm.

4.5.3 Porogen feeding mechanism and reservoir

In the pneumatic-based design, the insertion head picks up the porogens from the reservoir directly so, practically no feeding mechanism is required. There are two methods for placing the porogen reservoir under the porogen insertion head.

In the first method, the porogen reservoir is fixed at a specific location and the insertion head is carried by an X-Y positioning device to the reservoir. For this goal to be facilitated, either the X-Y micro-stage that carries the whole porogen insertion mechanism (as presented in Figure 4-3) can be used, or another X-Y micro-stage that has smaller dimensions can be included into the system. A new X-Y micro-stage occupies some spaces that in turn increase the size of the whole 3D printing machine. Larger dimensions and the additional micro-stages increase the cost of the final machine. For fabricating a typical scaffold, the insertion head may need to insert lots of porogens on the compacted powder layers. In other words, the porogen insertion head should be carried between the porogen reservoir and the workspace several times, and using the main X-Y micro-stage of the 3D printing machine for this purpose can raise the maintenance cost and time.

the second way involves using a mechanism to move the reservoir, instead of the insertion head. To accomplish this aim, a motor can be employed to carry the porogen reservoir on a

certain path. A schematic figure of the system and the flow chart of the process are demonstrated in Figure 4-32 and Figure 4-33, respectively. For inserting the required number of porogens at the pre-determined locations of each layer, the motor rotates counter-clock-wise and brings the porogen reservoir from its initial position to the final position that is under the porogen insertion head. Motor stops from rotating at the angle of β, at the final position of the porogen reservoir, so the porogen insertion head has enough time for coming down into the porogen reservoir, picking up the porogens, and moving upward out of the porogen reservoir. In the next step, the motor rotates clock-wise and returns the porogen reservoir to its initial position. Motor stops at the initial position of the porogen reservoir while the porogen insertion head places the porogens on the powder bed. Then, the porogen insertion head goes up, the motor brings the porogen reservoir under the porogen insertion head, and the cycle repeats as before until the porogens are inserted on the entire layer.

the cross section of the porogen reservoir is selected circular so the porogen insertion head has access to all the areas of the porogen reservoir and no porogen is stuck in the corners. The height of the reservoir should be long enough to make sure that no porogen can jump out of the porogen reservoir specifically when the porogen reservoir moves.

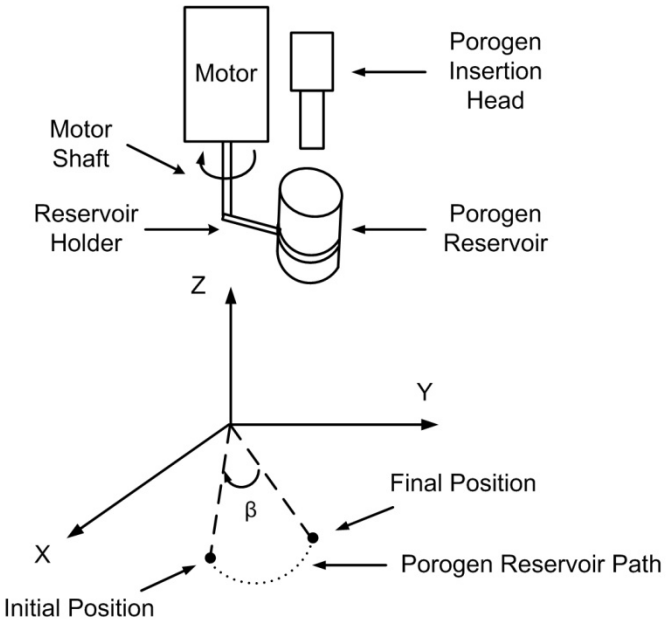

Figure 4-32: Schematic of the Moving Porogen Reservoir System

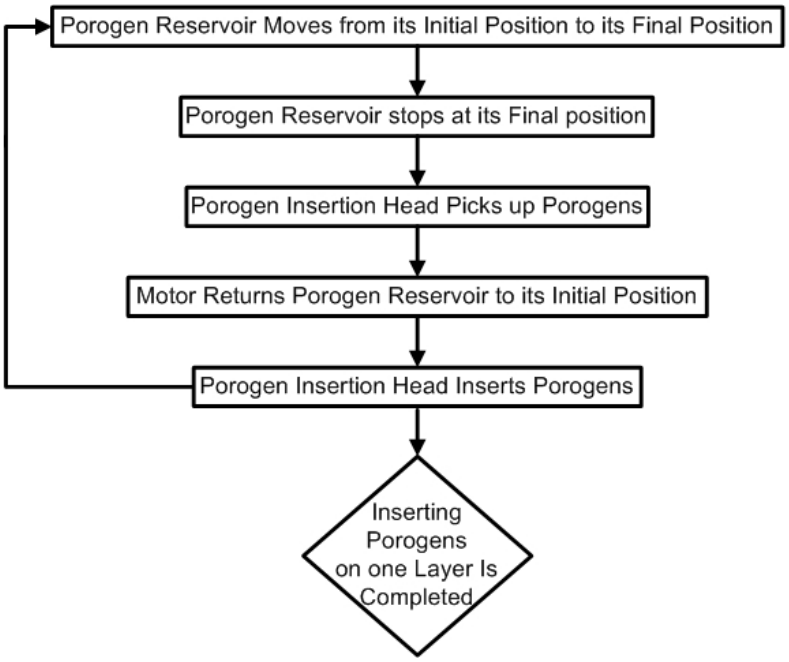

Figure 4-33: Flowchart of the Moving Porogen Reservoir System

the reservoir holder can be a rectangle that connects to the motor shaft at one end, and contains a through hole for carrying the porogen reservoir at the other end. To provide more flexibility for the reservoir holder to cover a wider range of angles during its rotation, the extra parts of the rectangle are cut. This modified version of the reservoir holder reduces the possibility of confliction between the reservoir holder and other parts of the system such as the Z-stage. The schematic of the reservoir holder is presented in Appendix A. The diameter of the hole that performs as the seating for the porogen reservoir should be selected slightly bigger than the outer diameter of the porogen reservoir. In this way, the clearance between the porogen reservoir and the reservoir holder facilitates small vibrations for the porogen reservoir during the rotation of the reservoir holder that in turn prevent the porogens to stick together and provide a more flat surface for the porogen powders in the porogen reservoir.

the reservoir holder is connected to the motor shaft by employing the part that is presented in Appendix A. The upper part of this connecting part contains a hole with the length and the

diameter of the motor shaft. The motor shaft is set into the hole by press fitting, and is secured there with a set screw. The outer diameter of the connecting part is equal to the diameter of the through hole in the reservoir holder. The reservoir holder is mounted on the connecting part, above the thread area, by press fitting, and it is secured in its place by a nut that is fastened under the reservoir holder on the thread area.

4.5.3.1 Motor Selection

Several parameters should be taken into account for selecting the required motor that carries the porogen reservoir. First of all, a general description of the motor application is required. In other words, it should be determined if the motor shaft will have complete rotations or it only passes a certain arc. In addition, all the stop points and motion periods have to be determined in detail. For this step, the flowchart of Figure 4-33 is beneficial.

Second effective parameter in the selection of the motor is space constraints. The total assigned space for the porogen insertion mechanism in the whole 3D printing machine is an envelope of 140×60×200 mm. Both the Z-stage and the motor should be fit in the Y-direction of this space, i.e., in 60 mm. For the first step of design, dimensions of the motor are selected equal to the dimensions of an available miniature motor in the Rapid Prototyping laboratory. Any required changes will be imposed in the next steps of the design. As a result, the diameter and the height of the required motor should be equal or smaller than 15mm and 70mm, respectively.

For calculating the weight constraints of the motor, the third involving factor, the assigned weight for the porogen insertion mechanism is taken into consideration. The maximum allowed weight for this mechanism that includes the weights of the vacuum sensor, the porogen insertion head, the porogen reservoir, the reservoir holder, the motor, the Z-stage, and the required fittings for connecting different parts of the system together is 2Kg. Conclusively, it is better to minimize the motor weight as much as possible. For this goal to be facilitated, similar to the previous case, the weight of the available miniature motor in the Rapid Prototyping laboratory is considered as the weight constraints that is 100g.

the load that is carried by the motor shaft and the moment of inertia around the motor shaft are important parameters in selecting the appropriate motor. In the current project, the motor

carries weights of the porogen reservoir, the reservoir holder, and the connecting components, as well as weight of the porogen particles in the porogen reservoir. For calculating weight of the required porogens for fabricating a bone scaffold with typical dimensions, a good estimation of the porogens volume is required. Figure 4-34 demonstrates a bone scaffold that has typical dimensions of the target scaffolds for the 3D printing machine. The presented scaffold has been fabricated for sheep's knee [46].

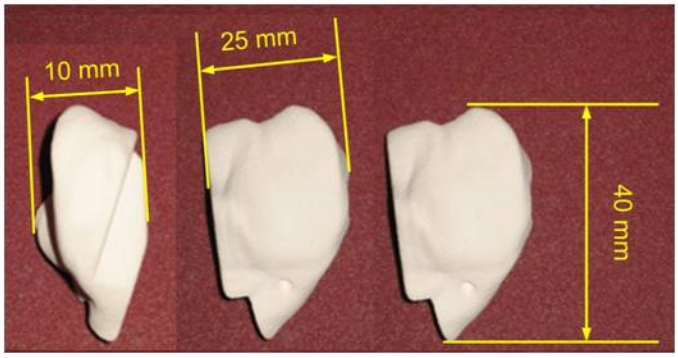

Figure 4-34: A Typical Bone Scaffold

Since the porogens make the macro pores in the scaffold structure, as discussed in 4.2.3, the volume of the used porogens can be assumed as the average of cancellous bone's porosity. Therefore, 70% is selected for calculating the porogens' weight and the reservoir's dimensions.

For a typical part with the porosity of 70% and the size of 10×25×40 mm, the total volume of porogens is 7000 mm^3. In the target 3D printing machine, powder particles made of PVA (Polyvinyl Alcohol) or PVB (Polyvinyl Butyral) will be used as porogen. The maximum density of PVA powder and PVB powder are 0.7 g/cm^3 [82] and 0.5 g/cm^3[90], respectively. As a result, the maximum mass of porogens is 4.9g.

the weights of other parts; including Porogen reservoir, Porogen reservoir holder, and connecting parts; are defined by using their SolidWorks models. The assigned material to all of these parts is aluminum alloy 6061with the density of 2.70 g/cm^3 [91]. As a result, the Porogen

reservoir has a volume of 7835 $mm^3$and is 21.15g, the Porogen reservoir holder has a volume of 2380 $mm^3$and is 6.43 g, and the connecting part has a volume of 447 $mm^3$and is 1.21 g. An approximate mass of 2 g is assigned to the nut. Therefore, the total load that is carried by the motor shaft is calculated as follows:

$$\Sigma F = 0.001 \times 4.9 \times 9.8 + 0.001 \times (21.15 + 6.43 + 1.21 + 2) \times 9.8 = 0.35 \text{ N}$$

For calculating moment of inertia around the motor shaft, the mass of all the parts is assumed to be located at one certain point with the distance of 50 mm from the motor shaft. This selected distance is approximately one third of the X–dimension of the envelope in which the porogen insertion mechanism should be fit. As a result, the moment of inertia around the motor shaft is equal to

$$\Sigma I = (4.9 + 21.15 + 6.43 + 1.21 + 2) \times 50^2 = 89.225 \text{ Kg mm}^2$$

the calculated moment of inertia around the motor shaft will be used later for calculating the torque and confirming if the selected motor is suitable for the current application or not. The calculated value of the moment of inertia is certainly greater than the real value for the designed system; however, it facilitates to use other types of material, with larger densities, as porogen. In addition, more number of porogen reservoirs that carry porogens of different sizes can be added to the system later. To provide this flexibility for the system, a larger value for the carried load by the motor, equal to 1N, is used for selecting the motor.

Other important parameters that should be taken into account for selecting an appropriate motor include the desired output speed of the motor; the power requirements, i.e., voltage and current that will be applied to the motor; environmental issues; and need of employing motion controller, encoder, and gearhead in the system.

To determine the desired speed of the motor it can be said that, since the process time should be minimized, the speed of the motor should be increased as much as possible. However, there are two stops at each cycle and the speed should not affect the accuracy of stop positions. In other words, the box should stop at its defined position without too much vibration and with a high accuracy. Large vibrations may cause the porogen particles to throw out of the reservoir on the workspace. Additionally, the porogen insertion head should not come down to the reservoir

for picking porogens up, unless when the porogen reservoir stops completely. Furthermore, the motion-stop-motion cycle should be smooth, so the porogens do not move to one side of the porogen reservoir due to their inertia of motion.

the 3D printing system should be capable of working in any industrial or academic environment. As a result, it is more reasonable to design the machine in a way that it will work with the city electricity supply. Therefore, the applied voltage to the machine will be 110 VAC/60 Hz. However, by using adaptors in the system, other voltages such as 12 VDC and 24 VDC can be available too.

the final 3D printing machine will work in the regular room temperature and humidity, or, in a condition similar to that, so there is no environmental issue for selecting the motor. In addition, the porogen insertion mechanism will be controlled by a global controller that will control the whole machine. Therefore, in the current project, selection of the required controller is not taken into consideration. To reduce the size and weight of the porogen insertion mechanism, it is preferred to not to use a gearhead for the motor; however, for detecting the stop positions that are presented in the flowchart of Figure 4-33, an encoder is required.

the motor is selected from the Maxon Company and its order number is 118638. The technical information about this product is presented in Appendix C. According to the catalogue of this product, its load stall torque is equal to 133 mNm. Since the moment of inertia around the motor shaft is $\Sigma I = 89.225\ \text{Kg mm}^2$, the starting acceleration of the motor is equal to

$$\alpha_0 = {}^{T_s}\!/_{I} = 133\,mNm \,/\, 89.225\,Kgmm^2 = 1490.6\,\frac{rad}{s^2} \qquad (4\text{-}5)$$

where T_s is load stall torque and I is moment of inertia around the motor shaft. By selecting $\omega = 200 rpm$ as the desired angular velocity for the motor, the required time for the system to start from the start point (stop position) and reach the desired velocity is calculated as:

$$t = \frac{\omega_d - \omega_0}{\alpha_0} = \frac{200\,rpm - 0}{1490.6\frac{rad}{s^2}} = \frac{200 \diagup 60\,\frac{rad}{s}}{1490.6\frac{rad}{s^2}} = 2.237\,ms \qquad (4\text{-}6)$$

where ω_d is the desired angular velocity for the motor and ω_0 is the starting velocity. The calculated value of the time is small enough; therefore, the selected motor is acceptable for the current application.

the motor is mounted on a reference plate, which in turn is mounted on the Y-stage, with a bracket-shape part. 2D sketches of the porogen reservoir, the reservoir holder, the connecting part, and the bracket-shape motor support are presented in Appendix B. The 3D model of the porogen reservoir mechanism is presented in Figure 4-35.

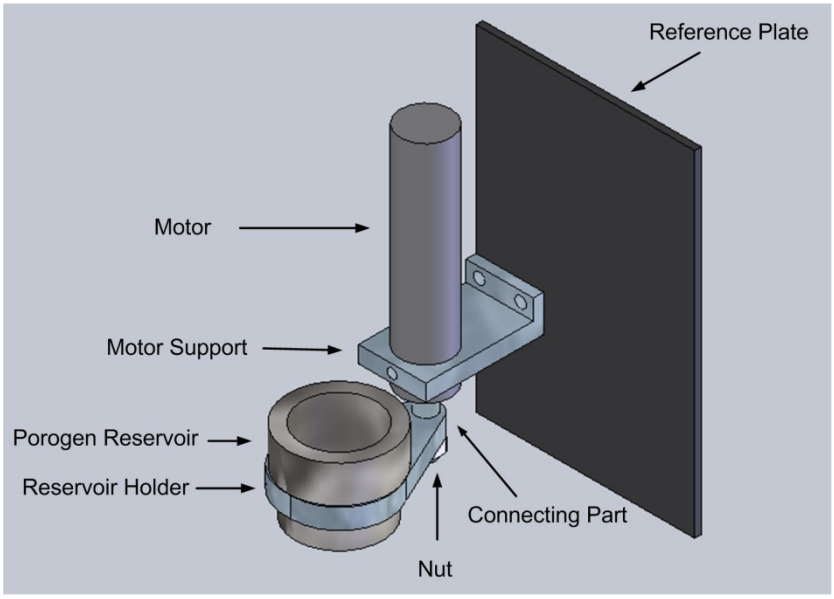

Figure 4-35: 3D Model of Porogen Reservoir Mechanism

4.6 Pushing Mechanism

When the particles are placed on the compacted powder bed, as demonstrated in Figure 4-1-a, a pushing mechanism is required to push the porogens inside the compacted powder layers such as Figure 4-1-b, before spreading the next layer of powder. Such a mechanism requires highly precise incremental displacements in the range of porogen diameters, because the porogen insertion mechanism should insert the porogens exactly inside the compacted powder layers without making any footprint on the powder surface or affecting the compacted powder distribution. The selected Z-stage in part 4.7 can facilitate the required well-controlled movement in the vertical direction for the pushing mechanism. The pushing head that interferes with the porogens should have a completely smooth surface, since the porogens may stick to the small sharp points in a non-smooth surface. To reduce the possibility of interfering between the pushing head and the powder layers, the surface of the pushing head should be perfectly parallel to the powder bed. the pushing process should be done before injecting binder to avoid stick of powder particles or porogens to the surface of the pushing head.

4.6.1 Solenoid-Head Design for the Pushing Head

In this design, the pushing head is fabricated separately from the insertion head. In other words, a linear solenoid is employed as the pushing head. In this system, the rest position of the pushing head is located at a higher level compare to the insertion head, so during the insertion process, the pushing head does not make any confliction with the insertion head. For the pushing step, the solenoid is actuated and the pushing head comes to a lower level compare to the insertion head. As a result, the pushing head can push the porogens inside the powder layer without any interference that may be caused by the insertion head.

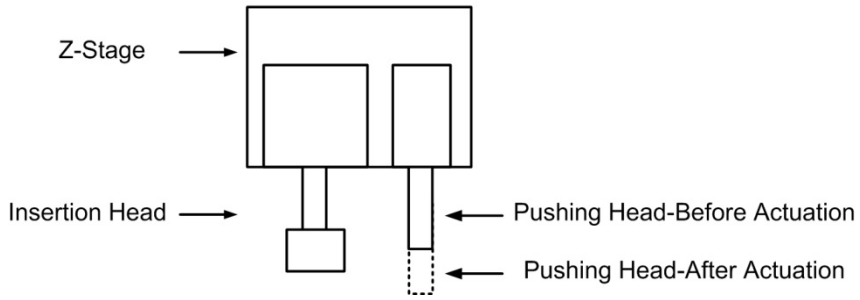

Figure 4-36: Pushing Head - Solenoid-Head

4.6.2 Twin-Heads Design for the Pushing Head

Although the presented design seems to be practical, in order to reduce the cost and size of the system, as well as minimizing the required time for the whole process, it is superior to fabricate the pushing head connected to the insertion head. A schematic of this design is presented in Figure 4-37. By employing the twin-heads design, the pushing head and the insertion head works simultaneously. In other words, the pushing head pushes the porogens into the compacted powder layers, when the insertion head places the porogens on the compacted powder layer in a neighbor row. Using such a system is beneficial for placing the porogen particles on the powder layers and pushing them inside the layers; however, a porogen reservoir with a larger cross section diameter should be used, so both the insertion head and the pushing head can enter to the porogen reservoir easily. In addition, when the insertion head is picking up the porogens, the pushing head may enter to the bunch of porogens in the porogen reservoir, therefore the system parameters should be set in a way that no porogen particle sticks to the pushing head in the reservoir.

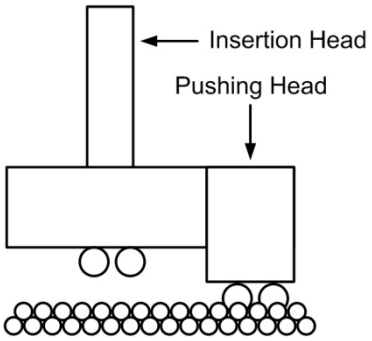

Figure 4-37: Pushing Head - Twin-Heads

4.6.3 Unified-Head Design for the Pushing Head

the drawbacks of the twin-head design leads to the unified design in which the pushing head and the insertion head have the same levels. In fact, in the unified design, the insertion head is manufactured a little bit larger, and the off center part of the insertion head is utilized as the pushing head. A schematic of the unified design is presented in Figure 4-38.

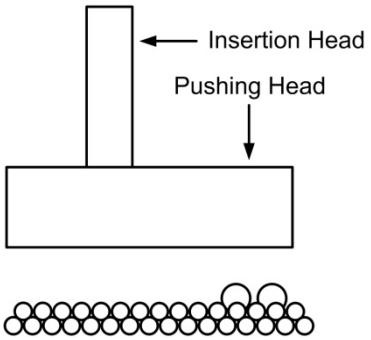

Figure 4-38: Pushing Head - Unified-Heads

4.6.4 Summary

When the porogen insertion mechanism inserts the porogens on the compacted powder layers, a pushing mechanism is required to jam the particles into the powder layers. A solenoid-head as presented in section 4.6.1 can be used for this purpose.

Building the pushing head integrated with the insertion head may reduce the cost and size of the mechanism and decrease the process time. For this goal to be facilitated, a twin-head design is presented in section 4.6.2, in which, the pushing head is integrated with the insertion head and has a small offset compare to it. As a result, when the insertion head inserts a group of porogens, the pushing head pushes the neighbour porogens into the powder layers. However, when the insertion head picks up the particles from the porogen reservoir, the pushing head may enter the bunch of porogens and get dirty. To eliminate this drawback of the twin-head design, the unified-head design is presented in section 4.6.3. in this design the pushing head does not have any offset with respect to the insertion head, and, in fact, the insertion head is employed as the pushing head too. Although this head is not capable of inserting the porogens on the powders layers and pushing them into the layers simultaneously, it can work fairly fast, because, after inserting each group of porogens, the head has to have only a small horizontal movement, so the pushing head part being located on top of the porogen particles and, then, push them into the layers by a vertical displacement. As a result, the unified-head design is selected for the pushing mechanism.

4.7 the Entire Porogen Insertion System

the height of the porogen reservoir is 24 mm, and, a minimum distance of 5 mm is kept between the bottom of the porogen reservoir and the workspace to guarantee prevention of any confliction. As a result, the Z-stage should be capable of traveling more than 29 mm, since after picking up the porogens the insertion head should be able to move upward out of the porogen reservoir and then, goes down and place the porogens on the powder bed. Other vital parameters in selecting an appropriate Z-stage include high precision, preferably less than 5 micron, which is 0.1 of the diameter of the smallest porogen; high speed movement, to minimize the process time; and low friction movement, to minimized damage to the stage since it has to pass several cycles

for manufacturing each part. In addition, the desired stage should be self controlled and its controller should be easily integrated with the global controller of the 3D printing machine. At last, dimensions of the Z-stage should be small enough, so it will be fit easily in the predetermined envelope for the porogen insertion mechanism, which is equal to 140×60×200 mm. The Y-dimension of this envelope is shared between the Z-stage and the porogen feeding mechanism's motor.

Compact Motorized 2" (50 mm) Travel Translation Stage that is a product of the THORLABS Company, with the Metric ITEM Number of MTS50X/M, is a suitable candidate for application in the porogen insertion mechanism. According to the catalogue of this product that is presented in Appendix C this stage has smooth and low-friction movements in a speed range of 100 nm/s to 0.4 mm/s. The minimum incremental motion of this stage is less than 50 nm and it travels up to 50 mm. The maximum load that can be carried by this stage when the stage is used in vertical direction is 4.5 Kg.

Figure 4-39 demonstrates the 3D model of the whole porogen insertion mechanism. The Z-stage is mounted on the reference plate, on which the motor is mounted. In the real 3D printing machine, the reference plate is replaced by the Y-stage. The finalized size of the holes in the porogen insertion rod, for connecting to the Z-stage, is determined based on the holes in the Z-stage's plate. Push-in fitting QS-1/8-4-I with the order number of 153012 from the Festo Company is used for connecting the insertion rod to the pneumatic circuit. 2D sketches of the insertion rod and the insertion cap are presented in Appendix B.

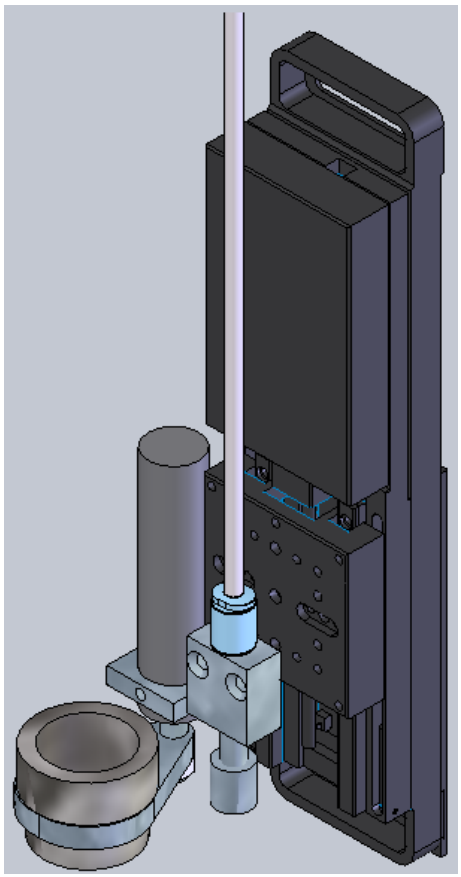

Figure 4-39: 3D Model of Porogen Insertion Mechanism

Figure 4-40 demonstrates the flowchart of the whole process. The required signals for starting each step of the process are presented in parallelograms. Each parallelogram includes the sender and the receiver of the signal.

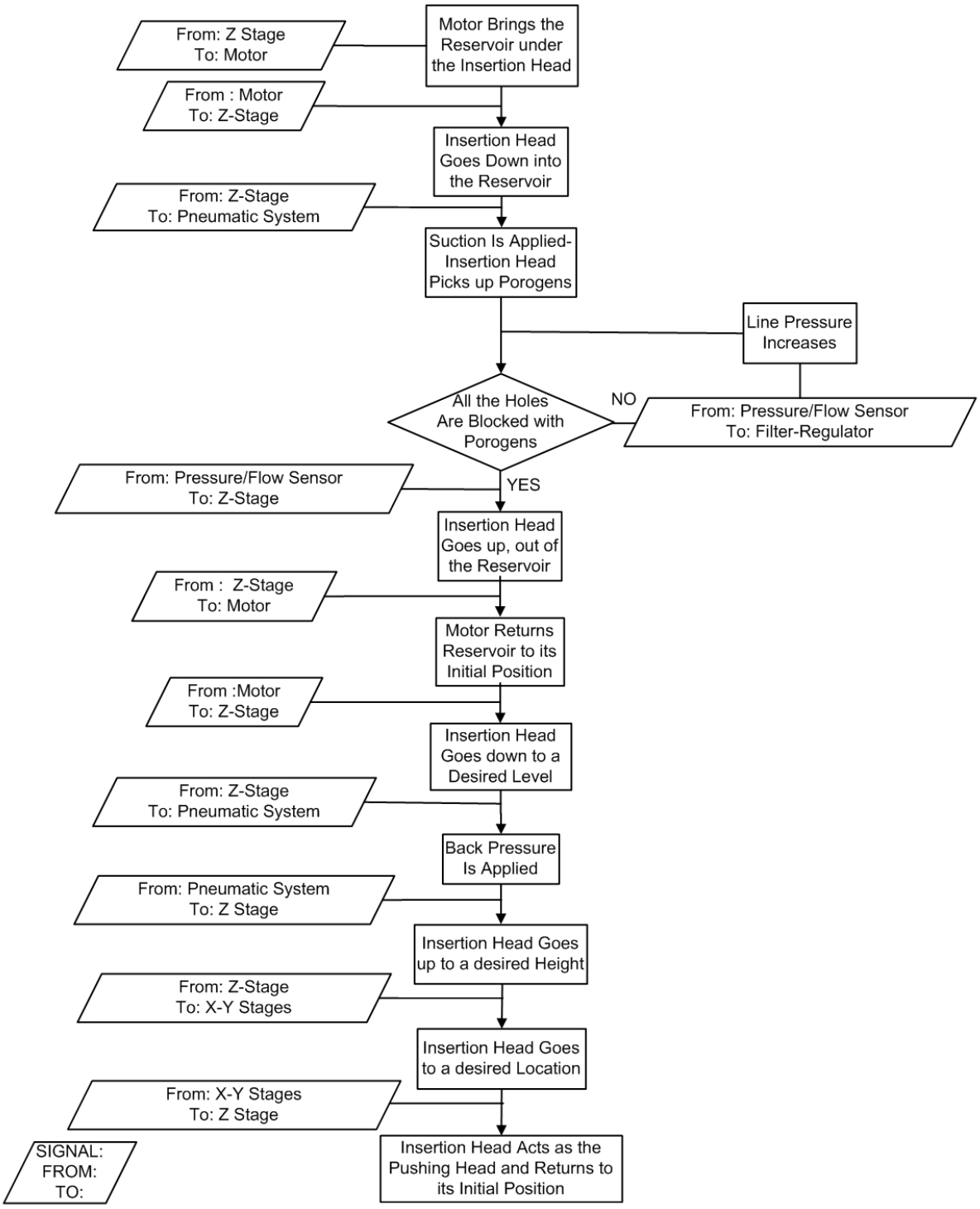

Figure 4-40: Flowchart of the Whole Process

Chapter 5
Experimental Results

5.1 Introduction

In the current chapter, the conducted experiments to assess the feasibility of the proposed system are presented. In the first part, the objectives of the experiments are explained, and the overall descriptions about the applied methods and the utilized pilot setup are given. To obtain some insights into the experiments' steps and the effective parameters, a preliminary experiment was designed and performed. The main experiment was conducted through twelve steps in a way that the results of each step determined the methodology of the next experiment. The pilot setup was also improved based on the results of each experiment. The conducted experiments proved the feasibility of the proposed system, i.e., the capability of the pneumatic-based porogen insertion head of picking up and inserting the porogens in a controlled manner.

5.2 Objectives and Methods

the presented porogen insertion mechanism, in the current work, is a completely new device for controlling the macro-pore distribution within bone scaffolds. Although all parts of the system have to work perfectly to facilitate the final goal of the system, the key proposed concept in the current design is employing a pneumatic system for picking up and placing porogens in pre-designed locations. In other words, the most important parameter that should be investigated is the practicality of the insertion head. As a result, the main experimental goal is the feasibility study of the proposed insertion head. The other parts of the system can only be selected after confirming that the presented insertion head is capable of inserting the porogens on the compacted powder layers at pre-designed locations.

In order to investigate the feasibility of the designed system, a pilot test setup as presented in Figure 5-1 was proposed. In this setup, the porogens are picked up and inserted without applying backpressure. The pneumatic circuit consists of the filter-regulator and the vacuum generator that are presented in Appendix C, as well as, a compressed gas reservoir. As demonstrated in Figure 5-1-a and Figure 5-1-b, the vacuum generator is connected to the insertion head directly. The insertion rod and the cylindrical part of the insertion cap, which are presented in Appendix B,

were manufactured by Machine Shop of the University of Waterloo. The insertion head was mounted on a 1/2" (12.7 mm) Travel Miniature Dovetail stage that is a product of THORLABS. This stage moves manually and has a 350 μm travel per revolution. The catalogue of this product is presented in Appendix C. The stage was mounted on a bracket shape support by means of some brackets and plates to make sure that the insertion cap surface was perfectly parallel to the microscope slide presented in Figure 5-1-c. The stage was capable of moving in three dimensions; however, in this experiment, only displacement along the Z-axis was required.

A modified version of the nut-screw design, which is presented in Figure 4-30, was used for the insertion cap. If the aluminum foil is glued onto the insertion cap directly, it is not possible to use the fabricated head, which has an individual hole pattern, more than once. As a result, a washer and a nut that were glued to each other as presented in Figure 5-2 were used as an intermediate part. A small clean piece of aluminum foil with a thickness of 60 μm was glued onto this intermediate part, and the intermediate part was then glued onto the end of the insertion cap. In the next step, micro holes were made in the aluminum foil by laser micro-drilling. The completed insertion cap was fastened onto the insertion rod, and the extra part of the aluminum foil was folded around the insertion cap to prevent the extra part from affecting “pick-up” and “placing” processes. It was important that, the intermediate part surface that was glued to the aluminum foil be kept fixed on a clean microscope slide so that these processes did not deform the aluminum foil. The completed insertion head is shown in Figure 5-1-c and Figure 5-1-d.

To determine the zero point of the system, a clean microscope slide was put on the metallic cube as presented in Figure 5-1-c, and the insertion head was moved downward until it touched the microscope slide. In this way, the upper surface of the microscope slide was defined as the zero point of the system. This method ensured that the insertion cap surface was perfectly parallel to the microscope slide. To run the experiment, a thin layer of porogens was distributed on the microscope slide, as demonstrated in Figure 5-1-d, and the insertion head picked up the particles from the microscope slide surface.

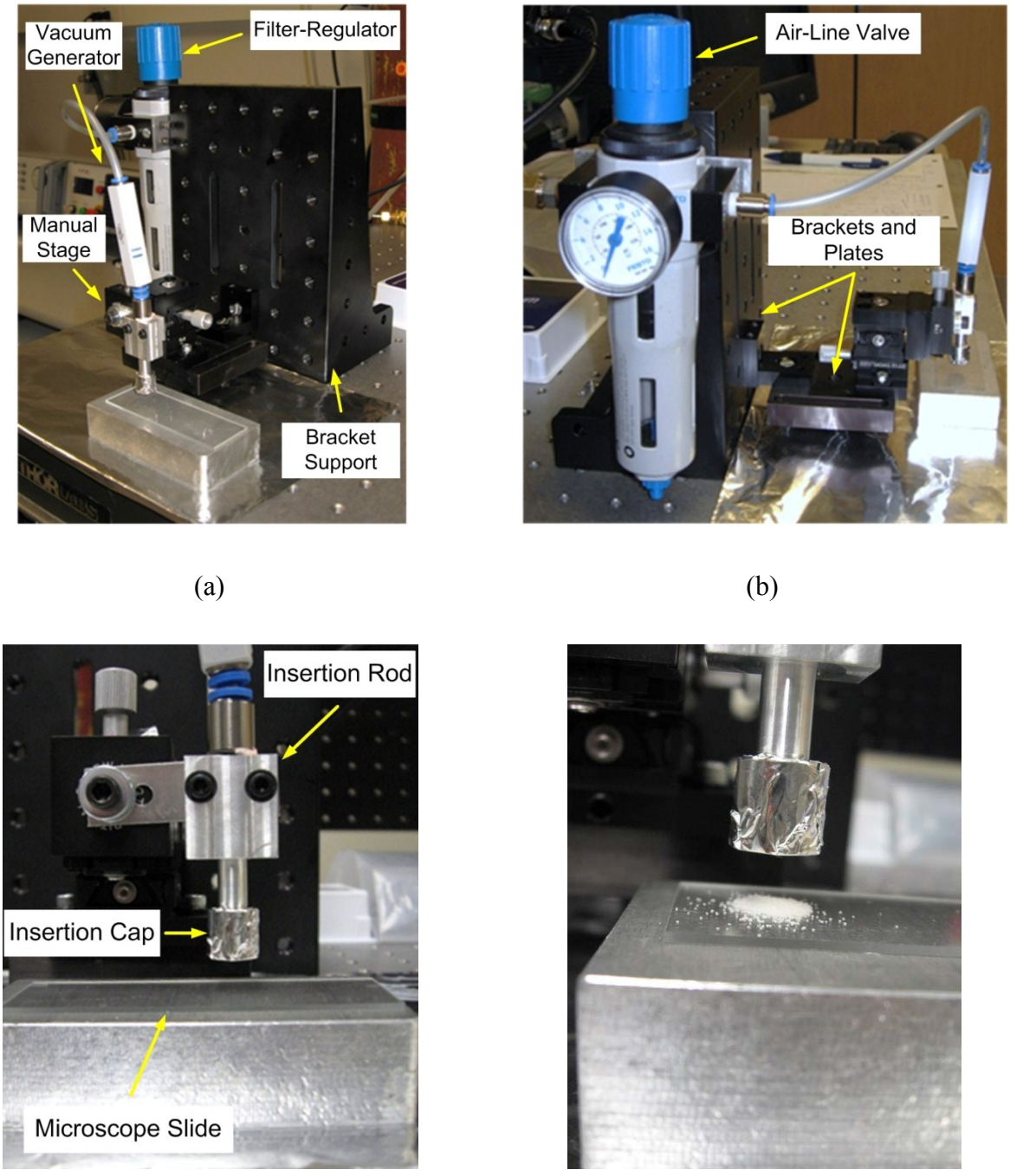

Figure 5-1: Pilot Test Setup 1 - Objectives and Methods a) Overall View of the Setup b) Side View of the Setup c) Front View of the Insertion Head d) Close View of the Insertion Head and the Porogens

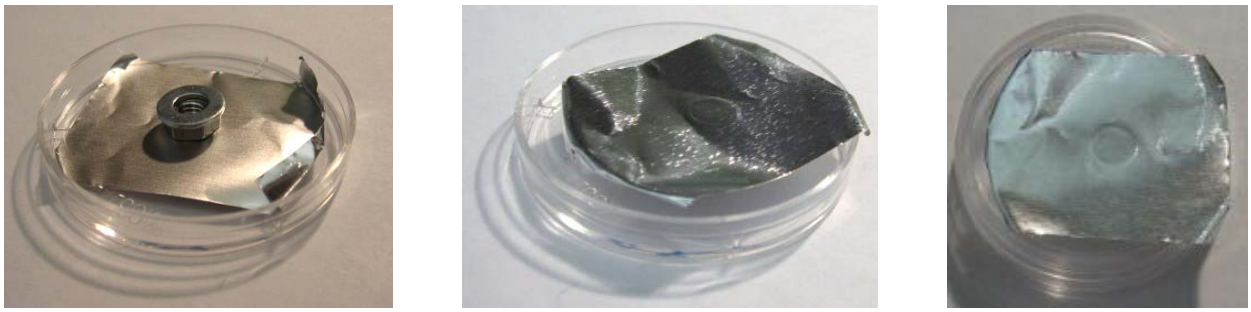

Figure 5-2: Intermediate Parts for Insertion Head

For laser micro-drilling, as discussed in section 4.5.2.1, a laser with short pulse duration, high peak power, and short wavelength is required. For this goal to be facilitated, Pulsed Ytterbium Fiber Laser with 1064 nm wavelength and 20 W power that is a product of the IPG PHOTONICS Company was employed. In order to evaluate the effect of the laser parameters on the size and quality of the drilled holes, the power of the laser was set at 100%, and a frequency of 20000 Hz was applied. Different samples of the aluminum foil glued onto the intermediate part were drilled by various durations of the laser. The results of this experiment are presented in Table 5-1. The discrepancy in the results is due to high sensitivity of the size of the drilled hole to the distance between the laser and the workpiece. In other words, to have a perfect drilled hole, the aluminum foil should be exactly located at the focal point of the laser; however, since the distance between the laser and the workpiece is set manually, the experimental error is high, and, accordingly, the repeatability of the system is very low.

Table 5-1: Micro-Drilling Results

Duration (s)	Hole Diameter (μm)
3	0
3	0
3	70
3	100
3	90
3	30
3	60-70
3	110
4	90
4	72
4	180
5	90
5	50
5	180
5	55
5	63
6	170

5.3 Preliminary Experiment

A preliminary experiment was designed to provide general information about the experiments' steps and effective parameters. For the preliminary experiment, the head with the hole size of 180 μm was used. In this way, an average line pressure equal to 3 bar was predicted to be enough for picking up the porogen particles. The maximum allowed input pressure for the vacuum generator is 6 bar, the pressure at which the vacuum generator provides its maximum suction. In this experiment 98% hydrolyzed PVA powder that was sieved with 250 μm sieve size was used as porogen. When the line pressure was set at 3 bar, the insertion head was moved downward until it picked up porogens. The distance at which the head grabbed porogens, was very close to the porogen powder's surface, and it could not be observed by the naked eye. For performing the "placing" process, a microscope slide with a sticky surface was held under the

insertion head at a close distance, and the air-line valve was closed so that the insertion head placed the porogens on the microscope slide. In this way, the porogens do not move around, and their distribution on the microscope slide represents their distribution on the insertion head.

When the insertion head was picking up the porogens from a short distance during the "pick-up" step, a cluster of particles accumulated at the insertion head hole. This phenomenon demonstrates that there were some attraction forces between the particles. A possible source of this problem is humidity, since the experiment was run under "room conditions", and humidity was not a control factor in the experiment. In addition to reducing the humidity, decreasing the size of the hole in the insertion head, or lowering the absolute value of the vacuum pressure, may partially solve this problem.

At "placing" step, some of the particles did not drop on the microscope slide, and they stuck to the surface of the insertion head, both at the location of the hole and outside of it. Figure 5-3 shows some stuck particles under microscope. One possible force that may cause the particles to stick to the insertion head surface is the electrostatic attraction between the polymeric PVA particles and the head surface. The electrostatic charge can be induced in particles during the powder preparation processes, i.e., grinding, sieving, etc. The preparation processes were done in the Rapid Prototyping laboratory in the University of Waterloo. In order to overcome this problem with the electrostatic charge, the same charge can be induced to the insertion head in a way that the insertion head surface repels the particles, and this repulsive force eliminates the effect of the attractive electrostatic force between the insertion head surface and the porogen particles. In addition, another porogen material, such as salt, that has a lower electrostatic charge can be used in the experiment to minimize the effect of the electrostatic force, which is a disturbance factor in the current experimental setup. Based on the behaviour of salt and PVA powders during the experiment, the electrostatic charges in these two materials were compared. To drop the particles that stick to the insertion head at the location of the hole, applying backpressure can be helpful. Although the solution presented for neutralizing the effect of the attractive electrostatic force between the powders and the insertion head may work perfectly, it should be taken into account that it it is not certain whether this force is the only source of attraction between the head and the particles. In other words, determining the present attractive forces in the current system, calls for plenty of research and experiments, which are not

mandatory for the final goal of the current project. In other words, the porogen insertion mechanism will work in an enclosure with well-controlled humidity and temperature, and the porogen particles that will be used in the real system will be produced by a more controlled and precise process to have pre-determined physical and geometrical properties. As a result, such undesired forces may be eliminated in the real system, and using a simple approach that can remove those porogens that are picked up due to the undesired forces from the insertion cap surface, is satisfactory for the purpose of the current project.

Conclusively, the important parameters in the current experiment include the hole size of the insertion cap, the distance between the insertion cap surface and the porogen powder surface, and the line pressure, which affects the vacuum pressure. By employing an insertion cap with a certain hole size, increasing the line pressure enables the system to pick up porogens from a farther distance; however, it can increase the number of grabbed particles as well. Therefore, determining optimum values for the line pressure and the picking up distance, and understanding their correlation with the insertion cap's hole size, are crucial for the porogen insertion mechanism to perform its task perfectly. With the aim of minimizing the effect of the disturbance factors on the experiments' results, Sodium Chloride GR ACS Crystals with the item number of SX0420-1 that is a product of EMD^{TM}, which is referred as salt in the current report, were sieved with the number 60 sieve (250 μm) and used as porogen. In order to have more repeatable results, the porogens were sieved with the number 100 sieve (150 μm) as well, and those porogens that could not pass the 150 μm sieve were selected for the experiment. As a result, the selected size of the used porogens was 200±50 μm.

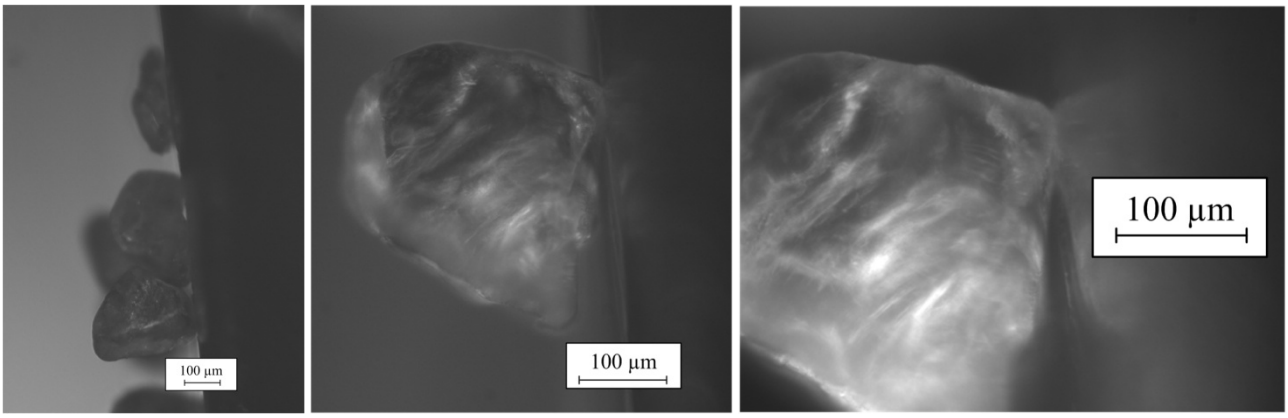

(a) (b) (c)

Figure 5-3: Stuck Particles to the Surface of the Insertion Head- a) 5× Magnification b) 10× Magnification c) 20× Magnification

5.4 Main Experiments

5.4.1 Experiment Number 1

the well-known Factorial Method with one central point was applied for designing the rest of the experiments. The experimental setup presented in Figure 5-1 was employed to perform "pick-up" and "placing" processes with the salt porogens of 200±50 µm. In order to separate the stuck particles from the head and keep only those ones that were sucked by the vacuum pressure, the insertion head was shaken by gentle manual impacts after picking up the porogens and before placing them. The control factors that are involved in the "pick-up" process and their assigned levels are presented in Table 5-2. Insertion heads with hole diameters of 30 µm and 90 µm were used to pick the porogens up from the distances of 700 µm and 2800 µmby applying 1 bar and 6 bar line pressure. The central points of the control factors were selected as 70 µm for the hole size, 1400 µm for the distance, and 4 bar for the line pressure. Since the maximum allowed input pressure for the vacuum generator is 6 bar, and the minimum pressure value that can be detected by the filter-regulator is 0.4 bar, these values were selected as the maximum and the minimum pressure in the experiment. One gentle impact was manually applied to the head before the "placing" process, and, then, the insertion head placed the porogens on a sticky microscope slide

from a distance of 700 µm. The number of dropped porogens due to the impact, the number of porogens that remained on the surface of the insertion head after the impact, and the number of inserted porogens through "placing" process were counted. After each trial, the stuck particles were cleaned from the insertion head using blowing air.

Table 5-2: Control Factors and their Levels – Experiment Number 1

Trial	Hole Diameter (µm)	Line Pressure(bar)	Head Surface Distance from Zero Point (µm)
1	30	0.4	2800
2	30	0.4	700
3	30	6	2800
4	30	6	700
5	90	0.4	2800
6	90	0.4	700
7	90	6	2800
8	90	6	700
9	70	4	1400

of the nine trials presented in Table 5-2, the results of trials 5 through 8 are listed in Table 5-3. Each trial was run two times to reduce the effect of the experimental errors on the results. According to Table 5-3, the system cannot pick up any porogens from the distance of 2800 µm, i.e., trials number 5 and number 7; however, the distance of 700 µm is close enough for the insertion head to pick up a bunch of particles. According to trials number 6 and number 8, when the system works with the line pressure of 1 bar, one single impact drops most of the porogens except for those that stick to the surface of the insertion head. In other words, the imposed impact is greater than the generated vacuum force and drops the porogens that are picked up by the vacuum force. This observation leads to the conclusion that the imposed impact is a significant factor in the current experiment. Therefore, using an automatic vibrator for generating the vibration increases the repeatability of the experiment and provides the opportunity to determine the magnitude of the required vibration all of which facilitate a better control on the process. To accomplish this goal, a miniature motor that is used for producing vibration in cellphone model TM520 product of LG was employed. Determining the disturbance factors that

cause discrepancy in the results of trial number 8, requires a better understanding of the effective parameters that in turn calls for running more experiments.

Table 5-3: Results of Experiment – Experiment Number 1

Number of Porogens That are:	Run / Trial	Total Number of Picked Up Porogens in Each Run			
		1		2	
Drop with Impact	5	0	0	0	0
Inserted through "placing"		0		0	
Stuck to Head		0		0	
Drop with Impact	6	16	19	16	27
Inserted through "placing"		0		0	
Stuck to Head		3		11	
Drop with Impact	7	0	0	0	0
Inserted through "placing"		0		0	
Stuck to Head		0		0	
Drop with Impact	8	6	6	12	17
Inserted through "placing"		0		1	
Stuck to Head		0		4	

5.4.2 Experiment Number 2

In the second experiment, factorial design was used to perform sensitivity analysis on the control factors. ¼ fraction design with four central points and three replicates that results 28 runs was applied. The setup of the experiment was similar to the experimental setup that was used in section 5.4.1, except, in the current experiment, the miniature motor selected in section 5.4.1 was mounted on the insertion cap for providing vibration. Figure 5-4 shows the insertion head and the miniature motor. The porogen particles that were used in this experiment were the same as the porogen particles that were used in Experiment Number 1.

Figure 5-4: Installed Miniature Motor on the Insertion Cap

the control factors that involve in the "pick-up" process of the current experiment and their assigned levels are presented in Table 5-4. 1VDC and 3VDC, and the central point of 2VDC, were applied to the miniature motor to provide vibration for the duration of 1 S and 5 S, and the central point of 3 S. Since the distance between the insertion head surface and the porogens in "pick-up" step was recognized to be too far in experiment 1, a lower value was assigned to this factor in the current experiment. The "placing" process was performed similar to Experiment Number 1.

Table 5-4: Control Factors and their Levels – Experiment Number 2

Factor	Levels		
Hole Diameter (μm)	30	70	90
Line Pressure(bar)	0.4	4	6
Head Surface Distance from Zero Point (μm)	700	1400	2100
Applied Voltage to Motor (V)	1	2	3
Time of vibration (S)	1	3	5

the results of the current experiment are presented in Table 5-5. The system was able to insert porogens only in two cases, i.e., trials number 18 and number 20, and, therefore, none of the control factors were recognized as significant. This result demonstrates that, the assigned levels to factors were not suitable, so the real effect of them is not observed.

Table 5-5: Results of Experiment – Experiment Number 2

Trial	Hole Diameter	Line Pressure	Distance	Voltage	Time	Number of Inserted porogens
1	30	0.4	700	3	5	0
2	90	0.4	700	1	1	0
3	30	6	700	1	5	0
4	90	6	700	3	1	0
5	30	0.4	2100	3	1	0
6	90	0.4	2100	1	5	0
7	30	6	2100	1	1	0
8	90	6	2100	3	5	0
9	30	0.4	700	3	5	0
10	90	0.4	700	1	1	0
11	30	6	700	1	5	0
12	90	6	700	3	1	0
13	30	0.4	2100	3	1	0
14	90	0.4	2100	1	5	0
15	30	6	2100	1	1	0
16	90	6	2100	3	5	0
17	30	0.4	700	3	5	0
18	90	0.4	700	1	1	1
19	30	6	700	1	5	0
20	90	6	700	3	1	2
21	30	0.4	2100	3	1	0
22	90	0.4	2100	1	5	0
23	30	6	2100	1	1	0
24	90	6	2100	3	5	0
25	70	3	1400	2	3	0
26	70	3	1400	2	3	0
27	70	3	1400	2	3	0
28	70	3	1400	2	3	0

5.4.3 Experiment Number 3

the only convinced information that is resulted from sections 5.4.1 and 5.4.2 is that, the system cannot pick the porogens up from the distances equal or farther than 1400 µm. According to the first two experiments, it can be predicted that, the applied voltage and the shaking duration should be minimized to ensure that the vibration effect is not greater than the evacuation force. By lowering the vibration effect and picking up the porogens from a closer distance, a lower vacuum force can be applied for performing the experiment. Since the two trials in which the insertion head picks up particles in Experiment Number 2 the head hole was 90 µm, it can be suggested that, the larger hole sizes may be more capable of picking up the porogens. As a result, a lower line pressure can be applied.

the experimental setup in the Experiment Number 3 was the same as the experimental setup that was used in section 5.4.2. The focus of the current experiment was on determining the effect of the vacuum force, which corresponds to the hole diameter and the line pressure, and the vibrating conditions, which corresponds to the applied voltage to the motor and the shaking duration, on the number of inserted porogens. Therefore, to reduce the number of required experiments, the distance of the insertion head from the zero point and the duration of vibration were assumed as constant factors in the current experiment. The involved constant factors and the control factors of the current experiment are presented in Table 5-6 and Table 5-7, respectively.

Table 5-6: Constant Factors and their Values – Experiment Number 3

Head Surface Distance from Zero Point (µm)	2
Time of vibration (S)	1

Table 5-7: Control Factors and their Levels – Experiment Number 3

Factor	Levels	
Hole Diameter (µm)	70	90
Line Pressure(bar)	0.4	2
Applied Voltage to Motor (V)	1	1.5

An experiment that was designed through ½ fraction factorial with three replicates was performed on the control factors, and the results are presented in Table 5-8. In one hand, no porogen was inserted on the microscope slide in all the trials except trial number 11. Therefore, a lower vibration should be imposed to the system that can be facilitated through reducing the applied voltage to the motor or decreasing the time of vibration. However, measuring shorter durations than 1 s is not possible to be performed accurately by employing the available instruments. As a result, this factor cannot be changed and it has to be kept at its minimum value, i.e., 1 s. On the other hand, in some of the trials, the surface of the head was not completely cleaned by the applied vibration. Although the stuck particles did not fall down during the insertion process except in one case, it is more reliable to provide a completely clean surface that in turn is associated with applying higher vibration. To compensate the effect of greater vibration, a higher line pressure is required. Moreover, it is better to change the location of the miniature motor, and mount it on the insertion rod, instead of the insertion head cap. In this way, changing the intermediate part of the insertion cap that consists of washer, nut, and aluminum foil, in order to have the desired hole size in the system, will be easier. In addition, for all of the insertion caps, the relative position of the motor to the surface of the insertion cap remains the same that in turn eliminates any possible noise due to the place of the motor. Furthermore, since the insertion rod has a flat surface, a better mounting is possible for the motor on the insertion rod, compare to the mounting of the motor on the circular surface of the insertion cap. Figure 5-5 shows the new location of the miniature motor in the system.

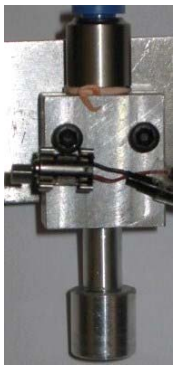

Figure 5-5: Installed Miniature Motor on the Insertion Rod

Table 5-8: Results of Experiment – Experiment Number 3

Trial	Hole Diameter	Line Pressure	Voltage	Number of Inserted porogens
1	70	0.4	1.5	0
2	90	0.4	1	0
3	70	2	1	0
4	90	2	1.5	0
5	70	0.4	1.5	0
6	90	0.4	1	0
7	70	2	1	0
8	90	2	1.5	0
9	70	0.4	1.5	0
10	90	0.4	1	0
11	70	2	1	3
12	90	2	1.5	0

5.4.4 Experiment Number 4

Using aluminum foil for fabricating insertion head imposes some problems to the system. First of all, as discussed in section 5.1, the repeatability of generating hole in the aluminum foil is low. In addition, since the aluminum foil is easily deformed, the surface of the insertion head is easily folded due to cyclic suction that is applied during "pick-up" process. Furthermore, since the zero point of the system is at the top surface of the microscope slide and the porogens are distributed on the microscope slide, during "pick-up" process, some of the porogens touch the insertion head surface and their foot print remain on the head after the whole process. As a result, each head can be used for a limited number of experiments, and, after that, the surface properties of the head will be changed. Variation in the head surface properties during the experiment can affect the experiment's results, and, in fact, the surface condition acts as a disturbance factor in the experiment. As a consequence, employing a tougher material, i.e., a thicker sheet of metal, for fabricating the insertion head is strongly beneficial, since in this way, every fabricated head can be used in several experiments without imposing any undesired effect. However, micro drilling of thick plates requires specific laser's characteristics, as well as, preferably a motion mechanism to move the workpiece toward the laser in a way that the focal point of the laser is

kept located at the solid phase of the workpiece at every moment of the drilling process, when the laser drills the depth of the workpiece [86]. Since such a self-controlled motion system is not available to be used in the current project, a unified insertion cap design, as presented in section 4.5.2, was used. The used insertion cap contained a 2×2 matrix of holes with the size of 150 µm, and it was manufactured by Machine Shop of the University of Waterloo. The hole size of 150 µm is the smallest hole size that could be drilled in the machine shop of the University of Waterloo. Since this hole size is not far off compare to the available hole sizes for the experiment, this value is acceptable for the insertion head's hole. Additionally, this new manufactured head facilitates the opportunity of study on the behaviour of the matrix of holes, instead of one single hole, during "pick-up" and "placing" processes. The surface of the cap was polished with 1 µm and 0.3 µm Aluminum oxide powders, respectively, to provide a smoother surface and minimize the possibility of the stuck porogens to the sharp points on the surface. Figure 5-6 shows the insertion cap, the matrix of 2× 2 holes and the surface of the head.

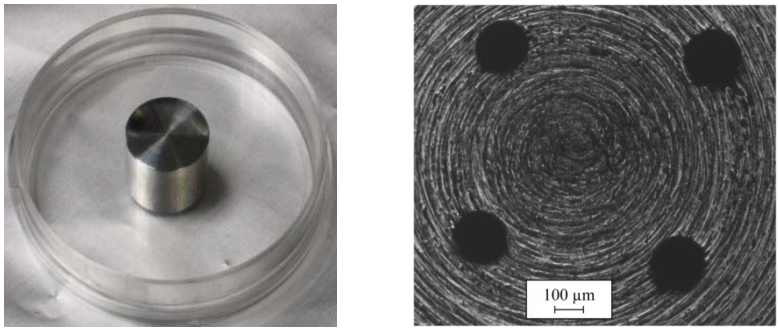

(a) (b)

Figure 5-6: Insertion Cap a) Unified Design Cap b) Matrix of 2×2 of Holes, 5X

A full factorial analysis with three center points was used for the current experiment. Two replicates were assumed per trial to minimize the effect of the experimental errors on the results. The involved control factors, as well as, their levels and center points are presented in Table 5-9.

Table 5-9: Control Factors, their Levels and Center points – Experiment Number 4

Factor	Levels		
Line Pressure (bar)	0.4	4	6
Applied Voltage to Motor (V)	1	2	3
Head Surface Distance from Zero Point (μm)	700	875	1050
Time of Vibration (s)	1	2	3

In all of the trials either a bunch of porogens or no porogen was placed. Additionally, after vibrating the insertion head and before "placing" process, there were lots of residual porogens on the insertion head. As a result, the summation of forces that kept the porogens on the head including the vacuum force, forces between particles, and forces between particles and the insertion head surface was larger than the force that was made by vibration, which caused porogens to drop from the surface. The result that no porogen dropped after turning off the gas valve, which reduces the vacuum force to zero level, leads to an undeniable conclusion that, the forces between particles and between head surface and particles were greater than the vacuum force in a sense that the effect of vacuum force in the current experiment was negligible in some of the trials. In other words, since the stuck porogens made a half-sphere with the radios of ~1 mm around the matrix of holes, even if any porogen was released after turning off the gas valve, it was trapped by other porogens that form the lower surface of the sphere, and this fact can be considered as a source of the problem that there was no inserted particle in some of the trials.

5.4.5 Experiment Number 5

the method of performing the fifth experiment was different from the previous experiments in a sense that, in this experiment the line pressure was set at a low, constant value, i.e., 0.5 bar, and the insertion head was moved very slowly toward the porogens that were distributed on the microscope slide. In this way, the particles were picked up easily and nicely at low pressure and

from a distance that could be observed by the naked eye. The interesting result of the experiment is that, when the porogens were picked up from such a far distance, only a few number of particles, i.e., less than 4, were picked up at each hole. In this experiment, a very thin layer of particles that was almost composed of one layer of particles was used as the powder bed. The experiment was repeated randomly without using any specific experiment design. The results of the current experiment demonstrate that the designed insertion mechanism has the capability of picking up a few number of porogens; however, the particles are not placed when the line pressure is turned off. As a result, applying a back pressure is necessary for inserting the particles. For the sake of the simplicity, a circuit as presented schematically in Figure 5-7 can be used for generating back pressure in the insertion head. During "pick-up" process, the regular valve is closed, and gas flow goes to right hand side branch that includes the vacuum generator, so the effective pressure in the insertion head is the vacuum pressure. For "placing" step, the valve is opened, so the gas enters the left hand side as well. Since the effect of the positive pressure for blowing down the particles is larger than the effect of the negative pressure that is generated by the vacuum generator and sucks the particles toward the insertion cap, the particles are inserted when the regular valve opens.

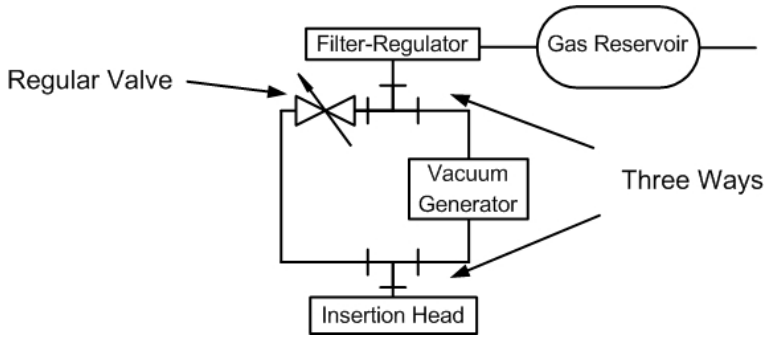

Figure 5-7: Schematic of Pneumatic Circuit for Generating Vacuum Pressure and Back Pressure

5.4.6 Experiment Number 6

Although the results of section 5.4.5 revealed that the presented system is able to pick up a few number of porogens, that experiment did not simulate the porogen reservoir conditions

accurately. In other words, either a new porogen reservoir and a porogen feeding mechanism should be designed to provide a thin layer of porogens, with the thickness of one porogen, under the insertion head, or the system's capability of picking up porogens from the current reservoir should be confirmed through experiment. In order to facilitate this goal, an updated experimental setup was used. This new setup is presented in Figure 5-8. The system was equipped with the pneumatic circuit that is presented in Figure 5-7 for generating back pressure in "placing" step. The new setup provided a more precise zero point for the system as well. In order to determine the zero point of the system accurately, a bunch of porogen particles were distributed in a cubic dish as shown in Figure 5-8-c. The particles formed a hill, and a clean microscope slide with the thickness of 1.01 mm was put on top of the hill. The cubic dish was shaken slowly, and the microscope slide was kept manually in a horizontal position, so as to make a flat, horizontal, non-compacted surface for the hill of particles under the microscope slide. Then, the insertion head was moved down until the surface of the insertion cap touched the surface of the microscope slide. These two surfaces should be set to be perfectly parallel. The point at which the insertion cap surface touched the microscope slide surface, and they were perfectly parallel was selected as the zero point of the system. In this way, the distance between the insertion cap and the surface of the particle bed was equal to the summation of the distance of the insertion cap surface from the zero point, which was measured fairly accurately by counting the number of turns of the manual stage, and the thickness of the microscope slide, which was known exactly. When the zero point of the system was determined, the microscope slide was removed with caution, in order to avoid changing the porogens distribution, which in turn left behind the porogens with a perfectly flat surface as presented in Figure 5-8-d.

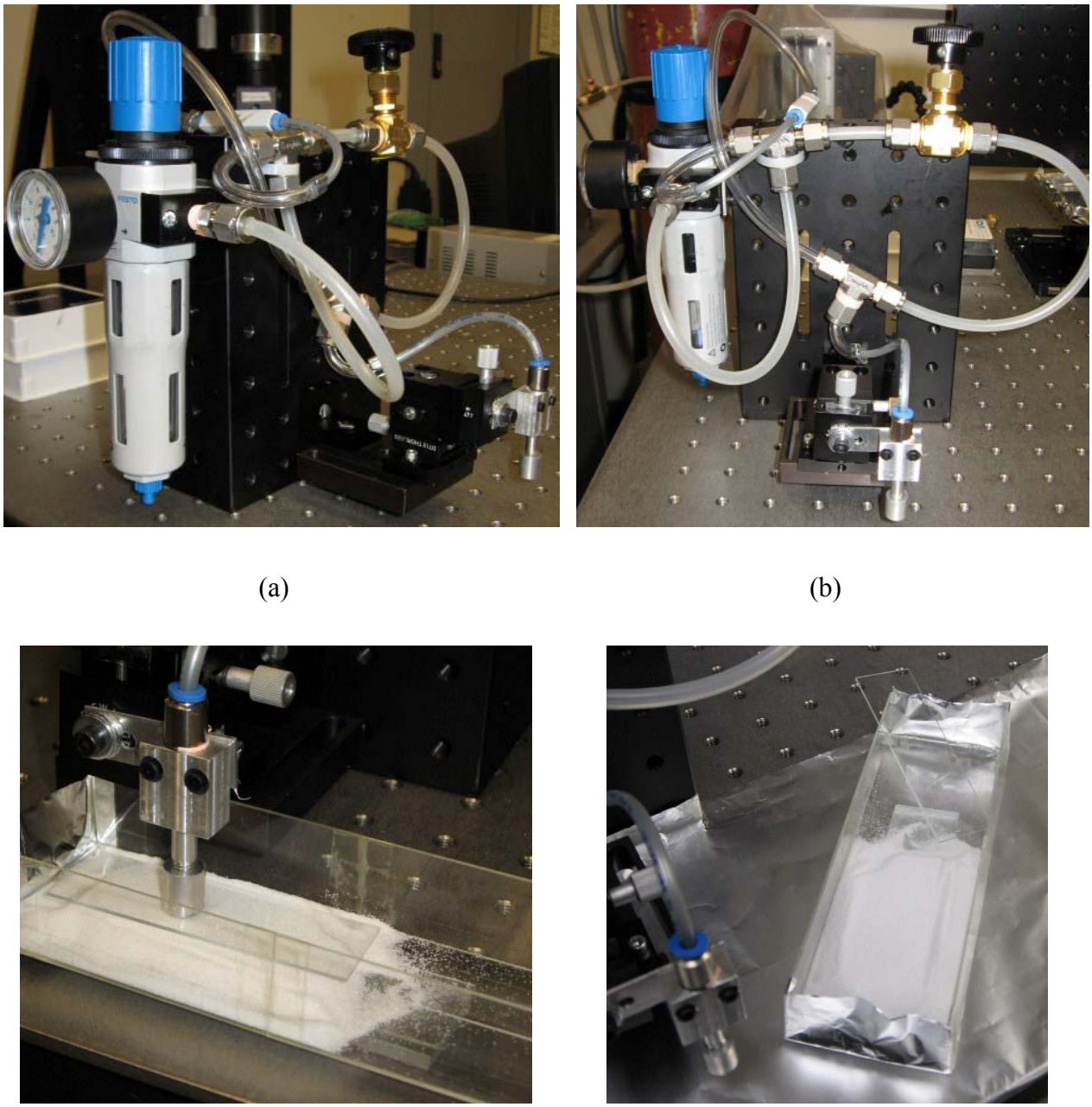

(a) (b)

(c) (d)

Figure 5-8: Pilot Test Setup 2 - Experiment Number 6 a) Side View of the Setup b) Front View of the Setup c) Determining the Zero Point of the System d) Flat Surface of the Porogens in the Porogen Reservoir

According to the results of section 5.4.5, the system should be able to pick up a limited number of porogens from a far distance and by applying a low pressure. Therefore, the current experiment was designed in a smaller range of the lower pressures and the closer distances compare to the previous experiments. The experiment was run by employing the insertion cap with a 2×2 matrix of holes. Since the particles were supposed to be picked up from a far distance, the head had to remain clean, and no vibration needed to be applied in the system. The control factors in the current experiment, as well as, their levels and center points are presented in Table 5-10. The well-known response surface design with two replicates per trial and three center points was run for the factors.

Table 5-10: Control Factors, their Levels and Center Points – Experiment Number 6

Factor	Levels		
Line Pressure (bar)	0.4	0.6	1
Head Surface Distance from Zero Point (µm)	125	300	650

the results of the current experiment are presented in Table 5-11. In all of the trials, the system picked up nothing, except in three cases including trial number 2, trial number 9, and trial number 16 in which a bunch of particles were picked up by the system. In addition, in the distance of 125 µm, some of the grabbed particles were not fallen by applying the back pressure, and vibration had to be applied for dropping them from the head surface. Moreover, some clusters of salt were observed in the salt reservoir that is a dish with the closed lead and is used for reserving grinded, sieved salt porogens. This observation indicated that, moisture had a significant effect on sticking particles together.

Table 5-11: Results of Experiment – Experiment Number 6

Trial	Line Pressure	Distance	Number of Inserted porogens
1	0.4	125	0
2	1	125	Cluster
3	0.4	650	0
4	1	650	0
5	0.6	300	0
6	0.6	300	0
7	0.6	300	0
8	0.4	300	0
9	1	300	Cluster
10	0.6	125	0
11	0.6	650	0
12	0.6	300	0
13	0.6	300	0
14	0.6	300	0
15	0.4	125	0
16	1	125	Cluster
17	0.4	650	0
18	1	650	0
19	0.6	300	0
20	0.6	300	0
21	0.6	300	0
22	0.4	300	0
23	1	300	0
24	0.6	125	0
25	0.6	650	0
26	0.6	300	0
27	0.6	300	0
28	0.6	300	0

5.4.7 Experiment Number 7

According to the results of the presented experiments in sections 5.4.1 to 5.4.6, it can be concluded that, the Response Surface Method is not a suitable approach for finding the optimum values for the control factors at this step; because, in this method, data is mainly collected from end points of the range, and only one point between the extermums, i.e., the middle point, is taken into consideration. In the performed experiments, the number of inserted particles in the trials that corresponded to the extermum values of the control factors were 0 or a cluster. As a result, fitting an appropriate curve to the collected data for finding the optimum values of the control factors is not reasonable.

By considering the trials number 2 and 24 of Experiment Number 6, it seems that 125 μm is an appropriate distance for picking the particles up, and only pressure should be set at a suitable value for picking up only one particle. Moreover, according to trial number 23 of Experiment Number 6, it can be declared that, 300 μm is too far for the insertion head to pick up any particle by the vacuum that is generated when the line pressure is 1 bar or less. As a result, selecting a midpoint between 300 μm and 125 μm is a reasonable selection for the distance between the surface of the insertion cap and the porogens. Especially, by considering the fact that, at the distance of 125 μm some of the particles stuck to the insertion cap surface in a way that the vibration had to be applied for separating them.

therefore, the well-known “one variable at a time” method was used for the current experiment. The experiment was designed to have a constant distance, equal to 212.5 μm, between the insertion cap surface and the porogen particles, and the line pressure was increased from 0.4 bar to 1 bar by the steps of 0.2 bar. Since, the system picked up a bunch of particles when the line pressure was 0.4 bar the rest of the experiment was not performed, and, instead of that, the number of picked up porogens from the distance of 125 μm and 300 μm when the line pressure is 0.4 bar was counted. In both of these cases, the system picked up a cluster of particles. Comparing the results of the current experiment with the results of Experiment Number 6 proves that, the experimental error is very large. Since the only manual instrument that is used in the current experiment is the Z-stage, equipping the system with a more accurate stage, in terms of the measured and displayed value of the distance, is crucial.

5.4.8 Experiment Number 8

the updated experimental setup is presented in Figure 5-9. The manual Z-stage was replaced by a Digital Vernier Height Gauge that is a product of the STm Company and is equipped with a digital screen for showing the displacement in mm with two digits resolution. The digital vernier and the insertion head that was mounted on the vernier are shown in Figure 5-10. The system is moved in vertical direction by rotating the black wheel that is located at the back of the vernier as presented in Figure 5-10-c.

Figure 5-9: Pilot Test Setup 3 - Experiment Number 8

(a)

(b)

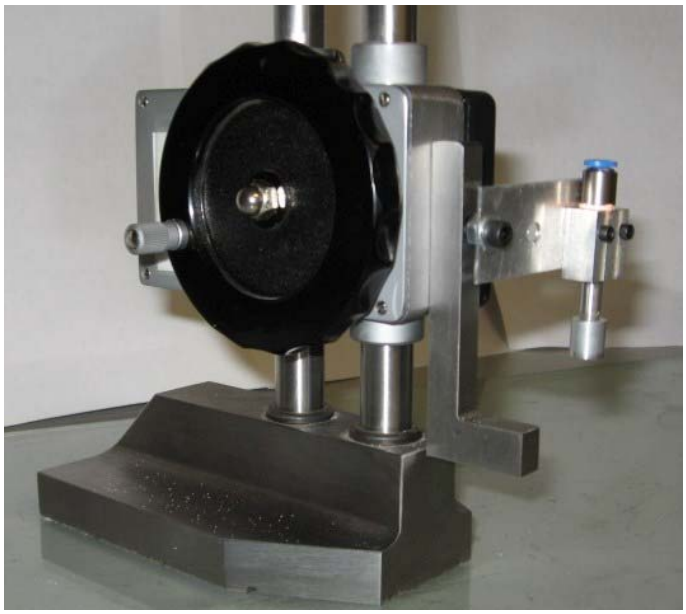

(c)

Figure 5-10: Digital Vernier and Mounted Insertion Head a) Overall View of the Setup b) Close Front View of the Setup c) Close Back view of the Setup

the number of inserted porogens that were picked up in different conditions of the line pressure and the picking up distance were counted. The results of the experiment are presented in Table 5-12. According to the results, the system did not pick any porogen up from the distances equal or farther than 110 µm; however, from the distance of 60 µm the system picked up 24 particles at the line pressure of 0.4 bar and 18 particles at the line pressure of 1 bar. In addition, some of the particles stuck to the head in a way that the back pressure could not separate them from the insertion cap surface, and a manual impact had to be applied to the system. These observations lead to the conclusion that, most likely, the distance should be set somewhere between 60 µm and 110 µm. Moreover, since at the lower line pressure the system picked up more particles, i.e., 24 particles at 0.4 bar and 18 particles at 1 bar, it can be understood that the surface of the powder bed was not completely horizontal. In fact, although the zero point was set at the surface of the microscope slide in an accurate way, and the distance from the zero point was measured accurately, the microscope slide might have a slope that in turn caused different distances from the powder surface, even when the same height was measured. In other words, the real distance between the insertion cap surface and powder surface in the reservoir was dependent on the X-Y position of the picked up porogens. Furthermore, increasing the number of replications can minimize the experimental errors' effects.

Table 5-12: Results of Experiment – Experiment Number 8

Distance (µm) / Pressure (bar)	510	310	210	110	60
0.4	0	0	0	0	24
0.6	0	0	0	0	-
0.8	0	0	0	0	-
1	0	0	0	0	18

5.4.9 Experiment Number 9

In order to have a more accurate zero point, two plastic dishes that have equal height were located at both sides of the porogen reservoir as shown in Figure 5-11, and they acted as holders

for the microscope slide. For determining the zero point through this modified version of the illustrated method in section 5.4.6, the porogen reservoir was shaken slowly, and the microscope slide was moved downward gradually until it was placed on the both dishes. In this way, it could be ensured that the porogen particles had an exactly horizontal and flat surface in all the points that were touched by the microscope slide.

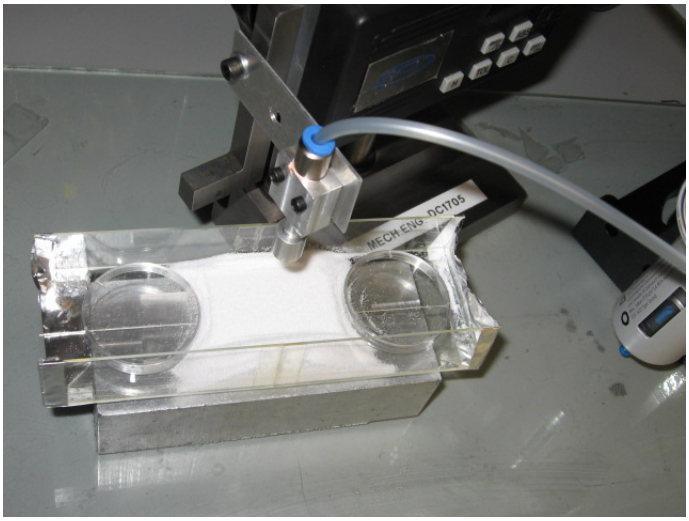

Figure 5-11: Using Plastic Dishes for Determining the System's Zero Point Accurately

the experiment was performed similar to Experiment Number 8, by applying the line pressure of 0.4 and picking up the porogens from the distance of 110 µm. In this condition, a cluster of particles was picked up that shows a huge difference from the results of Experiment Number 8. This discrepancy between the results of these two experiments can be related to the different approaches for setting the zero point of the system. As a result, the experiment was performed again by assuming larger distances as presented in Table 5-13.

Table 5-13: Results of Experiment – Experiment Number 9

Distance (µm) / Pressure (bar)	510	310	210	190
0.4	0	0	22	cluster

0.6	cluster	-	-	-

the other proposed method for determining the zero point of the system more accurately was using a new type of porogen reservoir as presented in Figure 5-12. In this method, porogens were poured in a small plastic dish and spread by moving a microscope slide, as presented in Figure 5-12-b, from one side of the dish to the other side. As a result, no compaction force was applied on the powders, and a flat surface for porogens, as shown in Figure 5-12-c, was provided. Then, the zero point ccould be set by putting a microscope slide on the dish edge, and the top surface of the microscope slide was considered as the zero point of the system through the same method that was used in section 5.4.6.

(a) (b) (c)

Figure 5-12: Plastic Dish Reservoir a) Reservoir Before Spreading the Porogens b) Spreding the Porogens in the Reservoir c) Flat surface of the porogens in the Reservoir

In order to select the best method for determining the zero point of the system, the repeatability of each method was investigated through a set of experiments that are presented with their results in Table 5-14 to Table 5-17 for the glass cube reservoir method that is presented in Figure 5-11, which may impose a lower compaction to the powders in the reservoir, and Table 5-18 to Table 5-21 for the plastic dish reservoir method that is presented in Figure 5-12. In all of these experiments, the system did not pick any particle up from the distances equal

or farther than 210 µm; however, it showed different behaviours in the distances closer than 210 µm that are highlighted in all these tables. The standard deviation was calculated for all the combinations of the line pressure and distance, for the highlighted trials of Table 5-14 to Table 5-21. For this goal to be facilitated, a value of 40 was assigned to the number of porogens in those trials in which a cluster of particles was picked up. The calculated standard deviations and their average, for each type of reservoir, are shown in Table 5-22. According to the presented values in Table 5-22, determining the zero point of the system through the demonstrated method in Figure 5-11 provides more repeatable results, since it has a lower value for the average of the standard deviations. As a result, this method was selected for the rest of the experiments.

Table 5-14: Repeatability Study – Glass Cube Reservoir – Lower Compaction – Run 1

Distance (µm) / Pressure (bar)	510	310	210	110	10
0.4	0	0	0	0	0
1	0	0	0	0	0

Table 5-15: Repeatability Study – Glass Cube Reservoir – Lower Compaction – Run 2

Distance (µm) / Pressure (bar)	510	310	210	110	10
0.4	0	0	0	1	2
1	0	0	0	0	cluster

Table 5-16: Repeatability Study – Glass Cube Reservoir – Lower Compaction – Run 3

Distance (µm) / Pressure (bar)	510	310	210	110	10
0.4	0	0	0	0	cluster
1	0	0	0	9	cluster

Table 5-17: Repeatability Study – Glass Cube Reservoir – Lower Compaction – Run 4

Distance (µm) / Pressure (bar)	510	310	210	110	10
0.4	0	0	0	0	0
1	0	0	0	0	cluster

Table 5-18 : Repeatability Study – Plastic Dish Reservoir – Higher Compaction – Run 1

Distance (µm) / Pressure (bar)	510	310	210	110	10
0.4	0	0	0	0	0
1	0	0	0	0	cluster

Table 5-19: Repeatability Study – Plastic Dish Reservoir – Higher Compaction – Run 2

Distance (µm) / Pressure (bar)	510	310	210	110	10
0.4	0	0	0	around 20	cluster
1	0	0	0	0	0

Table 5-20: Repeatability Study – Plastic Dish Reservoir – Higher Compaction – Run 3

Distance (µm) / Pressure (bar)	510	310	210	110	10
0.4	0	0	0	0	0
1	0	0	0	3	cluster

Table 5-21: Repeatability Study – Plastic Dish Reservoir – Higher Compaction – Run 4

Distance (µm) / Pressure (bar)	510	310	210	110	10
0.4	0	0	0	0	0
1	0	0	0	0	0

Table 5-22: Standard Deviations a) Glass Cube Reservoir – Lower Compaction b) Plastic Dish Reservoir – Higher Compaction

Distance (µm) / Pressure (bar)	110	10
0.4	0.43	17.05
1	3.9	17.32
Average	9.68	

(a)

Distance (µm) / Pressure (bar)	110	10
0.4	8.66	17.32
1	1.3	20
Average	11.82	

(b)

5.4.10 Experiment Number 10

In this experiment, the experimental setup that is presented in Figure 5-10 was employed. According to the observation of section 5.4.5, it seems that, picking up the porogens from a thin layer of powder provides better results, since in this way, the effect of the layers on each other, i.e., the attraction forces between the particles, is reduced. Subsequently, the zero point of the system was determined through the method that is presented in Figure 5-11, except, instead of the plastic dishes, two microscope slides with the thickness of 1.01 mm, as presented in Figure 5-13, were used as holders. As a result, the layer of porogens in the reservoir had a thickness of 1.01mm.

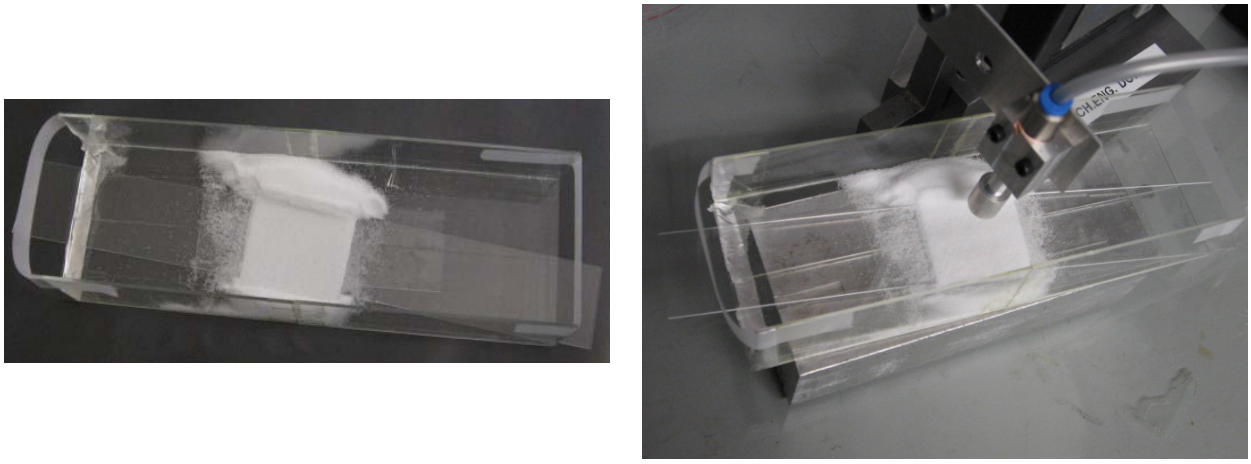

Figure 5-13: Microscope Slide Holders for Determinig Zero Point

Since in Experiment Number 9, the system usually did not pick up any porogen when the line pressure of 0.4 bar was applied, higher line pressures were considered in the current experiment. In order to minimize the effect of moisture, the powders were preheated at $100^{\circ c}$ for 5 minutes. Additionally, in each experiment, a low amount of powders was used, as shown in Figure 5-13, and the experiment was lasted no longer than 5 minutes. Experiment Number 9 proves that, the threshold of the distance between the insertion cap surface and the powder surface is located between 10 µm and 110 µm; however, since in this experiment some of the parameters were changed, a sensitivity evaluation experiment was required to assess those values of the factors that are close to the threshold points. The control factors and their levels, as well as the experimental results, are presented in Table 5-23. Comparing the results of the current experiment with the results of the experiments in section 5.4.9 that are presented in Table 5-14 to Table 5-17 confirms that, preheating the particles is not enough to completely neutralize the effect of the moisture that acts as a disturbance factor in the system. In other words, although when the particles are preheated the moisture is decreased, during the preparation process for the experiment, the environmental moisture affects the particles in a way that the effect of preheating is eliminated, and the particles present a sticky nature.

Table 5-23: Results of Experiment – Experiment Number 10

Distance (µm) / Pressure (bar)	610	510	310	210	110
0.6	0	0	0	0	0
1	0	0	0	around30	-

5.4.11 Experiment Number 11

Experiment Number 10 revealed that, preheating is not sufficient for removing moisture from the system, completely. In order to overcome to this potential problem, i.e., stuck particles because of moisture, the particles should be heated continuously during “pick-up” process. For this goal to be facilitated the particles were poured in a glass dish, and the zero point of the system was determined through the method that is demonstrated in Figure 5-8. The dish was

located on a heater under the insertion head. After the zero point of the system was determined, the heater was turned on, and the temperature was set at 100°c. The experimental setup is presented in Figure 5-14.

Figure 5-14: Pilot Test Setup 4 - Experiment Number 11

the line pressure was kept constant at 1 bar, and the distance between the insertion cap surface and the powder surface was changed to find out the appropriate distance for picking up a few number of porogens. The results of this experiment are presented in Table 5-24. According to this table, in most of the trials, the system was able to pick up and place a few number of particles successfully. Although in some of the trials; i.e., trials number 1, 2, 3, 8, and 9; there was a small number of particles that were stuck to the insertion cap surface, these particles did

not fall down during the experiment, and, as discussed in section 5.4.1, applying vibration on the insertion head can remove them before “placing” process. A small discrepancy can be observed in the results of the current experiment that can be related to the method that was used for determining the zero point of the system. This problem is discussed in section 5.4.8 and 5.4.9 in detail. The proposed method for solving this problem that was employed in Experiment Number 9 cannot be used in the current experimental setup, due to geometrical limitations; however, using a longer plate for mounting the insertion head on the digital vernier and using a larger glass dish as porogen reservoir can solve this problem. The current experiment lead to an undeniable conclusion that heating the powders during “pick-up” process has a major effect on removing moisture that in turn increases the repeatability of the system significantly.

Table 5-24: Results of Experiment – Experiment Number 11

Trial	Distance (µm)	Number of Inserted Porogens	Insertion Cap Surface	Placement	Comments
1	1010	3	a few particles on the edge of the cap	back pressure	all particles are picked up by two holes
2	190	4	a few particles on the edge of the cap	back pressure	-
3	210	0	-	-	-
	30	4	a few particles on the edge of the cap and 2 particles on its surface	back pressure	-
4	410	0	-	-	-
	310	10	head is clean	back pressure	-
5	510	0	-	-	-
	410	5	head is clean	back pressure	-
6	510	0	-	-	-
	410	2	head is clean	back pressure	-
7	470	2	head is clean	back pressure	-
8	420	0	-	-	distance is reduced step-wised
	210	0	-	-	
	80	cluster	particles on the surface of the cap	back pressure	-
9	510	cluster	particles on the surface of the cap	back pressure	-

5.4.12 Experiment Number 12

This experiment was performed similar to Experiment Number 11, except, in the current experiment, unless Experiment Number 11, the porogens were picked up from a thin layer of powder. The goal of Experiment Number 12 was to compare the system's capability of picking up porogens from different types of powder beds, including a thin layer of powder and a bunch of layers. The line pressure was kept at 1 bar and the distance between the insertion cap surface and the powder bed surface was changed. The results of this experiment are presented in Table 5-25. According to this table, the same as Experiment Number 11, in all of the trials, back pressure had to be applied for inserting the particles. However, unless Experiment Number 11, in most of the trials the surface of the insertion cap was not clean, and particles stuck to it. In trials number 3 and 4 the stuck porogens dropped on the insertion bed, which was a sticky microscope slide as presented in section 5.4.1. Comparing the number of inserted particles in Experiment Number 11 and Experiment Number 12 demonstrates that, using a thin layer of powder does not offer any significant advantage over the bunch of layers.

Table 5-25: Results of Experiment – Experiment Number 12

Trial	Distance (μm)	Number of Inserted Porogens	Insertion Cap Surface	Placement	comment
1	510	0	-	-	distance is reduced step-wised with the steps of 50 μm
	60	0	-	-	
	0	10	particles on the surface of the cap	back pressure	-
2	110	0	-	-	-
	60	cluster	-	back pressure	-
3	710	0	-	-	distance is reduced step-wised with the steps of 100 μm
	310	0	-	-	
	210	4	particles on the surface of the cap	back pressure	2 particles drop from edge of the cap
4	410	0	-	-	-
	310	2	particles on the surface of the cap	back pressure	1 particles drops from edge of the cap
5	810	0	-	-	-
	710	cluster	particles on the surface of the cap	back pressure	-

5.5 Conclusions

Through the performed experiments several parameters were recognized that those had considerable effects on the results of the experiment. These parameters can be classified in three major groups, including system parameters, experimental factors, and environmental issues. System parameters contain those parameters that should be set in the pilot setup and they remain the same for all the experiments. For instance, the insertion cap should be fabricated with a smooth surface to avoid porogens to stick to it. In addition, the size of the holes in the insertion cap may affect the number of grabbed particles. Particles size is also an important parameter. In the performed experiments, the size of the used particles is selected in the range of 150 μm to 250 μm that is a fairly wide range. Reducing the size range, for example using particles in the range of 190 μm to 210 μm, can improve the results of the experiments significantly. This

argument can be justified by the fact that, using particles that have fairly similar sizes provides a more even surface for the powder bed, as presented schematically in Figure 5-15, that in turn may reduce the number of stuck particles to both surface and edge of the insertion cap and increase the possibility of picking up particles from farther distances.

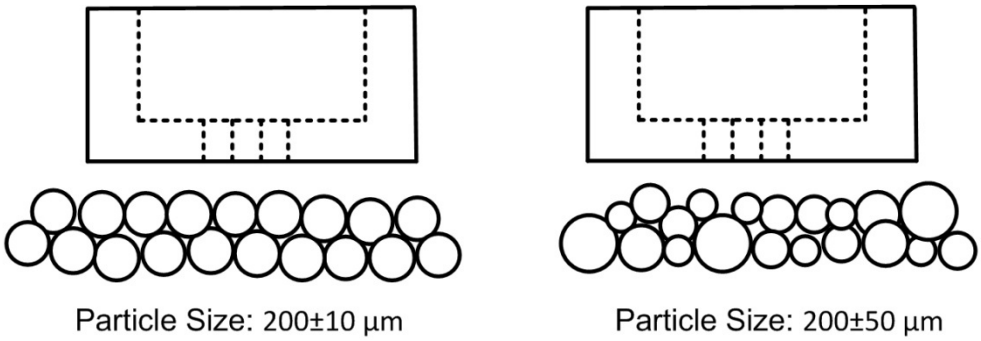

Figure 5-15: Insertion Cap and Different Powder Size Range

Experimental factors were explained during each experiment. For instance, the powder bed surface always should be completely flat and be perfectly parallel to the insertion cap surface; however, these parameters are set in every individual experiment separately. As a result, the method that is applied for flatting the powder surface and paralleling the cap surface to the powder bed surface should be a highly repeatable technique. Determining the zero point of the system in an accurate way without compressing the powders can be assumed as an experimental factor as well.

An important environmental factor that cannot be controlled completely in the employed pilot setups is moisture; however, the final porogen insertion mechanism will be installed in an enclosure with controlled humidity and temperature that in turn control the moisture.

Conclusively, Experiment Number 11 strongly proved that the designed porogen insertion mechanism is capable of picking up a few number of porogens, when the moisture is partially removed. In trials number 2 and 3 of this experiment, the system picked up only 4 porogens which means that all the holes pick up one and only one porogen. The designed system for

generating back pressure in “placing” step worked perfectly and placed the picked up particles easily and nicely. The only issue that was not solved completely in the current project is the stuck particles to the surface of the insertion cap; however, a number of effective parameters on this factor were recognized and some of them were investigated. First of all, by controlling humidity and temperature of the environment, moisture that is the most important factor that causes sticky nature for the particles can be eliminated. Moreover, as discussed earlier in the current section, using particles with more similar sizes can reduce the possibility of sticking particles to the insertion cap. In addition, the used particles in the performed experiments were ground with a coffee grinder, so, as presented in Figure 5-3, they have any arbitrary geometry. Utilizing more precise methods that provide powders with controlled geometries, for example produce spherical particles, can decline the chance of existence of sharp edges and corners, and, subsequently, stuck particles to the surface. At last, imposing vibration to the insertion head after picking up the particles can drop the stuck particles to the surface and leave only the picked up particles by evacuation.

Chapter 6
Conclusions and Future Work

6.1 Conclusion

Design of a novel porogen insertion mechanism is presented in this thesis. To facilitate this design, the following steps were completed.

1. A literature review on bone scaffolds and the role of porosity and pore distribution on the success of the tissue engineered bone scaffolds was conducted.

2. Since, to the best of the author's knowledge, providing heterogeneous pore distribution for the scaffolds has been recognized as an open problem in the field of tissue engineering, a mechanism that is capable of inserting porogens at pre-designed locations within the scaffold structure was developed in the current work. The proposed porogen insertion mechanism works synchronized with a three-dimensional printing (3DP) machine and provides customized porosity and pore distribution for the fabricated scaffolds. This machine has the capability of working with some other types of solid freeform fabrication (SFF) systems as well.

3. A prediction of bio-mechanical properties of a dual-porous scaffold composed of a cartilage substrate and a bone scaffold was conducted using the finite element technique. To judge the effect of two distinct porous architectures on strength and capability of cell ingrowth stimulation of the resultant structure, stiffness and principal strain histogram of the single and the dual-porous scaffolds were compared. Subsequently, to conquer the software limitations in modeling the actual size of the dual-porous scaffold, the results' (apparent stiffness and principal strain histogram) independency of size of the model was investigated as well. It can be concluded that the investigated mechanical properties of the dual-porous scaffold at 20% size ratio can be used to infer the mechanical properties of the actual size of the part.

4. Several alternative designs were presented for the porogen insertion mechanism, then, by employing the "value matrix" method, the best design was selected among them. The

proposed alternatives can be classified in two major categories including actuator-based and pneumatic-based systems. In actuator-based systems, a mechanical actuator opens and closes the path of porogen particles from a porogen reservoir to the build chamber with a designed frequency, in a way that, the porogens are brought from the porogen reservoir and inserted only at the pre-designed locations of the build chamber. Pneumatic-based systems utilize a pneumatic driven mechanism for picking up the porogens from the porogen reservoir and placing them at the pre-designed locations.

5. In both types of systems, possibility of inserting more than one porogen at a time was investigated.

6. the two proposed groups of designs are only concerned with placing the porogen particles on the build chamber; therefore, development of a pushing mechanism for jamming the particles into the compacted powder bed, which will form the main body of the fabricated scaffold, was taken into account as well.

7. Significant advantages of the pneumatic-based system over its actuator-based alternatives make it an excellent solution for facilitating the required application. As a result, the pneumatic-based system was selected in this thesis. Afterwards, a complete detail design of this system was presented, the required descriptions and sketches for fabricating the custom-made parts of the system were provided, and those parts that can be found off the shelf were selected and introduced by their catalogues.

8. Moreover, appropriate experiments were designed and performed, in order to investigate the feasibility of the designed system. To accomplish this goal, the required pilot test setups were developed successfully. The conducted experiments proved that the proposed mechanism is capable of picking up and inserting porogens in a controlled fashion. For instance, in Experiment Number 11, the system picked up only 4 porogens, which corresponds to one and only one porogen at each hole, from the distance of 190 μm and 30 μm when the line pressure was 1 bar. Also, in Experiment Number 12, the system picked up 4 particles from the distance of 210 μm under the line pressure of 1 bar.

6.2 Future Work

Based on the achievements of the preceding chapters, the future work for completion of the proposed system is described in followings.

1) Through the performed experiments in Chapter 5, several parameters such as powders size and shape, method of determining the zero point of the system, flatness of the porogens surface in the reservoir, etc. were nominated as effective parameters on the performance of the porogen insertion system. These parameters dictate some specific conditions for the system, and implementing some of these conditions calls for re-design of the porogen reservoir and the porogen feeding mechanism. For instance, it was claimed that the powder bed surface always should be completely flat and be perfectly parallel to the insertion cap surface; however, the porogen reservoir and the feeding mechanism that are currently designed and presented in section 4.5.3 provide a fairly flat surface for the powder bed, and there is no mechanism to guaranty that the powder bed is perfectly flat and completely parallel to the insertion cap surface. On the other hand, performing more experiments in controlled humidity and temperature environment can verify if these parameters have really significant effect or not. In other words, if the moisture is removed from the system completely, the porogen insertion head may be able to pick up the porogens from farther distances; therefore, the angle between the insertion cap surface and the powder bed would be negligible compare to the distance between them. Such experiments are also required for determining the optimum line pressure and picking up distance.

2) According to section 4.5.2.1, the insertion head should be brought very close to the compacted powder bed for inserting the picked up porogens during “placing” step, so the porogens are placed on the powder bed slowly, and they do not change the powders’ distribution in the build chamber. As a result, since during this process the holes of the insertion cap are very close to the build chamber, any leakage in those holes may suck in or blow out the compacted powders and change their distribution. Consequently, holes with small sizes should be fabricated in the insertion cap. In order to justify these arguments, appropriate experiments should be conducted with

the aim of investigating the effect of leakage on the compacted powder bed, as well as, determining the correlation between the porogen size, the insertion distance, and the density of the compacted powders, so as to avoid changing the distribution of the compacted powders.

3) According to the results of the recommended experiments, design and selection of the different parts of the system need to be updated. For example, after optimizing the line pressure and the distance for picking up one porogen at every hole, the flow rate/pressure changes during the process can be calculated, and, therefore, the appropriate sensor that is sensitive enough to measure the deviations of flow rate/pressure in the system can be selected.

4) Using the unified-head design has some advantages as discussed in section 4.6.4. However, the pushing head has to impose force to the particles for jamming them into the compacted powder layers. Since this force is applied several times for fabricating every single part, investigating the effect of such a force on the surface quality of the head is recommended.

5) Effect of the jammed porogens into the compacted powder layers on the distribution of the particles in these layers and the resulted stresses should be investigated analytically. For this purpose, the model that is proposed in Chapter 3 can be applied to provide a good estimation of the real scaffold.

6) the biomechanical properties of a scaffold with macro-pores can be compared with the biomechanical properties of a scaffold without macro-pores through finite element analysis to assess the effect of macro-pores on these properties. The modeling approach that is presented in this thesis (in Chapter 3) can be applied to find the optimum porosity for a bone scaffold with a heterogeneous internal structure, based on the biomechanical properties of the bone scaffold. Such findings can be confirmed through experiments by utilizing the generated scaffolds by the porogen insertion mechanism.

Bibliography

[1] Mikos, A.G., Herring, S.W., Ochareon, P., Elisseeff, J., Lu, H.H., Kandel, R., Schoen, F.J., Toner, M., Mooney, D., Atala, A., Van Dyke, M.E., Kaplan, D., Novakovic, G.V., "Engineering Complex Tissues", TISSUE ENGINEERING Volume 12, Number 12, 2006.

[2] ACFNEWSOURCE, "Canadian Scientists are Developing a New Way to Heal Bones Faster", 2003.
Available on: http://www.acfnewsource.org/science/bone_scaffold.html

[3] Encyclopedia of Surgery, definition of "Bone Grafting"
Available on: http://www.surgeryencyclopedia.com/A-Ce/Bone-Grafting.html

[4] Jančář, J., Slovíková, A., Amler, E., Krupa, P., Kecová, H., Plánka, L., Gál, P., Nečas, A., "Mechanical Response of Porous Scaffolds for Cartilage Engineering", Physiological Research, 56 (Suppl. 1): S17-S25, 2007.

[5] HOLLISTER, S.J., "Porous scaffold design for tissue engineering", nature materials, VOL 4, JULY 2005.

[6] Blitch, E.L., Ricotta, P.J., "Introduction to Bone Grafting", the Journal of Foot and Ankle Surgery 35(5):458-462, 1996.

[7] Sachlos, E., Czernuszka, J., "Making tissue engineering scaffolds work. Review: the application of solid freeform fabrication technology to the production of tissue engineering scaffolds (discussion 39–40)", Eur Cell Mater, 5, pp. 29–39, 2003.

[8] Yang, S., Leong, K.F., Du, Z., and Chua, C.K., "the design of scaffolds for use in tissue engineering. Part I. Traditional factors," Tissue Engineering, vol. 7, (6), pp. 679-689, 2001.

[9] Gibson, L., Harvard-MIT Division of Health Sciences and Technology, Course Note

"Structure-Property Relationships for Tissue Engineering Scaffolds", HST.523J: Cell-Matrix Mechanics.

[10] Hollister, S. J., "Designer Scaffolds for Tissue Reconstruction", presented at: International Workshop for Biomanufacturing, Tsinghua University, Beijing, China, 2005.

[11] Shanjani Y., Chanderashekar N., Toyserkani E., "Prediction of bio-mechanical properties of bone implant scaffold," Copyright © 2007 by ASME.

[12] Pourmohammadali H., "Application of Scaffolds for Cartilage Tissue engineering" , Department of MME, University of Waterloo, Unpublished.

[13] Karageorgiou, V., Kaplan, D., "Porosity of 3D biomaterial scaffolds and osteogenesis", Biomaterials 26, 5474–5491, 2005.

[14] Dellinger, J.G., Cesarano, J., and Jamison, R.D., "Robotic deposition of model hydroxyapatite scaffolds with multiple architectures and multiscale porosity for bone tissue engineering", Wiley InterScience, DOI: 10.1002/jbm.a.31072, 2007.

[15] Hollister, S.J., and Lin, C.Y., "Computational design of tissue engineering scaffolds", Comput. Methods Appl. Mech. Eng. 196, pp. 2991–2998, 2007.

[16] Sogutlu, S., and Koc, B., "Stochastic Modeling of Tissue Engineering Scaffolds with Varying Porosity Levels", Computer-Aided Design & Applications, Vol. 4, No. 5, pp. 661-670, 2007.

[17] Moore T., "Design and synthesis of biodegradable thermoplastic polyurethanes for tissue engineering ", PhD thesis, Swinburne University of Technology, 2005.

[18] Shanjani, Y., “Solid Freeform Fabrication of Osteochondral Scaffolds with a Controlled Porosity”, A research proposal presented to the University of Waterloo Department of Mechanical and Mechatronics Engineering Waterloo, Ontario, Canada, 2008.

[19] Chen, G., Ushida T., and Tateishia T., “Preparation of poly(-lactic acid) and poly(-lacticcoglycolic acid) foams by use of ice microparticulates”, Biomaterials, 22, pp. 2563-2567, 2001.

[20] Thomson, R.C., Shun, A.K., Yaszemski, M.J., and Mikos, A.G., “Polymer Scaffold Processing”, chapter 21 of Principles of Tissue engineering, second edition, Academic Pres., 2000.

[21] Yeong, W.Y., Chua, C.K., Leong, K.F., and Chandrasekaran, M., "Rapid prototyping in tissue engineering: challenges and potential," *Trends in Biotechnology,* vol. 22, (12), pp. 643-652, 2004.

[22] CASTLE ISLAND’S, Worldwide Guide to Rapid Prototyping, “the Most Important Commercial Rapid Prototyping Technologies at a Glance”.
Available at: http://home.att.net/~castleisland/rp_int1.htm

[23] Gbureck, U., Hölzel, T., Klammert, U., Würzler, K., Müller, F.A., and Barralet, J.E., “Resorbable Dicalcium Phosphate Bone Substitutes Prepared by 3D Powder Printing”, Advanced Functional Materials, vol. 17, pp. 3940-3945, 2007.

[24]Gbureck, U., Hölzel, T., Biermann, I., Barralet, J., and Grover, L., “Preparation of tricalcium phosphate/calcium pyrophosphate structures via rapid prototyping”, Journal of Materials Science: Materials in Medicine, vol. 19, pp. 1559-1563, 2008.

[25] Weinand, C., Pomerantseva, I., Neville, C.M., Gupta, R., Weinberg, E., Madisch, I., Shapiro, F., Abukawa, H., Troulis, M.J., and Vacanti, J.P. , “Hydrogel-[beta]-TCP scaffolds and stem cells for tissue engineering bone”, Bone, vol. 38, pp. 555-563, 2006.

[26] Leukers, B., Gülkan, H., Irsen, S., Milz, S., Tille, C., Schieker, M., and Seitz, H., "Hydroxyapatite scaffolds for bone tissue engineering made by 3D printing", Journal of Materials Science: Materials in Medicine, vol. 16, pp. 1121-1124, 2005.

[27] Taboas, J., Maddox R.D., Krebsbach P.H., Hollister S.J., and Chu T.M.G., "Controlled Local/Global and Micromacro-Porous 3D Plastic, Polymer and Ceramic/Cement Composite Scaffold Fabrication and Applications thereof", United States Patent, US 7,087,200 B2, Aug. 8, 2006.

[28] Lee, M., Dunn, J.C.Y., and Wu, B.M., "Scaffold fabrication by indirect three-dimensional printing, Biomaterials, vol. 26, pp. 4281-4289, 2005.

[29] Tay, B.Y., Zhang, S.X., Myint, M.H., Ng, F.L., Chandrasekaran, M., and Tan, L.K.A., "Processing of polycaprolactone porous structure for scaffold development, Journal of Materials Processing Technology, vol. 182, pp. 117-121, 2007.

[30] Lam, C.X.F., Moa, X.M., Teoha, S.H., and Hutmacher, D.W., "Scaffold development using 3D printing with a starch-based polymer" Materials Science and Engineering: C, vol. 20, (1-2), pp. 49-56, 2002.

[31] Sherwood J.K., Riley S.L., Palazzolo R., Brown, S.C., Monkhouse, D.C., Coates, M., Griffith, L.G., Landeen, L.K., Ratcliffe, A., "A three-dimensional Osteochondral composite scaffold for articular cartilage repair", Biomaterials 23: 4739–4751, 2002.

[32] Schwebel, Goetz & Sieben Personal Injury Attorneys, "Fractures/Broken Bones Data", Available on: http://www.schwebel.com/file/Fractures(1024).pdf

[33] Chandrashekar N., Course notes of "ME 598- Special Topics in Mechanical Engineering", Chapter 4 (the Biology and Mechanics of Bone), Department of Mechanical and Mechatronics Engineering, University of Waterloo, Winter 2008.

[34] nano werk, “Nanotechnology Scaffolds Aid Bone Grafts and Implants”, 2008
Available on: http://www.nanowerk.com/spotlight/spotid=8030.php

[35] Agency for Toxic Substances and Disease Registry, cancer fact sheet, 2002
Available on: http://www.atsdr.cdc.gov/COM/cancer-fs.html

[36] Blitch, E.L., Ricotta, P.J., “Introduction to Bone Grafting”, the Journal of Foot and Ankle Surgery 35(5):458-462, 1996.

[37] Nataraj, C., Silveira, E., Clark, J., Yonchek, J., Kirk, J., “Effect of Terminal Gamma Sterilization on Osteoinductivity”, ©2008 by RTI Biologics, Inc. (RTI), Reprinted by Zimmer, Inc. with permission of RTI, 2009.

[38] Malmström, J., Tandläkare, L., “On Bone Regeneration In Porous Bioceramics, Studies in humans and rabbits using freeform fabricated scaffolds”, Biomaterials Laboratory, Porto University, Porto, Portugal 2007.

[39] Mikos, A.G., and Temenoff, J.S., “Formation of highly porous biodegradable scaffolds for tissue engineering”, EJB Electronic Journal of Biotechnology ISSN: 0717-3458, Vol.3 No.2, Issue of August 15, 2000.

[40] Enderle, J., Blanchard, S., and Bronzino, J., “Introduction to Biomedical Engineering”, Elsevier academic Press, Second Edition, 2005.

[41] Mikos, A.G., Thorsen, A.J. , Czerwonka, L.A., Bao, Y., Langer, R., Winslow, D.N., and Vacanti, J.P., “Preparation and characterization of poly(L-lactic acid) foams”, POLYMER Volume 35 Number 5, 1994.

[42] Ghosh, S., Viana, J.C., Reis, R.L., and Mano, J.F., “the double porogen approach as a new technique for the fabrication of interconnected poly(L-lactic acid) and starch based biodegradable scaffolds”, J Mater Sci Mater Med. 2007.

[43] Mooney, D.J., Baldwin, D.F., Suh, N.P., Vacanti, J.P. and Langer, R., "Novel approach to fabricate porous sponges of poly(D,L-lactic-co-glycolic acid) without the use of organic solvents", Biomaterials 17, pp.1417-1422, 1996.

[44] CASTLE ISLAND'S, Worldwide Guide to Rapid Prototyping, "Functional Parts and Tools from Additive Fabrication".
Available at: http://home.att.net/~castleisland/tl_10.htm

[45] Chua, C.K., Leong, K.F., and Lim, C.S., "Rapid Prototyping principles and applications", Second Edition, World Scientific.

[46] Wei, C., "Rapid Fabrication Techniques for Anatomically-Shaped Calcium Polyphosphate Substrates for Implants to Repair Osteochondral Focal Defects ", thesis for the degree of Master of Applied Sciences in Mechanical and Mechatronics Engineering, University of Waterloo, Canada, 2007.

[47] CASTLE ISLAND'S, Worldwide Guide to Rapid Prototyping, "Fused Deposition Modeling".
Available at: http://home.att.net/~castleisland/fdm.htm

[48] CASTLE ISLAND'S, Worldwide Guide to Rapid Prototyping, "Laminated Object Manufacturing".
Available at: http://home.att.net/~castleisland/lom.htm

[49] Ge, Z., Jin, Z., and Cao, T., "Manufacture of degradable polymeric scaffolds for bone regeneration", Biomed. Mater. 3, 022001 (11pp), 2008.

[50] CASTLE ISLAND'S, Worldwide Guide to Rapid Prototyping, "Three Dimensional Printing".
Available at http://home.att.net/~castleisland/3dp.htm

[51] Szűcs, T.D., “Production of Hard Tissue Scaffolds Using Three-Dimensional Printing Method “, requirement of the award of degree of MASTER OF ENGINEERING (MEng) by research from DUBLIN CITY UNIVERSITY, 2008.

[52] Hamilton, D.J., “Formation of a nucleus pulposus-cartilage endplate construct *in vitro*”, Biomaterials 27, pp. 397–405, 2006.

[53] Omelon, S., “the effect of porous calcium polyphosphate processing conditions on its degradation and osteoconductivity”, Eighth International Conference on the Chemistry and Biology of Mineralized Tissues, 2004.

[54] Wan, C.K., Zhao, C.X., Chen, C.S., Tang, X.C.W., and Chen, Y.W., "Fabrication and characterization of porous calcium polyphosphate scaffolds," J Mater SCI, vol. 41, pp. 2429-2434, 2006.

[55] Waldman, S.D., Spiteri, C.G. , Grynpas, M.D., Pilliar, R.M., Hong, J., and Kandel, R.A., "Effect of bio-mechanical conditioning on cartilaginous tissue formation *in vitro*," J. Bone Joint Surg. Am., vol. 85-A, pp. 101-105, 2003.

[56] Kandel, R.A., Grynpas, M., Pilliar, R., Lee, J., Wang, J., Waldman, S., Zalzal, P., and Hurtig, M., "Repair of osteochondral defects with biphasic cartilage-calcium polyphosphate constructs in a sheep model," Biomaterial, vol. 27, pp. 4120-4131, 2006.

[57] Baksh, D., and Davies, J.E., "Three-dimensional matrices of calcium polyphosphates support bone growth *in vitro* and *in vivo*," J. Mater. Sci., vol. 9, pp. 743-748, 1998.

[58] Tarek, Y.E.S., Pilliar, R.M., and McCulloch, A.G., "Attachment, spreading, and matrix formation by human gingival fibroblasts on porous-structured titanium alloy and calcium polyphosphate substrates," Biomed. Mater. Res., vol. 61, pp. 482-492, 2002.

[59] Lee, Y.M., Seol, Y.G., Lim, Y.K., Kim, S., Han, S.B., Rhyu, I.C., Baek, S.H., Heo, S.J., Choi, J.Y., Klokkevold, P.R., and Chung, C.P., "Tissue-engineered growth of bone by marrow cell transplantation using porous calcium metaphosphate matrices," Biomed. Mater. Res., vol. 54, pp. 216-233, 2000.

[60] Pilliar, R.M., Filiaggi, M.J., Wells, J.D., Grynpas, M.D., and Kandel, R.A., "Porous calcium polyphosphate scaffolds for bone substitution applications - *in-vitro* characterization," Biomaterials, vol. 22, pp. 963-972, 2oo1.

[61] Grynpas, M.D., Pilliar, R.M., Kandel, R.A., Renlund, R., and Filiaggi, M., "Porous calcium polyphosphate scaffolds for bone substitute applications - *in vivo* studies," Biomaterials, vol. 23, pp. 2063-2070, 2003.

[62] Waldman, S.D., Grynpas, M.D., Pilliar, R.M., and Kandel, R.A., "Characterization of cartilaginous tissue formed on calcium polyphosphate substrates *in vitro*," J. Biomed. Mater. Res., vol. 62, pp. 323-330, 2002.

[63] Waldman, S.D., Spiteri, C.G., Grynpas, M.D., Pilliar, R.M., and Kandel, R.A., "Long-term intermittent compressive stimulation improves the composition and mechanical properties of tissue-engineered cartilage," Tissue Engineering, vol. 10, pp. 1323-1331, 2004.

[64] Waldman, S.D., Spiteri, C.G., Grynpas, M.D., Pilliar, R.M., and Kandel, R.A., "Long-term intermittent shear deformation improves the quality of cartilaginous tissue formed *in vitro*," J. Orthopaedic Res., vol. 21, pp. 590-596, 2003.

[65] Ignatius, A., Blessing, H., Liedert, A., Schmidt, C., Neidlinger-Wilke, C., Kaspar, D., Friemert, B., and Claes, L., "Tissue engineering of bone: effects of mechanical strain on osteoblastic cells in type I collagen matrices," Biomaterials, 26(3), pp. 311–318, 2005.

[66] Cleynenbreugel, T.,J Schrooten, Hans Van Oosterwyck, and Jos Vander Sloten, "Micro-CT-based screening of bio-mechanical and structural properties of bone tissue engineering scaffolds," Med Bio Eng Comput, 44, pp. 517-525, 2006.

[67] Cleynenbreugel, T.V., Schrooten, J., Oosterwyck, H.V., and Sloten, J.V., "Bio-mechanical Design of porous structures for bone growth Stimulation," European Cells and Materials, 5, Suppl. 2, pp. 94-95, 2003.

[68] Telen, S., Barthelat, F., and Brinson, L.C., "Mechanics considerations for micro-porous titanium as an orthopaedic implant material," J. Biomed Mater Res A., 69(4), pp.601-610, 2004.

[69] Kandel, R., Seguin, C., Hamilton, D., Grynpas, M., Pilliar, R., and Hurtig, M., "Toward bioengineering a scaffold-free nucleus pulposus," European Cells and Materials Vol. 10 Suppl. 3, page 42, 2005.

[70] Yuehuei, H., and Draughn, R.A., "Mechanical Testing of bone and the bone Implant Interface," CRC Press LLC, pp.181, 2000.

[71] Cleynenbreugel, V. T., Oosterwyck, V. H., Sloten, V. J., "Trabecular bone scaffolding using a biomimitic approach," Journal of Materials Science: Materials in Medicine, 13, pp. 1245-1249, 2002.

[72] Hollister, S., Brennan, J., and Kikuchi, N., "A homogenization sampling procedure for calculating trabecular bone effective stiffness and tissue level stress," J. of Bio-mech, 27(4), pp. 433–444, 1994.

[73] Duncan, R., and Turner, C., "Mechanotransduction and the functional response of bone to mechanical strain," Calcified Tissue International 57(5), pp. 344–358, 1995.

[74] Neathery, R. F., Applied strength of materials, New York, John Wiley & Sons, 1982.

[75] Wang, X., and Ni, Q., "Determination of cortical bone porosity and pore size distribution using a low field pulsed NMR approach", Journal of Orthopaedic Research 21, pp. 312-319, 2003.

[76] physicsworld.com, "NMR breakthrough for bone fracture", 2003.

Available at: http://physicsworld.com/cws/article/news/18528

[77] Bronner, F., Farach-Carson, M.C., Mikos, A.G., "Engineering of Functional Skeletal Tissues", Chapter 7: Migliaresi, C., Motta, A., DiBenedetto, A.T., "Injectable Scaffolds for Bone and Cartilage Regeneration", London: Springer, 2007.

[78] PI catalog, "Precision positioning stages and actuators Hexapod 6-axis alignment system", updated 2008.

[79] Catalog of Vacuum Generators, electropneumatic, 1.2, FESTO Company, 2007/10 – Subject to change – Products 2008.

[80] TEKNOCRAFT INC., "venture vacuum generators, what they are and how to design them into your system".
Available at: http://www.iqvalves.com/vacuumsysdesignguide.aspx

[81] ANVER, "Vacuum Pumps and Vacuum Generators", 2009.
Available at:
http://www.anver.com/document/vacuum%20components/vacuum%20generators/QVP%20Generators/modular_venturi_q-vp10.htm

[82] Mecadi, "PVA Powder", 2009.
Available at:
http://www.mecadi.com/en/chemicals_processing/polymers_shop/PVA_Powder/

[83] Groot, J.R., Nagohosian, J., Prisciandaro, J., and Butchko, D., "Introduction to Pneumatics and Pneumatic Circuit Problems for FPEF Trainer", Fluid Power Education Foundation, Available on: http://www.fpef.org

[84] Han, W., and Pryputniewicz, R.J., "Investigations of laser percussion drilling of small holes on thin sheet metals", Laser Beam Shaping V, Proceedings of SPIE Vol. 5525, 2004.

[85] Rizvi, N., Milne, D., Runisby, P., and Gower, M., "Laser Micromachining – New Developments and Applications", In Laser Applications in Microelectronic and Optoelectronic Manufacturing V, Proceedings of SPIE Vol. 3933, 2000.

[86] Clarke, J.A., Metalase Technologies, LLC, and Profeta, J.A., Aerotech, Inc., "Laser Micro-Drilling Applications".

[87] Zhu, X., Naumov, A.Y., Villeneuve, D.M., and Corkum, P.B., "Influence of laser parameters and material properties on micro-drilling with femtosecond laser pulses", Appl. Phys.A 69, pp. 367–371, 1999.

[88] Chichkov, B.N., Momma, C., Nolte, S., Alvensleben, F.V., and Tunnermann, A., "Femtosecond, picosecond and nanosecond laser ablation of solids", Appl. Phys. A 63, pp. 109-115, 1996.

[89] Karnakis, D., Rutterford, G., and Knowles, M.R.H., "High power DPSS laser micromachining of stainless steel and silicon for device Singulation", Oxford Lasers Ltd., Unit 8, Moorbrook Park, Didcot, Oxfordshire OX11 7HP, UK.

[90] COLLTEC, "Polyvinyl butyral", 2009.
Available at: http://www.colltec.de/Home_english/Polyvinyl_butyral/polyvinyl_butyral.html

[91] WIKIPEDIA, "6061 aluminium alloy"
Available at: http://en.wikipedia.org/wiki/6061_aluminium_alloy

Appendices

Appendix A

System Components

Schematic of Reservoir Holder

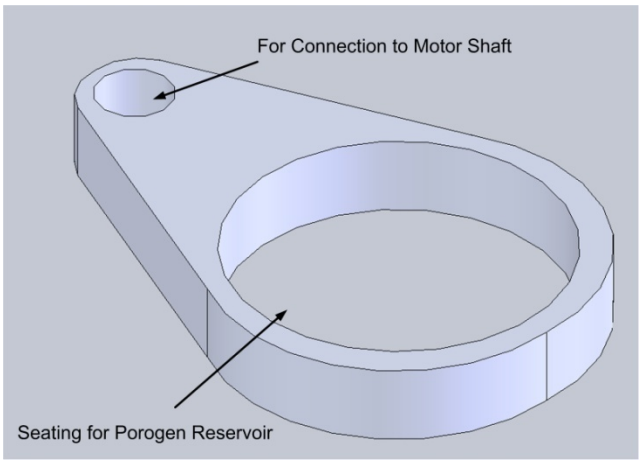

Part for Connecting Reservoir Holder to Motor Shaft

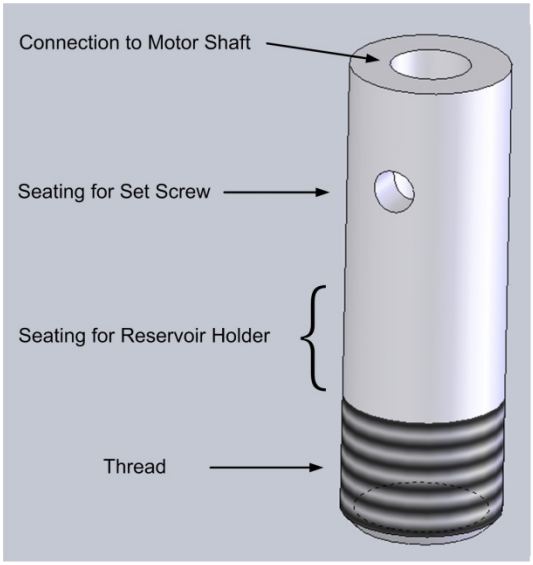

Appendix B

Parts Drawings

2D Sketch of Porogen Reservoir

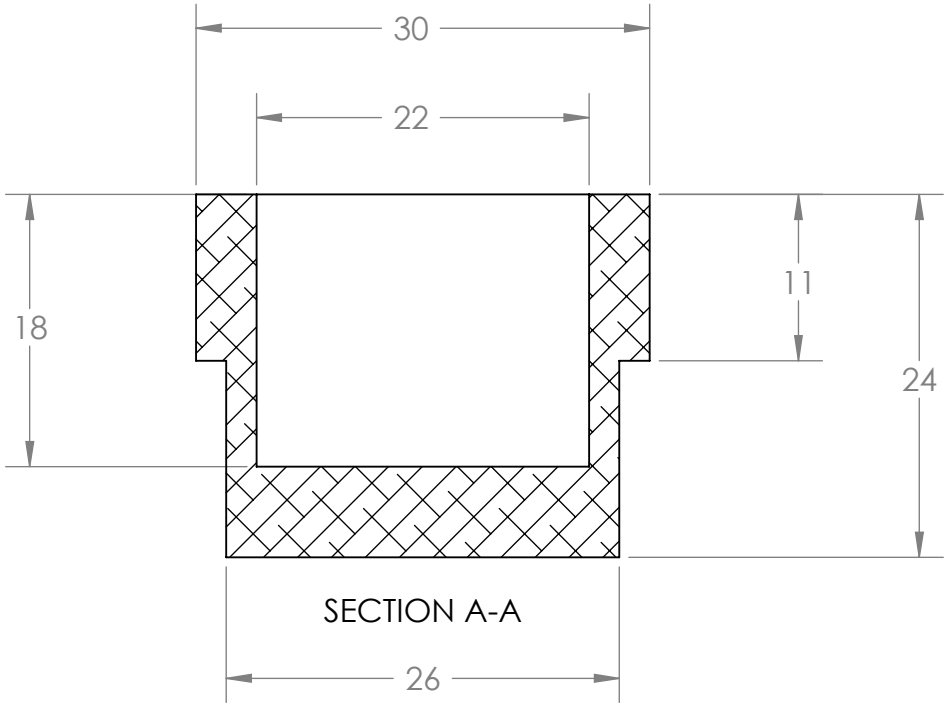

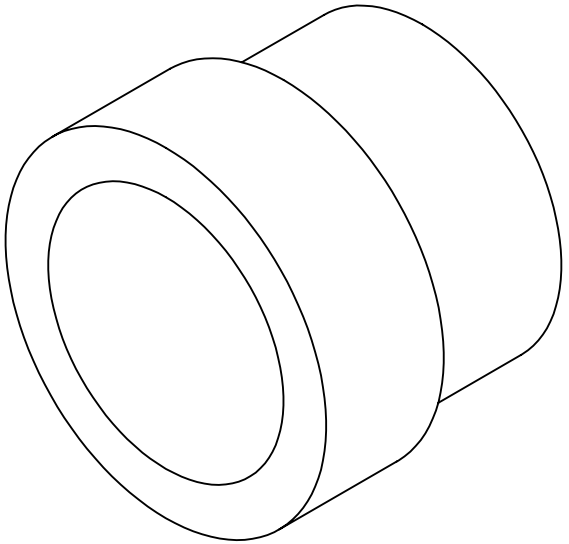

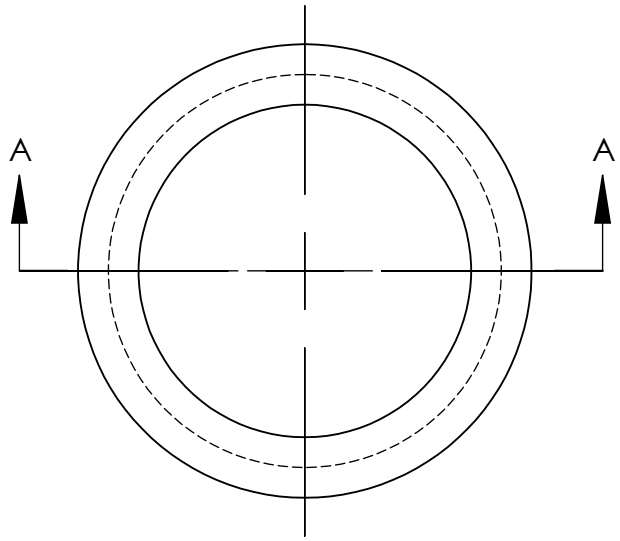

		NAME	DATE
UNLESS OTHERWISE SPECIFIED:			
DIMENSIONS ARE IN MILLIMETERS TOLERANCES: ZERO PLACE DECIMAL ±1mm ONE PLACE DECIMAL ± 0.1mm TWO PLACE DECIMAL ±0.01mm ANGULAR: MACH ± BEND ±	DRAWN		
	CHECKED		
	ENG APPR.		
	MFG APPR.		
	Q.A.		
INTERPRET GEOMETRIC TOLERANCING PER:	COMMENTS:		
MATERIAL ALUMINUM			
FINISH DO NOT SCALE DRAWING			

TITLE:

POROGEN RESERVOIR

SIZE	DWG. NO.	REV
A		
SCALE: 2:1	WEIGHT:	SHEET 1 OF 1

5 4 3 2 1

2D Sketch of Reservoir Holder

NOTES:
1. DEBURR ALL EDGES

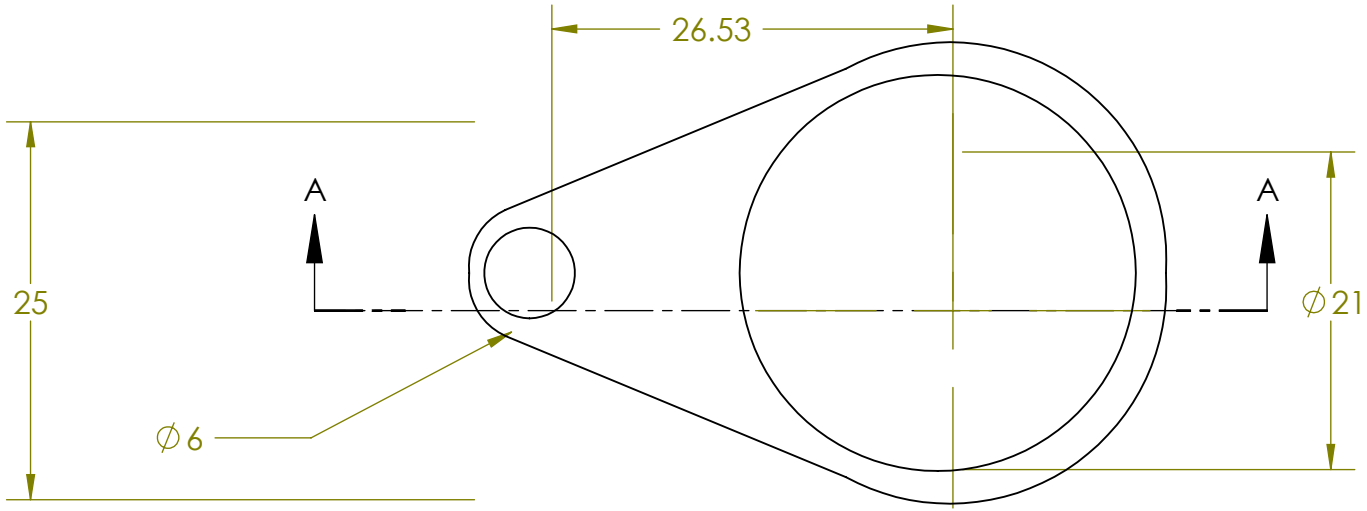

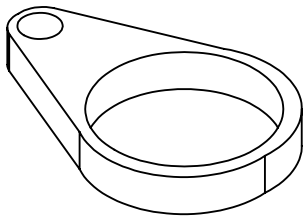

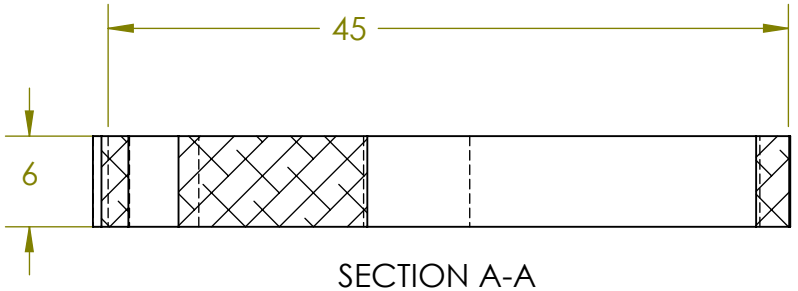

SECTION A-A
SCALE 2 : 1

UNLESS OTHERWISE SPECIFIED:		NAME	DATE
DIMENSIONS ARE IN MILLIMETERS TOLERANCES: ZERO PLACE DECIMAL ±1mm ONE PLACE DECIMAL ± 0.1mm TWO PLACE DECIMAL ±0.01mm ANGULAR: MACH ± BEND ±	DRAWN		
	CHECKED		
	ENG APPR.		
	MFG APPR.		
INTERPRET GEOMETRIC TOLERANCING PER:	Q.A.		
MATERIAL ALUMINUM	COMMENTS:		
FINISH			
DO NOT SCALE DRAWING			

TITLE: RESERVOIR HOLDER

SIZE	DWG. NO.	REV
A		
SCALE: 1:1	WEIGHT:	SHEET 1 OF 1

5 4 3 2 1

2D Sketch of Connecting Part

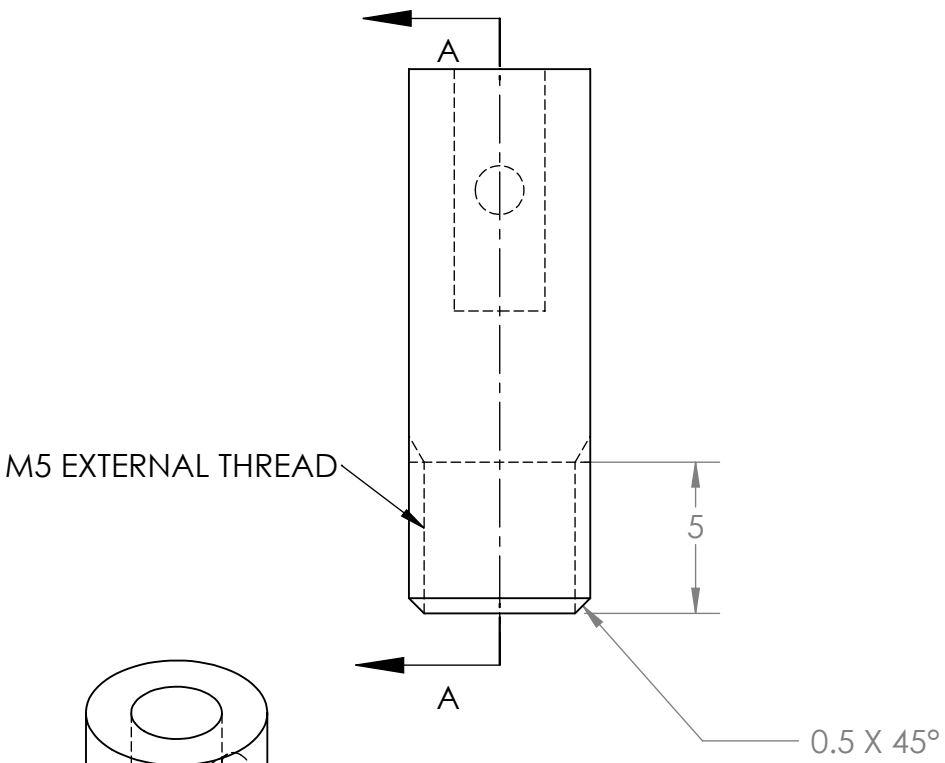

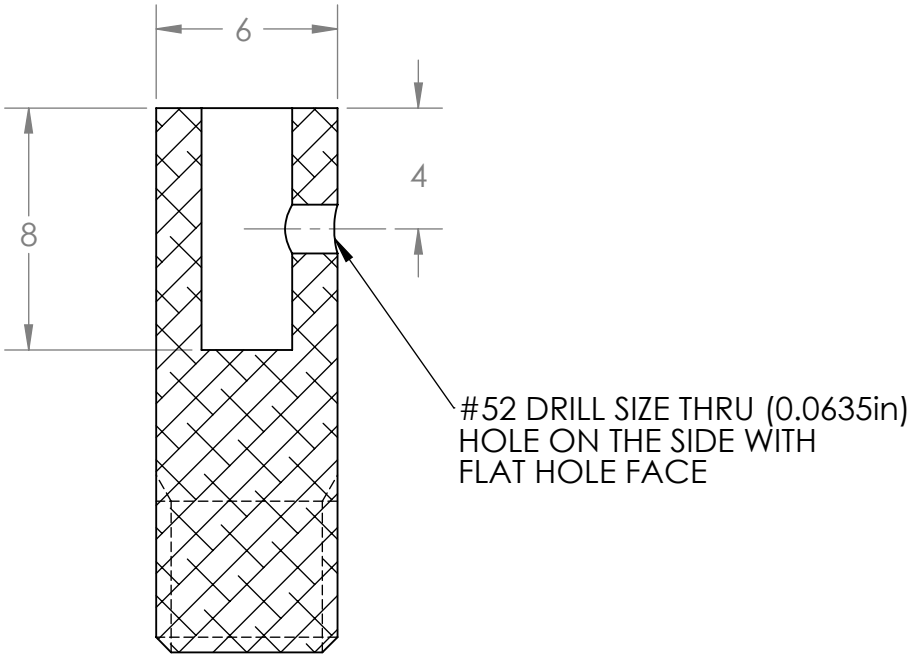

SECTION A-A
SCALE 4 : 1

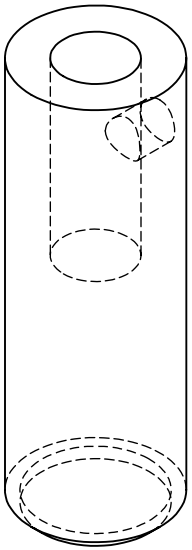

		NAME	DATE
UNLESS OTHERWISE SPECIFIED:			
DIMENSIONS ARE IN MILLIMETERS TOLERANCES: ZERO PLACE DECIMAL ±1mm ONE PLACE DECIMAL ± 0.1mm TWO PLACE DECIMAL ±0.01mm ANGULAR: MACH ± BEND ±	DRAWN		
	CHECKED		
	ENG APPR.		
	MFG APPR.		
INTERPRET GEOMETRIC TOLERANCING PER:	Q.A.		
MATERIAL ALUMINUM	COMMENTS:		
FINISH			
DO NOT SCALE DRAWING			

TITLE:

SIZE	DWG. NO.	REV
A	Part5	
SCALE: 1:1	WEIGHT:	SHEET 1 OF 1

5 4 3 2 1

2D Sketch of Bracket-Shape Motor Support

NOTES:
1. DEBURR ALL EDGES

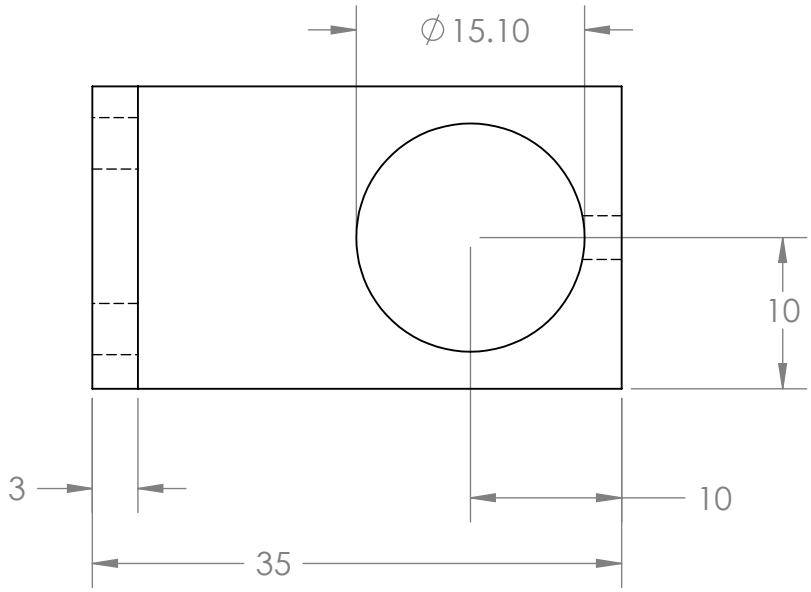

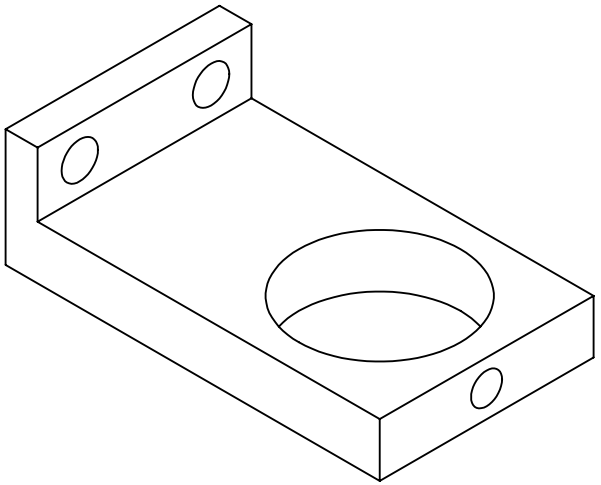

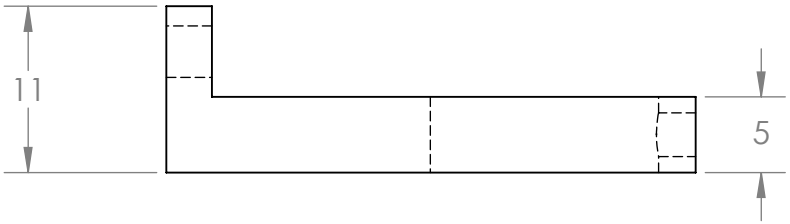

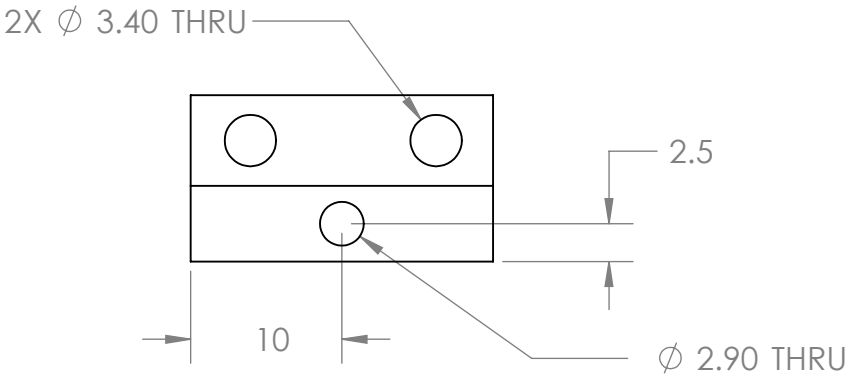

UNLESS OTHERWISE SPECIFIED:		NAME	DATE
DIMENSIONS ARE IN MILLIMETERS TOLERANCES: ZERO PLACE DECIMAL ±1mm ONE PLACE DECIMAL ± 0.1mm TWO PLACE DECIMAL ±0.01mm ANGULAR: MACH ± BEND ±	DRAWN		
	CHECKED		
	ENG APPR.		
	MFG APPR.		
INTERPRET GEOMETRIC TOLERANCING PER:	Q.A.		
MATERIAL ALUMINUM	COMMENTS:		
FINISH DO NOT SCALE DRAWING			

TITLE:

RESERVOIR MOTOR PLATE

SIZE	DWG. NO.	REV
A		

SCALE: 2:1 | WEIGHT: | SHEET 1 OF 1

5 4 3 2 1

2D Sketch of Insertion Rod

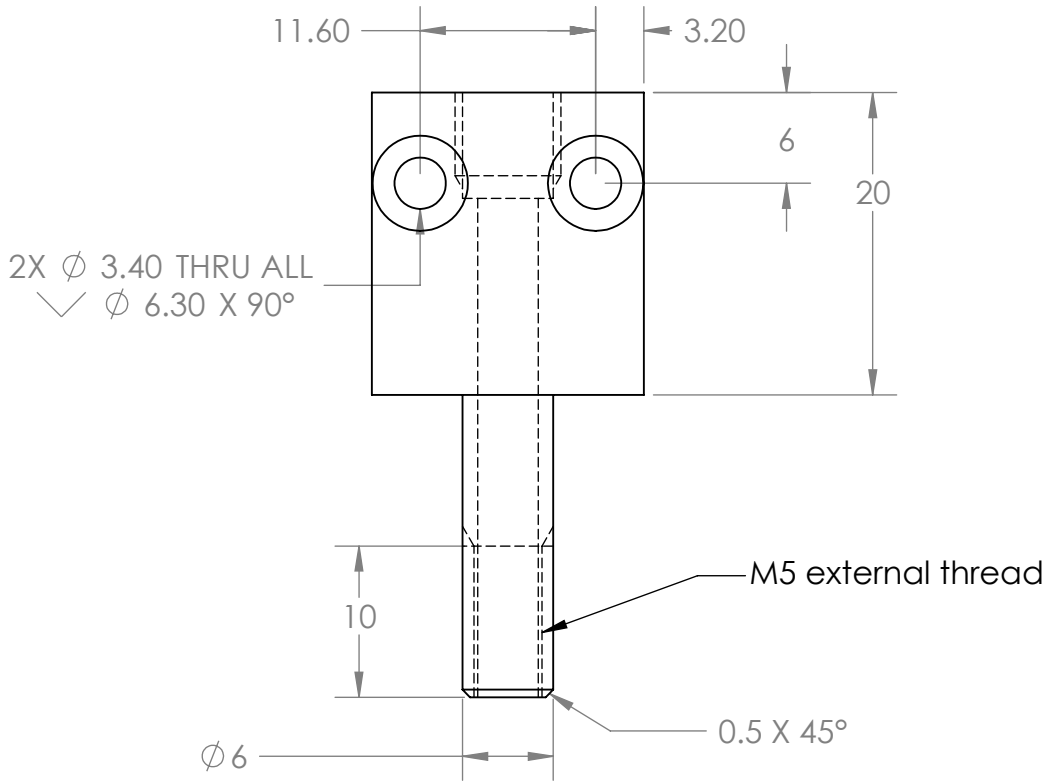

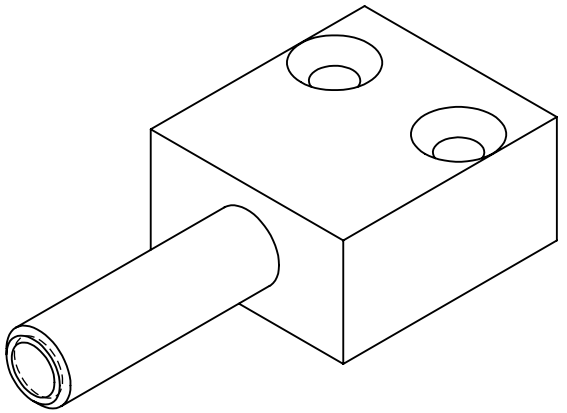

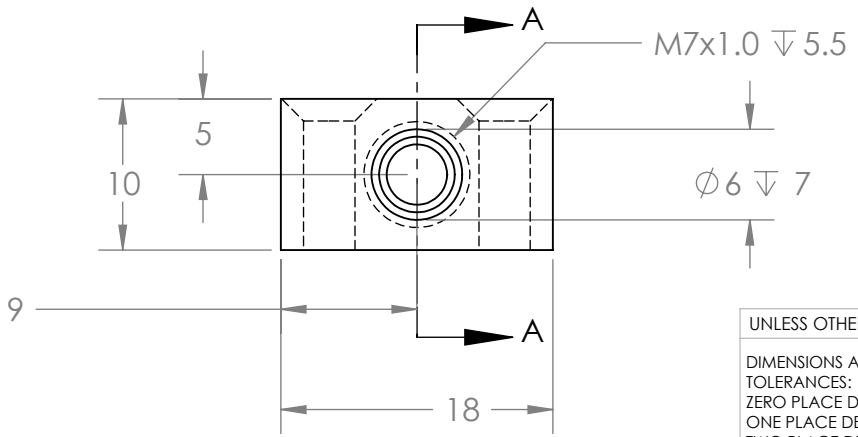

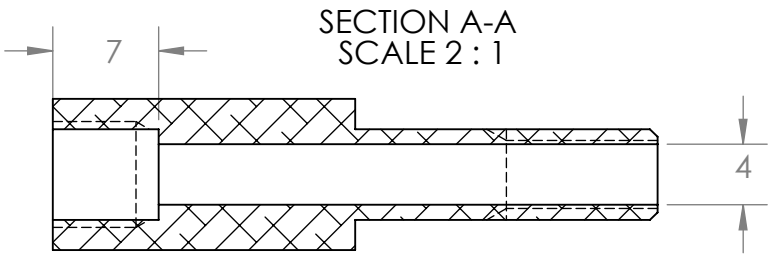

UNLESS OTHERWISE SPECIFIED:		NAME	DATE
DIMENSIONS ARE IN MILLIMETERS TOLERANCES: ZERO PLACE DECIMAL ±1mm ONE PLACE DECIMAL ± 0.1mm TWO PLACE DECIMAL ±0.01mm ANGULAR: MACH ± BEND ±	DRAWN		
	CHECKED		
	ENG APPR.		
	MFG APPR.		
	Q.A.		
	COMMENTS:		
INTERPRET GEOMETRIC TOLERANCING PER:			
MATERIAL ALUMINUM			
FINISH DO NOT SCALE DRAWING			

TITLE:

INSERTION ROD

SIZE	DWG. NO.	REV
A		
SCALE: 1:1	WEIGHT:	SHEET 1 OF 1

5 4 3 2 1

2D Sketch of Insertion Cap (cylindrical type and unified design type)

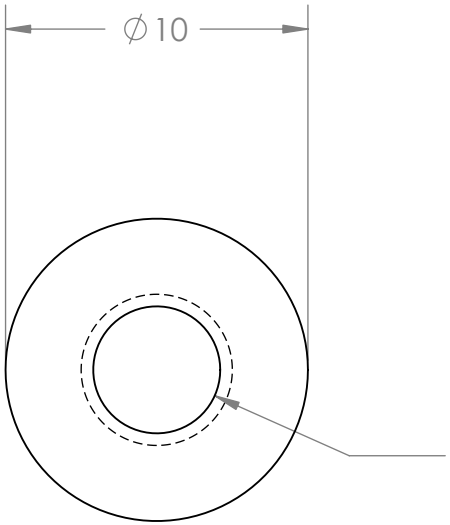

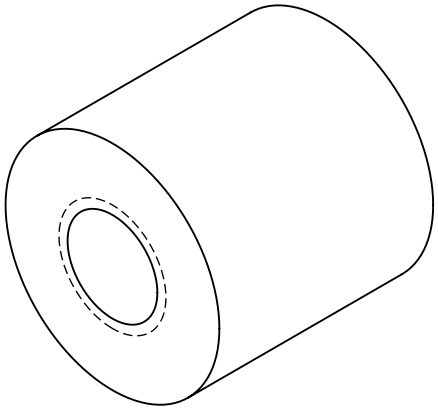

UNLESS OTHERWISE SPECIFIED:		NAME	DATE
DIMENSIONS ARE IN MILLIMETERS TOLERANCES: ZERO PLACE DECIMAL ±1mm ONE PLACE DECIMAL ± 0.1mm TWO PLACE DECIMAL ±0.01mm ANGULAR: MACH ± BEND ±	DRAWN		
	CHECKED		
	ENG APPR.		
	MFG APPR.		
	Q.A.		
INTERPRET GEOMETRIC TOLERANCING PER:	COMMENTS:		
MATERIAL ALUMINUM			
FINISH			
DO NOT SCALE DRAWING			

TITLE:

INSERTION-HEAD CAP

SIZE	DWG. NO.	REV
A		

SCALE: 1:1	WEIGHT:	SHEET 1 OF 1

5 4 3 2 1

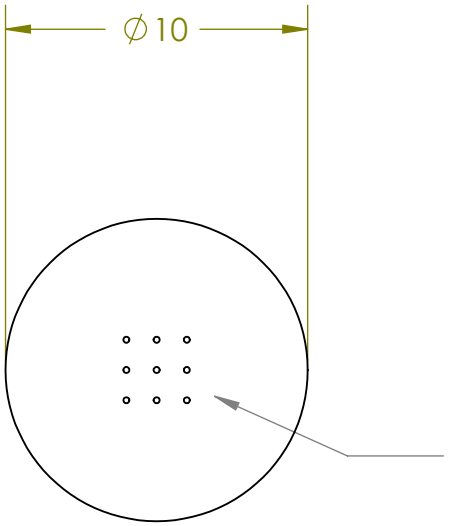

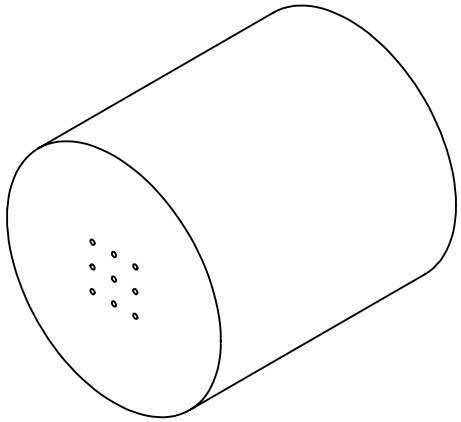

UNLESS OTHERWISE SPECIFIED:		NAME	DATE
DIMENSIONS ARE IN MILLIMETERS TOLERANCES: ZERO PLACE DECIMAL ±1mm ONE PLACE DECIMAL ± 0.1mm TWO PLACE DECIMAL ±0.01mm ANGULAR: MACH ± BEND ±	DRAWN		
	CHECKED		
	ENG APPR.		
	MFG APPR.		
INTERPRET GEOMETRIC TOLERANCING PER:	Q.A.		
MATERIAL ALUMINUM	COMMENTS:		
FINISH			
DO NOT SCALE DRAWING			

TITLE:

INSERTION-HEAD CAP

SIZE	DWG. NO.	REV
A		

SCALE: 1:1	WEIGHT:	SHEET 1 OF 1

5 4 3 2 1

Appendix C

Catalogues of the Selected Components

Catalogue of Vacuum Generator VN-05-M-I2-PQ1-VQ1 Product of: Festo

https://xdki.festo.com/xdki/data/doc_engb/PDF/EN/VN_EN.PDF

Catalogue of Motor with the Order Number of 118638 Product of: Maxon

http://shop.maxonmotor.com/maxon/assets_external/Katalog_neu/eshop/Downloads/Katalog_PDF/maxon_dc_motor/RE-programm/new/newpdf_09/RE-13-118628_09_EN_071.pdf

Compact Motorized 2” (50 mm) Travel Translation Stage Product of: THORLABS

http://www.thorlabs.com/catalogPages/266.pdf

1/2" (12.7 mm) Travel Miniature Dovetail stage Product of: THORLABS

http://www.thorlabs.com/NewGroupPage9.cfm?ObjectGroup_ID=2952&pn=DT12/M&CFID=1587280&CFTOKEN=97662970

Catalogue of Filter-Regulator LFR-1/8-D-5M-MINI-RR-SA Product of: Festo

Filter regulator for D-Micro series LFR-...-D-5M-MICRO-RR-SA

Flowrate: 110...280 l/min

Cleanroom class ISO 45(FS209E class 100)

Filter regulator with manual condensate drain with 5 µm filter cartridges and gauge
LFR-...-D-5M-MICRO-RR-SA

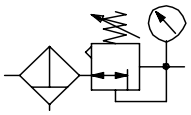

- Pressure range: 7 bar
- Two pressure gauge connections for flexible installation
- 5 µm filter cartridges
- Available with manual condensate drain
- Space saving design with filter and regulator in a single unit
- Good particle separation and high flow rate
- Good regulating characteristics with minimal hysteresis
- Setting values are secured by locking the rotary knob

Accessories

Mounting bracket
HFOE-D-MICRO

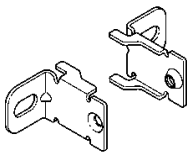

Connecting plate kit
PBL-1/8-D-MICRO

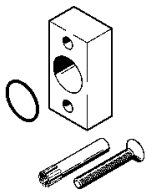

Threaded pin set
FRB-D-MICRO

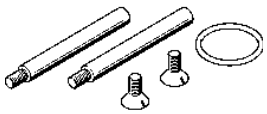

LFR-M5-D-7-5M-MICRO-RR-SA

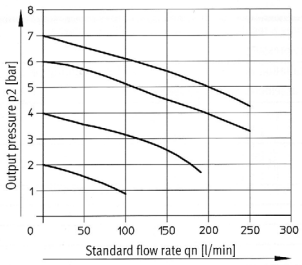

LFR-M7-D-7-5M-MICRO-RR-SA

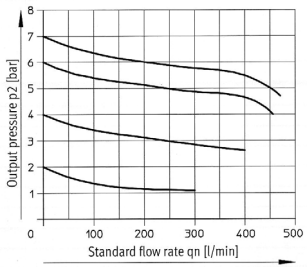

LFR-1/8-D-7-5M-MICRO-RR-SA

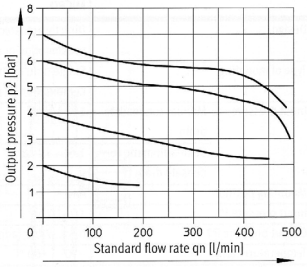

Type [5.0 µm]	Part No.	Connection	Std nominal flow rate at 7 bar [l/min]	Weight [kg]	Input pressure [bar]	Output pressure [bar]	Temperature range [°C]	Condensate volume [ml]
LFR-M5-D-5M-MICRO-RR-SA	15059901	M5 (Thread screw in housing)	110	0.08	1...10	0.5...7	-10...+60	3
LFR-M7-D-5M-MICRO-RR-SA	15059904	M7 (Thread in connection plate)	280	0.09				
LFR-1/8-D-5M-MICRO-RR-SA	15059905	G1/8 (Thread in connection plate)	250	0.09				

Filter regulator for D-Micro series LFR-...-D-5M-MICRO-RR-SA

Flowrate: 110...280 l/min

Cleanroom class ISO 5 (FS209E class 100)

LFR-M5-D-M5-MICRO-RR

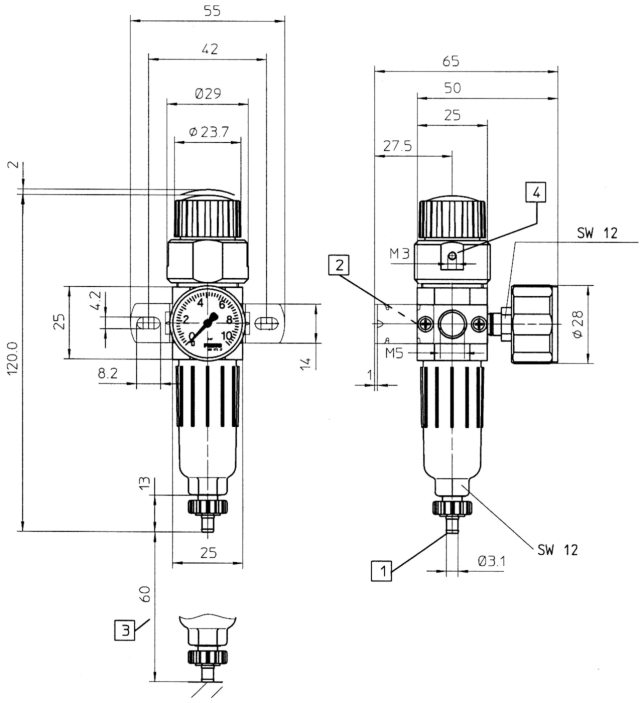

1 Barbed fitting for plastic tubing
2 Second pressure gauge connection
3 Installation dimension above ground level
4 Vacuum suction port M5

LFR-M7-D-M5-MICRO-RR
LFR-1/8-D-M5-MICRO-RR

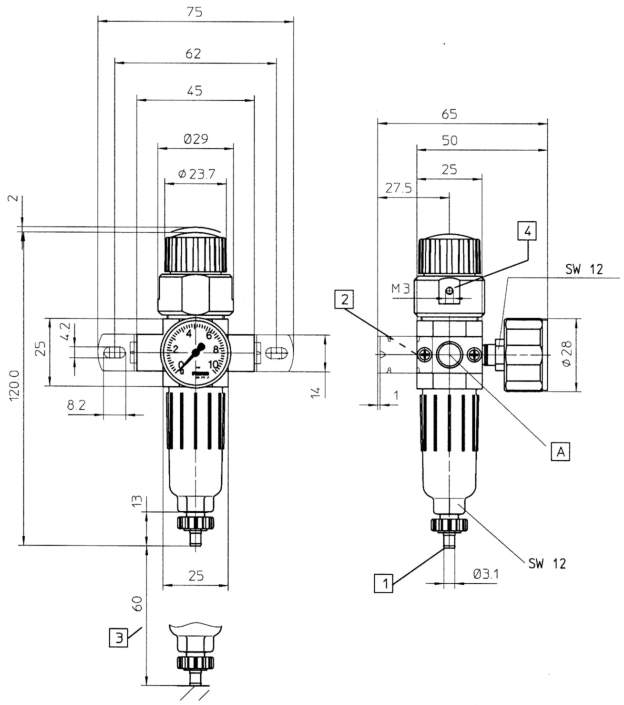

1 Barbed fitting for plastic tubing
2 Second pressure gauge connection
3 Installation dimension above ground level
4 Vacuum suction port M5

Type	A
LR-M7-D-5M-MICRO-RR	M7
LR-1/8-D-5M-MICRO-RR	G1/8

Filter regulator LFR-...-RR-SA

Flowrate: 750...10000 l/min

Cleanroom class ISO 5 (FS209E class 100)

Filter regulator with manual condensate drain with 40 µm filter cartridges and gauge
LFR-...-D-...-RR-SA

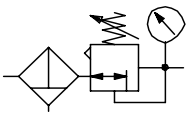

Filter regulator with manual condensate drain with 5 µm filter cartridges but without gauge
LFR-...-D-O-...-RR-SA

Filter regulator with manual condensate drain with 5 µm filter cartridges and gauge
LFR-...-D-5M-...-RR-SA

- Two pressure gauge connections for flexible installation
- Sintered filter with water separator
- Usual 40 µm filter cartridges. Optional with 5 µm filter cartridges
- Space-saving design with filter and regulator in a single unit
- Good particle separation and high flow rate
- Good regulating characteristics with minimal hysteresis
- Setting values are secured by rotary knob.
- Input pressure; 1...16 bar
- Operating pressure; 0.5 ...12 bar
- Temperature range; -10...+60 °C
- Mounting; Vertical ±5°

MINI and MIDI sizes
Directly actuated diaphragm regulator valve

MAXI size
Pilot-actuated piston regulating valve

Accessories
Mounting bracket
HFOE-D-MINI
HFOE-D-MIDI/MAXI

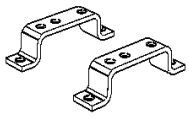

Type	Part No.	Type	Part No.	Connection	Std nominal flowrate]l/min]	Condensate volume [ml]	Weight [kg]
LFR-1/8-D-MINI-RR-SA	15024394	LFR-1/8-D-O-MINI-RR-SA	15024425	G1/8	750	22	0.460
LFR-1/4-D-MINI-RR-SA	15024396	LFR-1/4-D-O-MINI-RR-SA	15024426	G1/4	1400		
LFR-3/8-D-MINI-RR-SA	15024397	LFR-3/8-D-O-MINI-RR-SA	15024428	G3/8	1600		
LFR-1/4-D-MIDI-RR-SA	15024398	LFR-1/4-D-O-MIDI-RR-SA	15024429	G1/4	2000	43	0.920
LFR-3/8-D-MIDI-RR-SA	15024399	LFR-3/8-D-O-MIDI-RR-SA	15024430	G3/8	3100		
LFR-1/2-D-MIDI-RR-SA	15024401	LFR-1/2-D-O-MIDI-RR-SA	15024431	G1/2	3400		
LFR-3/4-D-MIDI-RR-SA	15024402	LFR-3/4-D-O-MIDI-RR-SA	15024432	G3/4	3400		
LFR-1/2-D-MAXI-RR-SA	15024382	LFR-1/2-D-O-MAXI-RR-SA	15024387	G1/2	9400	80	1.470
LFR-3/4-D-MAXI-RR-SA	15024385	LFR-3/4-D-O-MAXI-RR-SA	15024388	G3/4	9700		
LFR-1-D-MAXI-RR-SA	15024386	LFR-1-D-O-MAXI-RR-SA	15024391	G1	10000		
LFR-1/8-D-5M-MINI-RR-SA	15024440	LFR-1/8-D-5M-O-MINI-RR-SA	15024458	G1/8	650	22	0.460
LFR-1/4-D-5M-MINI-RR-SA	15024441	LFR-1/4-D-5M-O-MINI-RR-SA	15024459	G1/4	1200		
LFR-3/8-D-5M-MINI-RR-SA	15024442	LFR-3/8-D-5M-O-MINI-RR-SA	15024460	G3/8	1350		
LFR-1/4-D-5M-MIDI-RR-SA	15024443	LFR-1/4-D-5M-O-MIDI-RR-SA	15024461	G1/4	1600	43	0.920
LFR-3/8-D-5M-MIDI-RR-SA	15024444	LFR-3/8-D-5M-O-MIDI-RR-SA	15024462	G3/8	2400		
LFR-1/2-D-5M-MIDI-RR-SA	15024446	LFR-1/2-D-5M-O-MIDI-RR-SA	15024463	G1/2	2500		
LFR-3/4-D-5M-MIDI-RR-SA	15024447	LFR-3/4-D-5M-O-MIDI-RR-SA	15024464	G3/4	2600		
LFR-1/2-D-5M-MAXI-RR-SA	15024436	LFR-1/2-D-5M-O-MAXI-RR-SA	15024455	G1/2	7580	80	1.470
LFR-3/4-D-5M-MAXI-RR-SA	15024438	LFR-3/4-D-5M-O-MAXI-RR-SA	15024456	G3/4	7600		
LFR-1-D-5M-MAXI-RR-SA	15024439	LFR-1-D-5M-O-MAXI-RR-SA	15024457	G1	8000		

Filter regulator LFR-...-RR-SA

Flowrate: 750...10000 l/min

Cleanroom class ISO 5 (FS209E class 100)

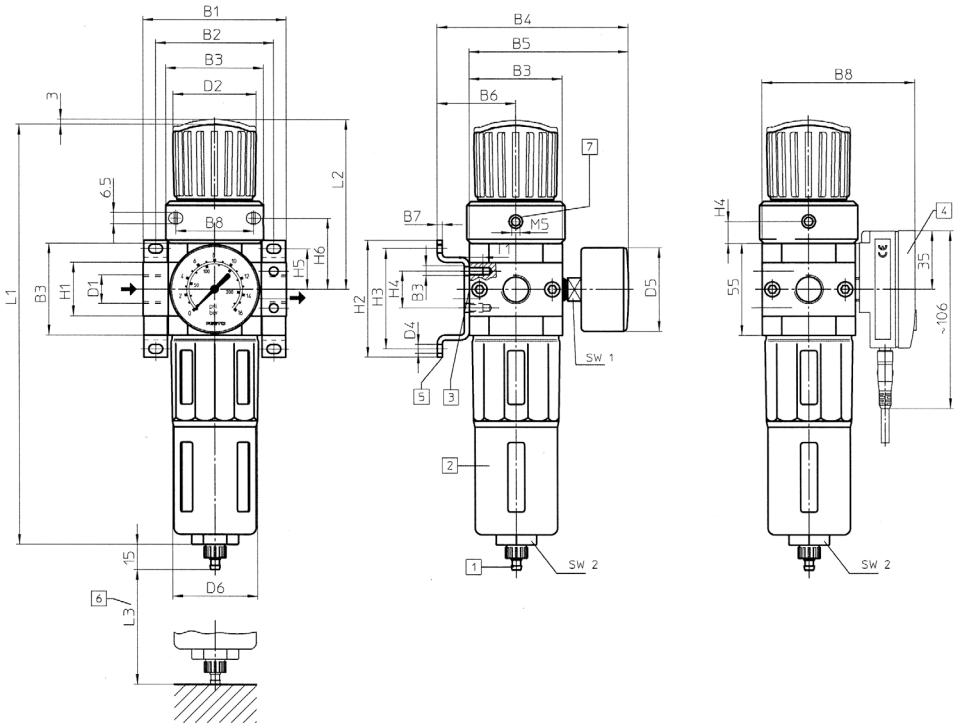

1 Barbed fittings for plastic tubing
2 Metal bowl guard
3 Second pressure gauge Connection
4 Pressure sensor SDE1- ... -R
5 Mounting bracket HFOE-D-... (not included in scope of delivery)
6 Installation dimensions
7 Vacuum suction port

Type	B1	B2	B3	B4	B5	B6	B7	D1	D2	D3	D4	D5
LFR-1/8-D-MINI-RR-SA	64	28	40	92	76	36	75	G1/8	31	43	M4	41
LFR-1/4-D-MINI-RR-SA								G1/4				
LFR-3/8-D-MINI-RR-SA	70							G3/8				
LFR-1/4-D-MIDI-RR-SA	85	46	55	111,5	95	44	91	G1/4	50	58	M5	49
LFR-3/8-D-MIDI-RR-SA								G3/8				
LFR-1/2-D-MIDI-RR-SA								G1/2				
LFR-3/4-D-MIDI-RR-SA								G3/4				
LFR-1/2-D-MAXI-RR-SA	96	51	66	124	107	50	100	G1/2	31	43	M5	49
LFR-3/4-D-MAXI-RR-SA								G3/4				
LFR-1-D-MAXI-RR-SA	116							G1				

Type	D6	H1	H2	H3	H4	L1	L2	L3	T1	SW1	SW2
LFR-1/8-D-MINI-RR-SA	38	20	38	35	9	193	69	60	7	14	24
LFR-1/4-D-MINI-RR-SA											
LFR-3/8-D-MINI-RR-SA											
LFR-1/4-D-MIDI-RR-SA	52	32	45,5	60	13	250	99	80	8	14	24
LFR-3/8-D-MIDI-RR-SA											
LFR-1/2-D-MIDI-RR-SA											
LFR-3/4-D-MIDI-RR-SA											
LFR-1/2-D-MAXI-RR-SA	65	32	51	60	9	252	82	90	8	14	24
LFR-3/4-D-MAXI-RR-SA											
LFR-1-D-MAXI-RR-SA		40									

Appendix D

ASME Publications Permission for Chapter 3

hajar sharif <hajarsharif@gmail.com>

Re: ASME PUBLICATIONS PERMISSION REQUEST FORM SUBMISSION

1 message

Beth Darchi <DarchiB@asme.org> **Fri, Jan 22, 2010 at 10:40 AM**
To: hajarsharif@gmail.com

Dear Mr. Sharif:
It is our pleasure to grant you permission to use ASME paper "ON THE BIO-MECHANICAL PROPERTIES OF A DUAL-POROUS OSTEOCHONDRAL SCAFFOLD," by Hajar Sharif, Yaser Shanjani, Mihaela Vlasea, Ehsan Toyserkani, Proceedings of IMECE2008, cited in your letter for inclusion in a master thesis entitled Development of a Novel Porogen Insertion System Used in Solid Freeform Fabrication of Porous Biodegradable Scaffolds with Heterogeneous Internal Architectures to be published by University of Waterloo.

As is customary, we ask that you ensure full acknowledgment of this material, the author(s), source and ASME as original publisher on all printed copies being distributed.

Many thanks for your interest in ASME publications.

Sincerely,
Beth Darchi
Permissions & Copyrights
ASME, 3 Park Avenue
New York, NY 10016
T: 212-591-7700
F: 212-591-7841
E: darchib@asme.org

>>> <webmaster@asme.org> 1/21/2010 7:23 PM >>>

ASME PUBLICATIONS PERMISSION REQUEST FORM HAS BEEN SUBMITTED:

ASME Publication Title: Proceedings of IMECE2008
Complete List of Authors: Hajar Sharif, Yaser Shanjani, Mihaela Vlasea, Ehsan Toyserkani
Paper Title (Conference/Journal): ON THE BIO-MECHANICAL PROPERTIES OF A DUAL-POROUS OSTEOCHONDRAL SCAFFOLD
Paper Number (Conference): 68108
Volume Number (Journal): 0
Page(s) in the publication of

the permission request:
Year of Publication: 2008
I would like to... Photocopy for Academic/Non-Commercial Use
Portion to be used: Entire Article
List Figure Numbers: 0
List Table Numbers: 0
Number of Copies:
Usage: Electronic
Title of outside publication: Development of a Novel Porogen Insertion System Used in Solid Freeform Fabrication of Porous Biodegradable Scaffolds with Heterogeneous Internal Architectures
Publisher: University of Waterloo
Comments: I want to use my ASME Paper as a part of my master thesis.

I am wondering if you can provide me the permission as soon as possible, since my thesis has to be approved by our university before January 22nd., 4:00 pm eastern time.

thank you for cooperation
Author: yes
First Name: Hajar
Last Name: Sharif
Address Line 1: Apt# 1205, 80 Mooregate Cres.,
Address Line 2:
City: Kitchener
State: Ontario
Zip: n2m5g1
Phone: 519 742 5114
Fax:
Email: hajarsharif@gmail.com